A MICROFLUIDIC PLATFORM TO STUDY CELL MIGRATION

by

SMITHA MALALUR NAGARAJA RAO

Presented to the Faculty of the Graduate School of

The University of Texas at Arlington in Partial Fulfillment

of the Requirements

for the Degree of

DOCTOR OF PHILOSOPHY

THE UNIVERSITY OF TEXAS AT ARLINGTON

December 2009

Dedicated to my grandparents.

ACKNOWLEDGEMENTS

I would like to thank my mentor Dr. J.-C. Chiao for his support, encouragement and guidance throughout this work. His vision and insight was an inspiration that helped me overcome initial failures and face the challenges. I also thank Dr. Victor Lin who took it upon himself to change an electrical engineer into a student of biology. Dr. Lin's patient training, guidance and faith in my abilities gave me the courage and confidence to conduct the experiments in his lab. I would also like to thank Dr. Kytai Nguyen and Dr. J. T. Hsieh for their valuable suggestions and use of their facilities. Dr. Nguyen always provided friendly advise from the stand point of a student and encouraged me never to give up. I would also like to thank Dr. Singhal from UNTHSC for providing us with cell samples and antibodies for testing. I would also like to acknowledge the help and support from Dr. Venkat Devarajan and Dr. Michael Vasilyev. I also thank Dr. Mingyu Lu and Dr. Weidong Zhou for their valuable suggestions.

This work would not have been possible without the help and suggestions of members, past and present of iMEMS. I would like to thank my colleagues Cory Huggins, Preeti Singhal, and Uday Tata for their help with the experiments along with my friend Praveen P.S for his time and help. I would also like to thank the help provided to me by Dr. Nguyen's students Amit, Maria, Hao and Daniel. I also thank the faculty and staff at The Nanofabrication and Teaching Facility, UTA and Department of Urology, UTSW Medical Center.

I am grateful to my family, specially my aunt and uncle Dr. Sudhamani Rao and Dr. Sateesh Babu who supported me and encouraged me. My endeavors would

not have been possible without my parents Mrs. Shoba Rao and Mr. M.S. Nagaraja Rao who believed in me and let me pursue my dreams so far away from home. Their love and blessings have helped me come a long way. My gratitude to my husband and best friend Nagesh Hatti who has stood by me, encouraged me and most importantly let me work things out at my own pace and time. I also thank my parents-in-law Mr. D.V. Hatti and Mrs. Sidamma Hatti for their words of encouragement, support and blessings. A special thanks to all my friends.

November 20, 2009

ABSTRACT

A MICROFLUIDIC PLATFORM TO STUDY CELL MIGRATION

SMITHA MALALUR NAGARAJA RAO, Ph.D.

The University of Texas at Arlington, 2009

Supervising Professor: Jung-Chih Chiao

Migration of cancer cells from the primary organ to distant sites is critical to the development of malignant metastasis. This is partly dependant on the various chemical factors present in the blood serum. Cell motility studies using conventional Boyden chamber assays require high volumes of reagents. The measurement provides only an end-point result and time-lapse study of the cell deformation and migration cannot be performed. We have designed and evaluated a poly-dimethylsiloxane (PDMS) microfluidic device in order to study cell migration in the presence of gradients. Photolithography and soft lithography processes were used to fabricate the PDMS devices from the negative photoresist (SU-8) molds. The devices were then soft bonded to standard tissue culture plates. Conventional tissue culture techniques were employed and the cell culture environment was not compromised. Using our proposed designs, we can obtain cell number, location, migration rate and time taken for cells to migrate in response to chemoattractants.

We propose two different methods to study cell migration in response to chemokine gradients. In the first method, the chemokines were continuously infused into the microfluidic system through a system of microchannels creating a sustainable gradient

and migration of cells in this gradient environment was monitored. This device consists of three inlets and one outlet. The inlets were used to introduce chemokines along with culture media and cells in suspension. Time lapse video micrographs were used to determine concentration gradients and cell response in the gradients. The channels were designed to be 100 μm wide and 100 μm in height with two mixing stages leading into the outlet. The outlet was designed to be 900 μm wide and 100 μm in height.

In the second method, the gradient was formed by diffusion over time in the microchannels after the chemoattractants were introduced. The device consists of two separate identical chambers that are interconnected by identical microchannels that are 10 μm high, 25 μm wide and 1 mm long. One chamber contains cells whose migration characteristics are to be evaluated, while the other chamber contains media with chemoattractants towards which the response of the cells needs to be analyzed. Time-lapse photography was used to determine the migration of cells in the microchannels and obtain information regarding migration rate, cell number and identify migration potential of various stimulants. Two such designs were tested. The first one had four reservoirs, two each for cell seeding and addition of chemoattractants. This reduced chemokine consumption compared to conventional assays however, we aimed to further reduce the volume of reagents required. The third design had only one reservoir each for cell seeding and addition of chemoattractants. Several cell lines were tested against various factors. Normal human epithelial prostate (HPV-7) cells were tested against growth factors. Similarly, prostate cancer (PC-3) cells, lung metastasized prostate cancer cells (PC-3-ML), breast cancer cells (MDA-MB-231), normal human mesangial (HMC) cells, kidney cancer (CaKi-2) cells were all tested against several antibodies and ionic chemicals. The migration rate, distance and cell numbers for each case were determined. Due to the ability of the microfluidic platform to mimic

physiological dimensions and provide information regarding cell migration, we have called this platform as MiMiC^{TM} standing for Microfluidic assay for Migration of Cells. This platform is cost effective and relies on very small volumes of reagents. It can maintain stable chemokine gradients in the channels, allow real-time quantitative study of cell migration and provide information about cellular dynamics and help in biomechanical analysis. The results demonstrate the utility of this microfluidic device as a platform to study cancer cell migration and point to potential applications in the identification of specific chemokine agents and drugs targeting cell migration. It also has the potential to be a complementary technique to Prostate specific antigen (PSA), that is used in Prostate cancer diagnosis. The device also allows high throughput assays and real time observation. It is our understanding that these techniques have not all been incorporated in a single device until now.

TABLE OF CONTENTS

LIST OF FIGURES

LIST OF TABLES

CHAPTER 1

INTRODUCTION

Metastasis of solid tumors from their primary site to distant sites often render the cancer incurable. For example, the metastasis of prostate cancer to the bone is associated with a very poor prognosis [1–4]. Metastasis is a complex multi-step process that involves invasive tumor cells entering the blood stream, attaching onto the walls of the blood vessels and invading a secondary organ leading to tumors [5]. This process may be partly determined by chemokines that serve to attract the cancer cells from the primary organ site to specific metastatic sites. Another phenomenon believed to be instrumental in cancer cell migration is epithelial-mesenchymal transition (EMT).

Epithelial cells are characterized by close, densely packed cells organized by the basement membrane. Cancer of the epithelial cells is called carcinomas and account for 85% of all cancers. The breakdown of the basement membrane allows the epithelial cells in a carcinoma to separate from the neighboring cells and become motile. These motile cancerous cells form tumors in secondary organs [6, 7].

For prostate cancer, several chemokines have been shown to be elevated in patients with advanced prostate carcinoma and may influence the migration of prostate cancer cells towards the bone [8–18].

One of the primary limitations of the study of cell migration has been the lack of a suitable cost-effective assay with applications in clinical assessments. Conventional assays using Boyden chamber models require a high volume of valuable reagents, and are limited in their scope of evaluation of cell migration [19, 20]. Further, the methods

measure cellular and biochemical gross response in cells responding to chemical stimulation and detailed cellular parameter analyses are not possible. Given the complexity of the changes in growth environment on the cells, the measurement of individual cell responses to the chemokine gradient may greatly enhance our understanding of cancer cell migration.

Towards this end, various microfluidic devices of different designs have been used to create controllable and steady concentration gradients of various chemokines for quantitative evaluation of chemotaxis on cell migration [21–24]. Unlike conventional Boyden chambers or transwell devices, microfluidic devices are able to provide stable chemokine gradients and real-time quantitative measurement of cell migration towards chemokine gradients. Moreover, microfluidic devices can dramatically reduce the quantity of the chemokines consumed in the testing process. Microfluidic devices use fractions of a microliter of reagent compared to the Boyden chamber arrays which requires more than 250 μl per well. In addition, stable chemical gradients can be generated, maintained and repeated over time. Finally, an array configuration allows for parallel testing, including multiple chemokine gradients [23, 25–28]. Microfluidic devices have been employed to investigate neutrophil and breast cancer cell chemotaxis [24, 29–31]. Thus, microfluidic devices represent a more cost-effective system to study chemotaxis of cancer cells, evaluate cell migration in vessel-like environments and can be fabricated as arrays that allow for the high-throughput evaluation for cell migration.

Microfluidic devices have several advantages over conventional macro-scale devices for biomedical applications. Some of the advantages may be summarized as follows:

1. Human physiology consists of large networks of microscale vessels connecting to larger conduits. Microfluidic devices can be fabricated to recreate a similar environment to analyze the various cellular responses
2. Microfluidic devices with Reynold's number typically less than one always provide non-turbulent laminar flows
3. Static and dynamic conditions can be realized and tested
4. Potentially single cell analysis can be performed
5. Small volumes, batch processing, high-throughput applications, small foot prints, use of low cost polymers make polymeric microfluidic devices cost effective

Thus microfluidic devices can potentially be used in a wide range of experiments requiring a controllable in-vitro environment. In order to use polymer based devices for cell studies, the behavior of cells need to be better understood. Our knowledge of cellular behavior and functions is from in vitro manipulation of cells. The current techniques are inadequate as they do not mimic the intricate microenvironments within the body because of which many cellular characteristics and phenomenon remain unidentified. Handling cells outside the body involves three major steps: isolation, culture and analysis. These steps have been successfully developed and practiced over time [32, 33]. These steps are easy to accomplish in the macro-scale, where the device size is compatible with existing instruments allowing easy access for handling and manipulation. However, in the micro-scale one of the major issues is interfacing the micro-scale devices with the macro-scale instruments and equipments allowing cell handling, manipulation and analysis. Furthermore the complete device should be robust, reliable and leak free. Several interface techniques have been developed and employed including interface adapters, fluidic couplers [34] and the most commonly used direct sample loading structures such as wells or reservoirs [35–38]. We have

proposed a design for a microfluidic platform that allows monitoring of cell migration under influence of chemokine gradients. The design for a continuous flow microfluidic platform providing gradients is presented in Chapter 2. The results and conclusions of the experiments are presented in Chapter 3. Chapter 4 introduces an alternative design for the microfluidic platform using static flow or no-flow condition. An array configuration of the static flow device is also presented. In an array configuration, it is possible to conduct high throughput assays. Several experiments with prostate cancer cells, breast cancer cells, vascular smooth muscle cells, kidney cancer cells have been performed to demonstrate the feasibility of using the device to study cell migration. Cell migration in response to various growth factors, antibodies, different growth media concentrations and patient serum extract was analyzed. The platform also has potential to be used as a means to assess cancer metastasis potential. Experiments and results to demonstrate that the platform provides a high-throughput, real time method to test, study and analyze cell migration and observe epithelial to mesenchymal transition (EMT) is presented in Chapter 5.

CHAPTER 2

MICROFLUIDIC PLATFORM: DESIGN AND FABRICATION

2.1 Materials

Microfluidic devices have been fabricated using several materials from silicon, glass, metals and polymers to ceramics. Silicon has been the most commonly used material due to the fact that fabrication technology required to process silicon is well established. Moreover the processes involved in forming various devices and structures from silicon are readily available. The silicon based technology relies on conventional CMOS processes making design, fabrication and testing such devices relatively easy. The use of silicon as a biomaterial has been debated [39–42]. Glass has been used mainly in biomedical applications since biochemical reactions in glass have been well characterized. Glass has the advantage that it is optically transparent when compared to silicon, metal and ceramics but it is brittle and can be fatal when used in-vivo. Metals and ceramics are relatively new and have limitations in biomedical applications. Gold, titanium and platinum are acceptable biocompatible materials while copper and aluminum are considered hazardous as they are prone to oxidation. The drawback in all these materials is that they are all rigid and cannot be used in applications requiring flexible or semi-flexible membranes or devices such as electrodes for biomedical applications.

Polymers have been incorporated in microfluidic devices in recent years. There are several advantages to using polymers. The surface properties of polymers can be altered to suit the application. Fabrication processes are comparatively easy allowing batch fabrication leading to cost efficiency. The greatest advantage of polymers is

that they can be modified to have required rigidity. Polymers can be flexible, optically transparent and biocompatible. Some of the polymers used include Parylene, Poly(methyl methacrylate) also known as PMMA, Polydimethylsiloxane (PDMS), Polyimide, SU-8 and hydrogels [43, 44]. The devices presented in this work are polymer based and fabricated by soft-lithography of PDMS.

2.1.1 Polydimethylsiloxane (PDMS)

Poly-dimethylsiloxane (PDMS) has been employed in microfluidic devices in the past [45–48]. The motility of cells on PDMS surfaces has also been reported [49]. PDMS can be easily molded to form channels of desired dimensions and is inexpensive. PDMS 3-dimensional structures have also been demonstrated [50]. In our novel design of the microfluidic device, the PDMS structures form the confinement chambers and channels of the microfluidic device. These chambers and channels are placed on culture dishes on which cells are seeded, cultured and monitored. Utilizing the culture dish as a substratum retains the well-characterized cell culture conditions for adherent cells, while the PDMS forms the superstructure to study cell migration. PDMS is optically transparent allowing for detailed optical interrogation and high quality image recording and documentation. In this study we successfully designed a microfluidic device to efficiently measure individual cell response and migration in response to chemical stimulation in detail. The results presented clearly demonstrate the efficacy and utility of the device design for cell motility analyses with implications in the study and analyses of cancer cell migration and metastasis.

PDMS is commercially available as a two part polymer kit under the name Sylgard^{TM} 184 from Dow Corning and RTV615 from GE. The kit consists of the PDMS base and curing agent that forms an elastomer by an organometallic cross-linking action between the siloxane base oligomers of the base comprising of vinyl ter-

minated end groups. The cross-linkers typically are dimethyl methylhydrogen siloxane or tetrakis(dimethysiloxylsilane) (TDS). The Si-CH_2-CH_2-Si linkages are formed by the addition of the SiH bond across the vinyl groups catalyzed by the platinum-based catalyst in the base solution. The base solution also consists of silica fillers [51]. Three-dimensional cross-linking is achieved due to the multiple reaction sites on the monomer and the cross-linking chains [52–56].

By varying the mixing ratio of the base and curing agent, the flexibility of the PDMS can be changed. Typical mixing ratio is 10:1 by weight of base and curing agent. As the quantity of the base is increased, the PDMS tends to become soft and beyond 40:1 ratio becomes very pliable. In our application, the device needs to retain its structure and maintain integrity of the patterns. Thus we have used the recommended 10:1 by weight of base to curing agent as the mixing ratio.

Patterning PDMS involves transferring a pattern from a master to the elastomeric material. This is commonly known as soft lithography, casting or molding. The master molds in turn can be made by wet chemical etching or photolithography. The fabrication process is discussed in detail in section [**?**].

2.2 Fabrication Process

Fabrication of devices from PDMS involves a number of steps. A master pattern was first formed by photolithography on silicon wafer. The pattern was hard baked to prepare it for the next step. The device pattern from the master was transferred onto the PDMS by soft lithography.The following sections describe the process in detail.

2.2.1 Photolithography

Photolithography is a process in which patterns are developed on a photosensitive polymer resin known as photoresists, when exposed to ultraviolet light. Pho-

toresists are light sensitive polymer resins that are sensitive to light in the ultraviolet and shorter wavelengths. The typical wavelengths are i-line (365 nm) and g-line (436 nm). They are used extensively in printed circuit board fabrication, microelectronics and other integrated circuit fabrication processes.

To begin with, the photoresist is coated on a substrate material, typically silicon wafer. The thickness of the photoresist being coated can be controlled by changing the spin coating speed. Spin coating is a procedure in which a uniform thin film is coated on the substrate by the centrifugal force on the wafer mounted on a vacuum chuck that can spin at controlled rates. The thickness of the resist coat can be determined by the spin speed, duration and ramp speeds.

When a photoresist is exposed to UV light, polymerization occurs hardening the material. The develop step further polymerizes the material, removes the non-polymerized resist completing the chemical reactions. Baking removes the solvents, improves adhesion of the material to the substrate and prepares the resist for further processing. Patterns of required shape and size (length and width) are transferred onto the resist by exposing the resist through a photomask containing the patterns. The regions of the resist that are not polymerized are washed away by the developer. Thus photoresists can be classified into positive and negative. In a positive photoresist, the regions of the resist exposed to the UV light through the photomask are developed out while in the negative photoresist, the regions not exposed to UV light are washed away by the developer. The choice of the type of photoresist depends on the design requirements. Generally negative tone photoresists provide higher aspect ratios and can reach as much as 450 μm in height. In our process we have used the negative photoresist SU-8-100 (Microchem, MA) [57]. The coating speed and times were obtained from the data sheets. The substrate was a 4" p-type silicon wafer. The complete process is summarized in Table 2.1. Once the master pattern was created

Table 2.1. Process parameters for SU-8-100 to obtain 100 μm feature height

	Process Step	Parameters
1.	Singe the wafer	1 hour at 150°C
2.	Spin coat	500 rpm with a ramp of 100 rpm/s. Hold for 5s 3000 rpm with a ramp of 300 rpm/s. Hold for 30s
3.	Soft Bake	30m at 65° 45m at 95°C
4.	Expose	32s
5.	Post exposure bake (PEB)	30m at 65°C 45m at 95°C
6.	Develop	10m in developer. Rinse with Isopropylalcohol (IPA)
7.	Hard bake	45m at 150°C

on the silicon wafer, the wafer was placed on a Pyrex® plate and PDMS is poured onto the mold and cured as shown in Fig. 2.1. As the PDMS cured, the patterns were transferred onto the PDMS from the master. The cured PDMS layer was cut and peeled from the silicon wafer. It was then diced, cleaned and prepared for use. Cleaning included soaking in detergent for up to an hour followed by DI water rinsing and 20 minutes soak in 75% Ethyl alcohol. The dies were then placed in sterilized dishes under the UV light of a tissue culture hood for 45 minutes.

2.2.2 PDMS Bonding

The device is made by bonding the cleaned PDMS die to a clean glass substrate. The surface of the cured PDMS can be modified to alter the reaction between PDMS and other surfaces. These modifications also alter the surface wetting characteristics of PDMS [51]. PDMS can be bonded to glass, Kapton or to PDMS itself by permanent or temporary bonds.

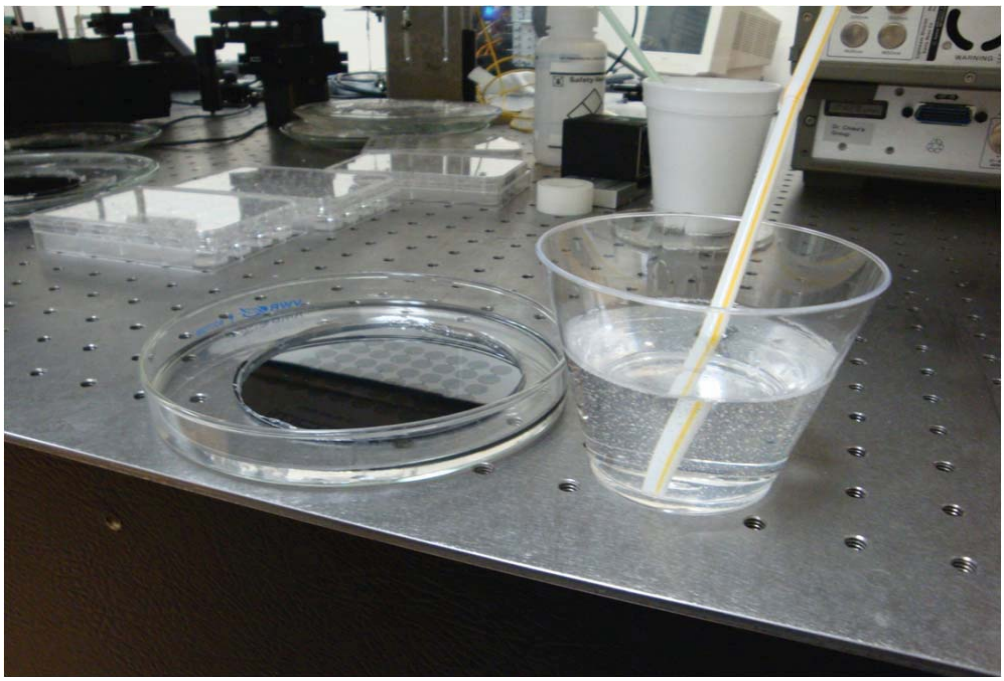

Figure 2.1. The PDMS mixture is degassed and poured on to the silicon wafer with the master pattern placed on Pyrex® plate and cured.

2.2.2.1 Temporary or Soft PDMS-Glass Bonding

Temporary bonds are formed by placing clean PDMS-PDMS or PDMS-glass in contact. Temporary bonds, allow the separation of PDMS and glass at the end of the experiments. This allows easy access for further processing. In order to create a leak free bond, the surface of the materials in contact should be clean and free of voids. To prepare for soft-bonding, the glass was cleaned by rinsing in IPA and blow drying with compressed dry air inside a tissue culture hood to keep it free of bacterial contamination. The PDMS was cleaned first using scotch-tape (3M, MN), rinsed with iso-propyl alcohol and placed to dry in the tissue culture hood under UV light. The clean and dried glass and PDMS were carefully brought in contact with the device side facing the glass and pressed. Care was taken not to touch the active surfaces of the device as this can prevent bonding.

2.2.2.2 Permanent PDMS-Glass Bonding

PDMS can be bonded permanently to glass, Kapton or PDMS itself [58]. This can be achieved by activating the surface of the PDMS with ionized oxygen. Exposing the PDMS surface to the ionized oxygen in the chamber of a reactive ion etcher (RIE) for 20 seconds renders the surface hydrophillic and if a similarly activated PDMS, clean glass or Kapton is brought in contact a permanent bond is formed. This method has several disadvantages including a very short time to bring the parts together to bond. Also, once exposed to the ionized oxygen, the surface cannot be modified again. For our process we used an alternative method of using a corona discharge electrode for PDMS surface treatment. PDMS was cleaned and dried and a corona discharge electrode (Model:BD-20AC, Electro-Technic Products Inc.) was used to activate the surface of the PDMS. When this activated surface was brought in contact with glass or similarly activated Kapton or PDMS, a permanent chemical bond was formed sealing the contacting surfaces. Such devices have been known to have bond strengths of the order of 500 kPa [59].

In our proposed device, the cells attach and proliferate on a glass substrate in channels defined by the PDMS die. The PDMS structures serve to confine the media, mix them in the "U" shaped channels and form a gradient in the outlet. The PDMS die with the microchannels, inlets, outlet and the mixer network was permanantly bonded to a glass substrate by activating the surface using the corona electrode. Another important issue to consider, although the cells do not attach and proliferate on the PDMS and were only in close contact with it, was the biocompatibility of PDMS. The next chapter discusses the experiments conducted to assess biocompatibility of PDMS by determining proliferation of prostate cancer cells (PC-3) and

vascular smooth muscle cells (VSMC) on cured PDMS with different base to curing agent ratios with and without surface activation.

2.3 PDMS Biocompatibility

In our proposed device, the cells attach and proliferate on a glass substrate in channels defined by the PDMS die. It was important to assess the cytotoxicity of PDMS in order to determine the optimum conditions required to culture the cells and monitor their migration in response to the chemoattractants.

2.3.1 Characterization of PDMS

PDMS has been analyzed and characterized for cell culture applications [60]. We have tested PDMS specifically with human aortic vascular smooth muscle cells (HASMC) and prostate cancer cells (PC-3) by assessing their proliferation on PDMS. The tests were conducted on cured PDMS made of different base to curing agent ratios to determine the most suitable ratio for cell culture applications. Different base to curing agent ratios yield PDMS samples that have different properties. For ratios up to 20:1 the properties remain similar and the PDMS remains firm but flexible retaining structures with high elasticity. However, beyond 50:1 the PDMS does not fully cure and becomes difficult to handle. therefore, we tested PDMS base to curing agent ratios of 10:1, 30:1 and 50:1 by weight.

2.3.1.1 Contact Angle Measurement

In order for the cells to attach to the surface and proliferate, the surface needs to be hydrophilic in nature. However, PDMS is hydrophobic in nature. It has been shown that the surface properties of PDMS can be altered by exposing to ionized oxygen or treating with a corona electrode [58]. The surface activation process is

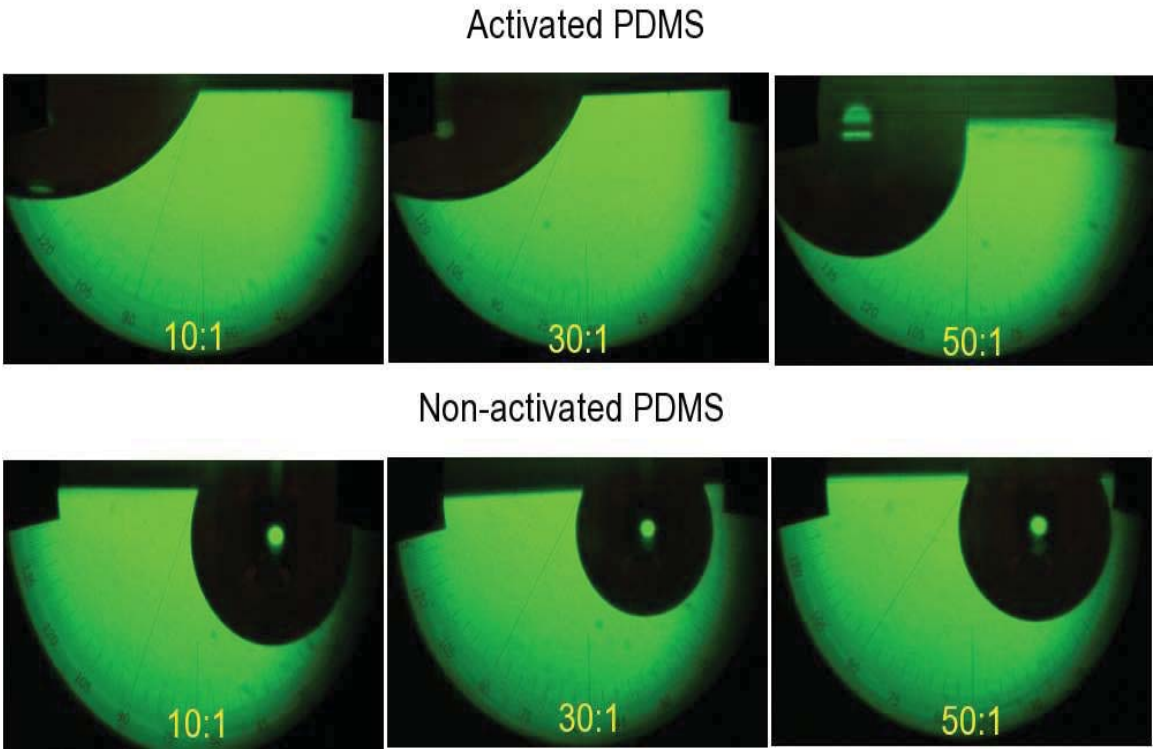

Figure 2.2. Contact angle measurement of PDMS with base to curing agent ratios of 10:1, 30:1 and 50:1, 24hrs with and without surface activation.

believed to change the hydrophobic property of PDMS. The three different PDMS mixtures, 10:1, 30:1 and 50:1 with n=3 were all cured in 6-well plates. Thus there were 3 wells each of PDMS 10:1, 30:1 and 50:1. The first such set was used as control. A second similar set was treated with the corona electrode and left inside a tissue culture hood for 24 hours. A third set was treated with corona electrode prior (not exceeding 60 minutes) to testing. It was found that non-activated PDMS or the control was highly hydrophobic in nature. PDMS activated and placed in the hood for 24 hours was less hydrophobic, except for 50:1 and the immediately activated PDMS was hydrophilic. This was determined by the contact angle formed by a droplet of water on the PDMS surface which indicates surface wetting properties.

A contact angle of less than 90° indicates hydrophilic surface while an angle greater than 90° indicates hydrophobicity. The results of the contact angle measurements are summarized in Table 2.2 and micrographs of the droplet formation on the PDMS is shown in Fig. 2.2.

Table 2.2. Contact angle measurements for PDMS samples that was activated immediately (1 hour prior to testing), activated (24 hrs prior to testing) and control (non-treated) PDMS samples with base to curing agent ratios of 10:1, 30:1 and 50:1

Surface Treatment	10:1	30:1	50:1
Activated immediately	0° ± 3°	0° ± 3°	0° ± 3°
Activated	68° ± 3°	61° ± 3°	90° ± 3°
Control	115° ± 3°	124° ± 3°	129° ± 3°

2.3.1.2 Tests for Biocompatibility

PC-3 cells cultured in DMEM were trypsinized and counted (refer Appendix A). A known number of cells (3000 per well) were seeded on activated, activated immediately and non-activated PDMS with base to curing agent ratios of 10:1, 30:1 and 50:1 cured in 6-well plates. Cells were also seeded at the same time in standard 6-well culture plates as control. All the seeded plates were placed in the incubator at 37°C and 5% CO_2 for 3 days after which the numbers of live cells in each well were counted. By comparing with the control, the effect of using different PDMS for cell culture was assessed. Fig. 2.3 shows PC-3 cells after three days of culture on PDMS substrates with different surface treatments. It was clear that there was cell death in the non-activated PDMS and therefore was not suitable for cell growth. Activated PDMS was similar to control whereas there were fewer cells in the immediately acti-

vated PDMS when compared to control. The results can be quantitatively analyzed by assessing the cell numbers.

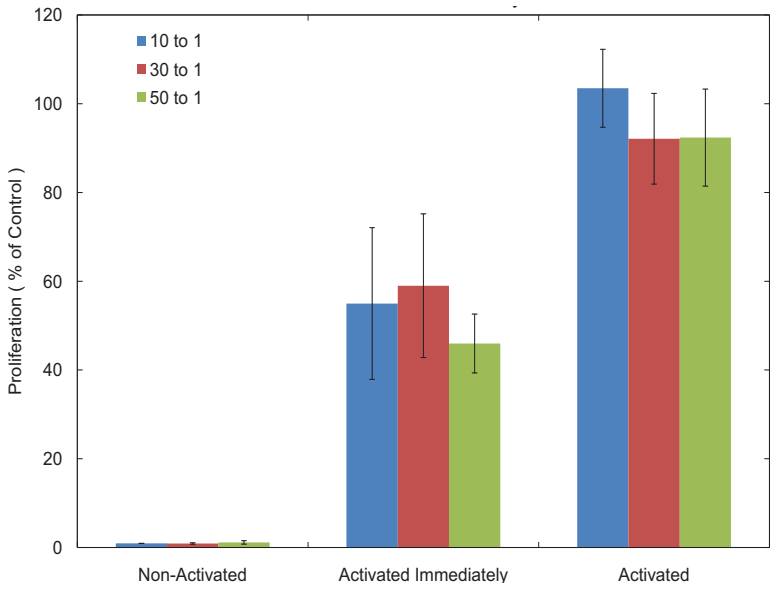

Figure 2.3. PC-3 proliferation on 10:1, 30:1 and 50:1 PDMS that has not been activated, immediately activated and activated 24 hrs prior to cell seeding compared to control after 3 days.

Analysis of individual PDMS samples with different base to curing agent ratios and surface treatments, can be used to select the best combination required for cell culture. The plot of the number of cells as percentage of control for PDMS that is immediately activated, activated and non-activated is as shown in Figs. 2.4, 2.5 and 2.6. It can be seen that the PDMS substratum that was activated (24 hours prior to cell seeding) had the highest number of cells and the non-activated PDMS had the least. Thus, PDMS that is activated 24 hours prior to cell seeding could be used for cell culture. The cell proliferation as percentage of control for each of the PDMS mixing ratios and with surface modifications tested is as represented in Figs. 2.7, 2.8 and 2.9. Similar experiments were conducted with human aortic smooth muscle cells

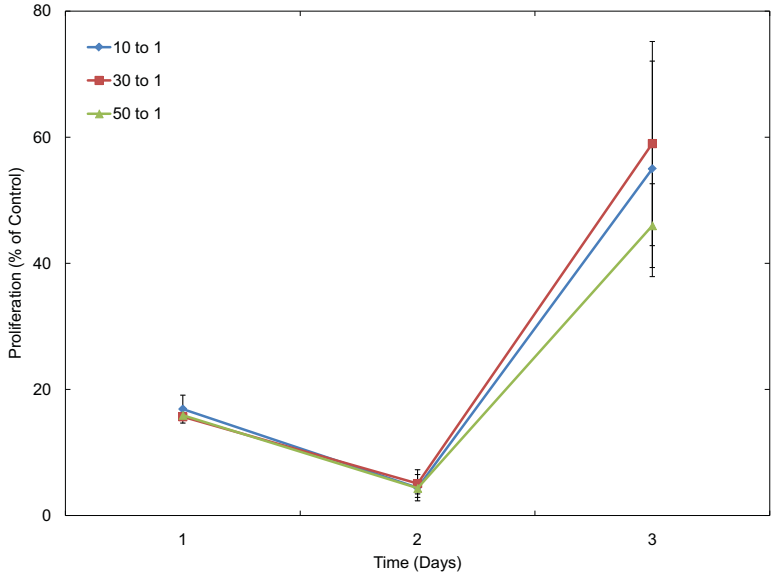

Figure 2.4. PC-3 proliferation on 10:1, 30:1 and 50:1 PDMS that has been activated immediately as percentage of control after 3 days.

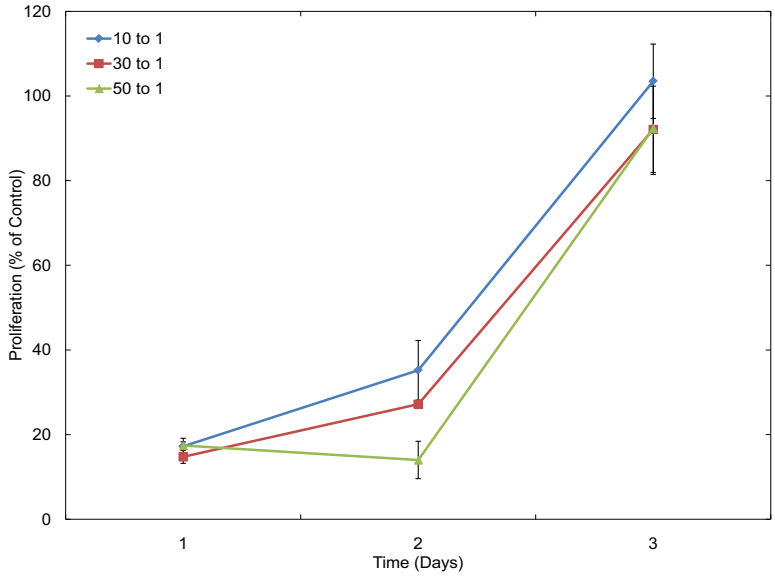

Figure 2.5. PC-3 proliferation on 10:1, 30:1 and 50:1 PDMS that has been activated as percentage of control after 3 days.

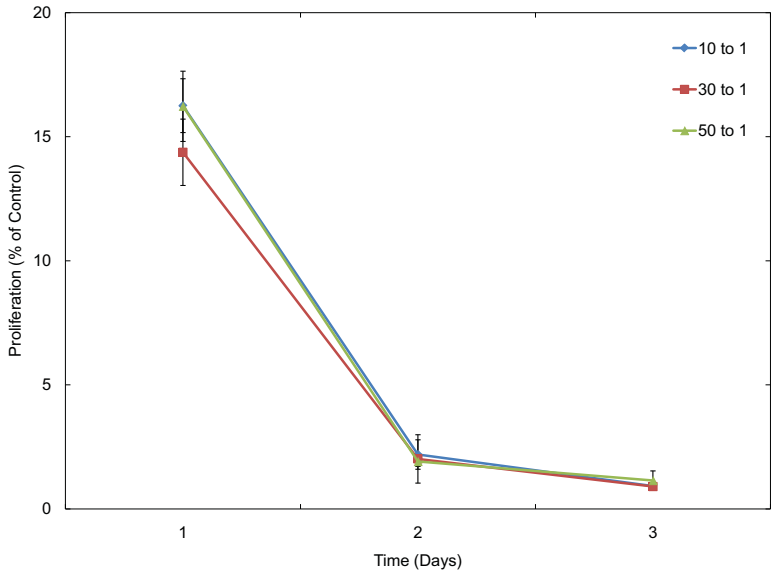

Figure 2.6. PC-3 proliferation on 10:1, 30:1 and 50:1 PDMS that has not been activated as percentage of control after 3 days.

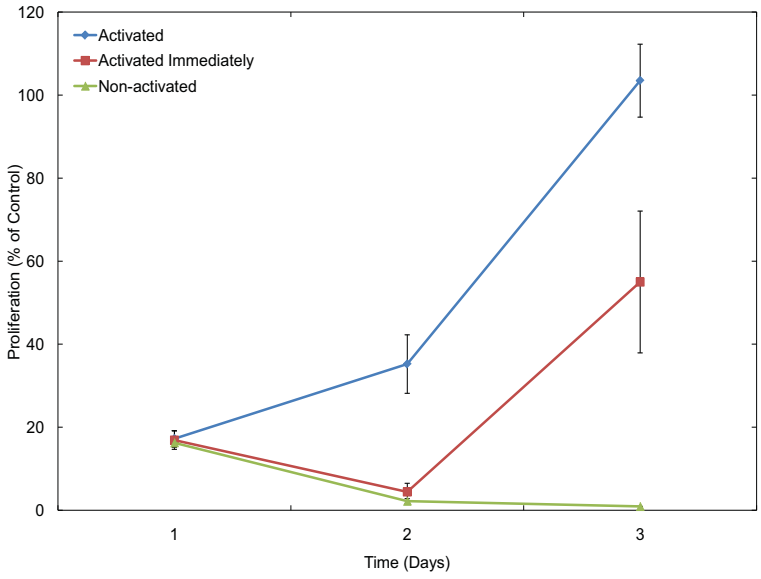

Figure 2.7. PC-3 proliferation on 10:1 PDMS with and without different surface treatments.

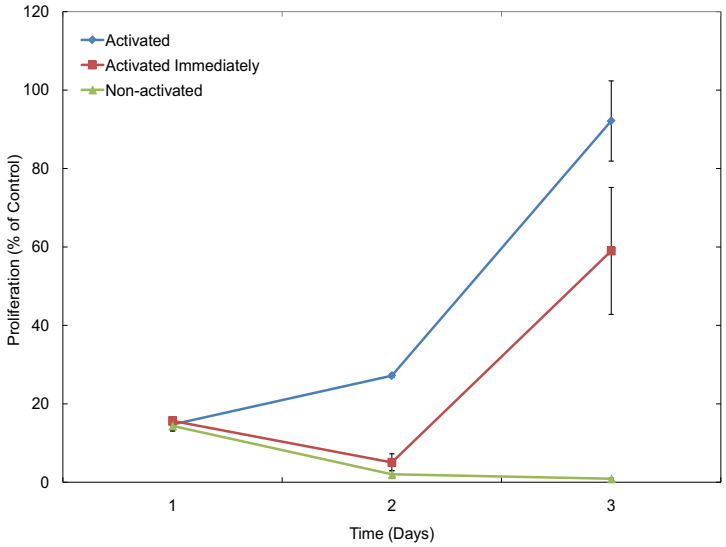

Figure 2.8. PC-3 proliferation on 30:1 PDMS with and without different surface treatments.

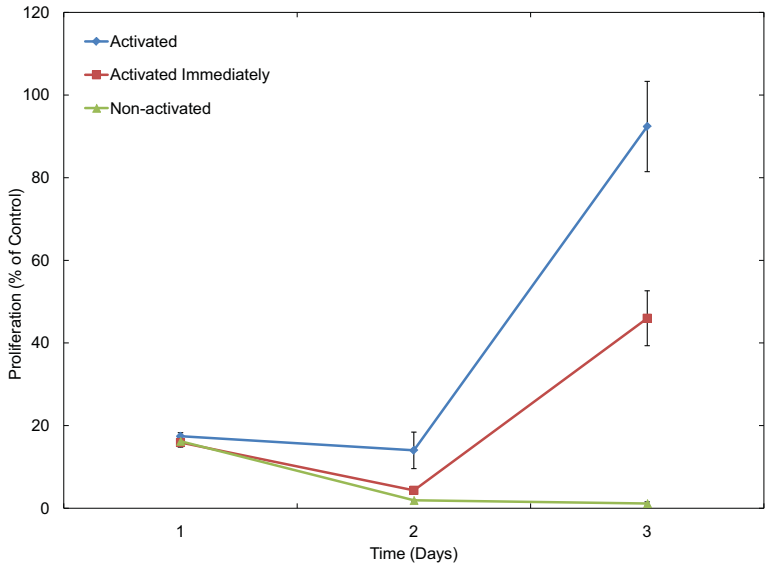

Figure 2.9. PC-3 proliferation on 50:1 PDMS with and without different surface treatments.

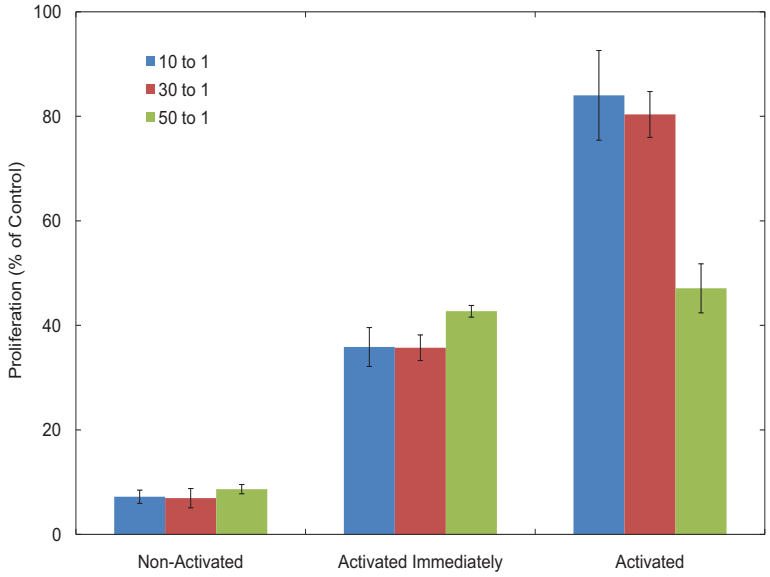

Figure 2.10. HASMC proliferation on 10:1, 30:1 and 50:1 PDMS that has not been activated, immediately activated and activated 24 hrs prior to cell seeding compared to control after 3 days.

(HASMC) cultured in DMEM as shown in Figs. 2.10 - 2.16. As before, the control in this experiment was HASMC cells seeded on traditional 6 well plates in the same culture media. HASMC cell proliferation after 3 days was compared to the control. Using these data, the combination of the PDMS and surface treatment best suited for PC-3 and HASMC culture was determined.

From the results it was determined that non-activated PDMS was insufficient to sustain PC-3 and HASMC's. PDMS base to curing agent ratio did not show any effect on PC-3 growth while 10:1 and 30:1 PDMS when activated were preferred by HASMC's.

Thus the results show that PDMS in some form can be successfully used in tissue culture work. In our proposed design, PDMS structures serve to confine the media and cells creating a microenvironment that can be monitored and analyzed. The microfluidic platform was formed by the temporary or permanent bonding of

PDMS with glass or tissue culture substratum thus the cell growth was on a standard substratum and the PDMS structures did not have any effect on cell growth and proliferation.

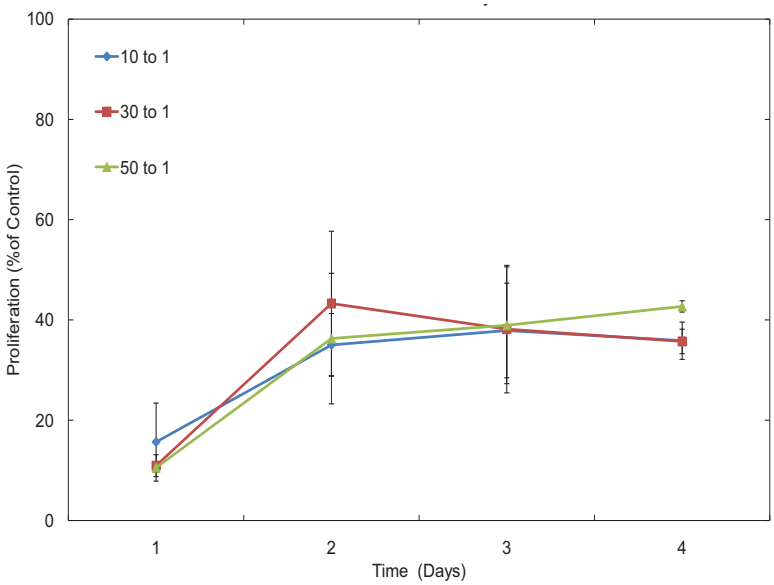

Figure 2.11. HASMC proliferation on 10:1, 30:1 and 50:1 PDMS that has been activated immediately as percentage of control after 3 days.

In summary, different PDMS mixtures were made by mixing 10:1, 30:1 and 50:1 base to curing agent by weight. The three mixtures of PDMS have distinct differences in their physical properties and in their surface wetting characteristics. The various mixtures of PDMS were poured into standard 6 wall plates and allowed to cure. The cured PDMS inside the well plates were treated or activated with the corona arcing electrode. The samples were separated into (1) non-activated, (2) activated not more than 60 minutes before cell seeding and (3) activated 24 hours prior to cell seeding. The control was cell culture on standard well plates. By seeding the same number of cells in each of the experimental conditions, the percentage of cell proliferation was determined. It was concluded that

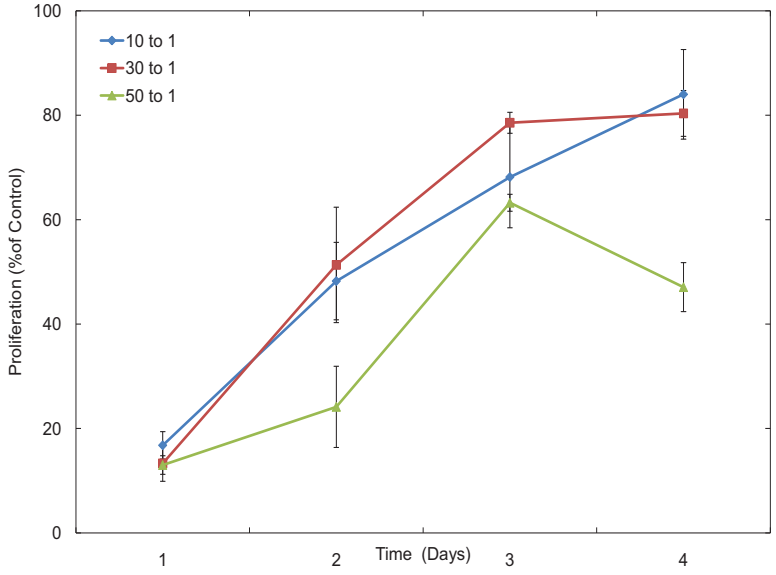

Figure 2.12. HASMC proliferation on 10:1, 30:1 and 50:1 PDMS that has been activated as percentage of control after 4 days.

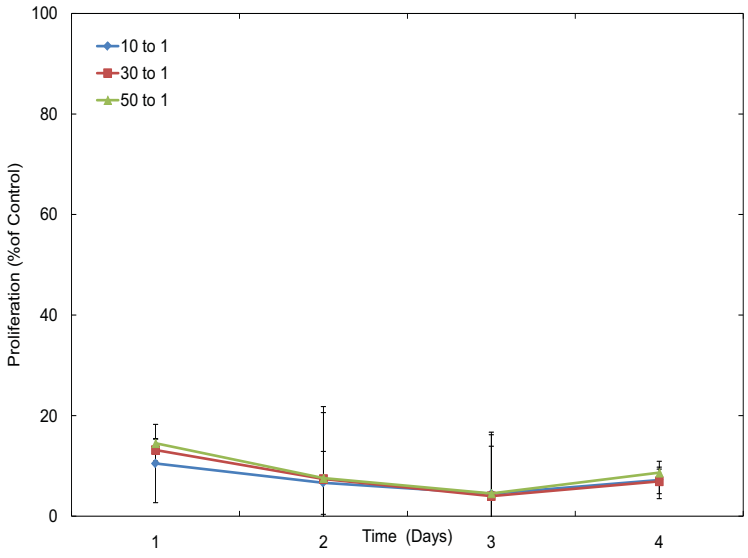

Figure 2.13. HASMC proliferation on 10:1, 30:1 and 50:1 PDMS that has not been activated as percentage of control after 4 days.

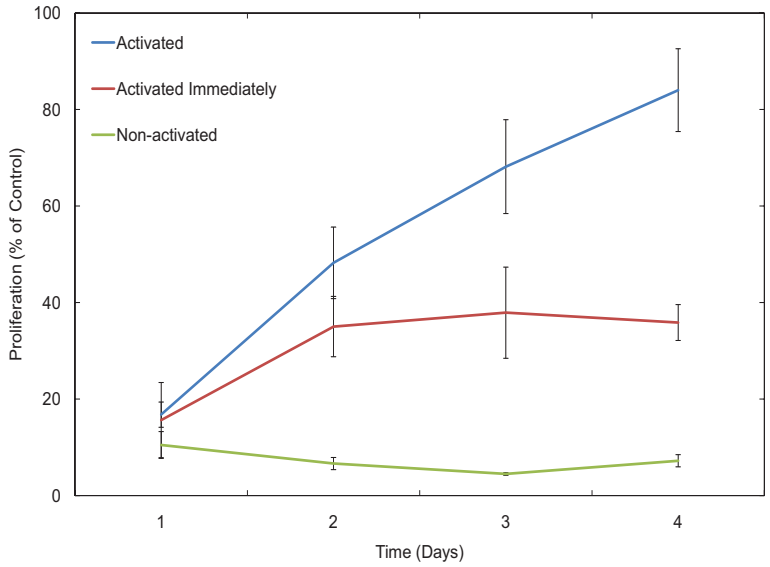

Figure 2.14. HASMC proliferation on 10:1 PDMS with and without different surface treatments.

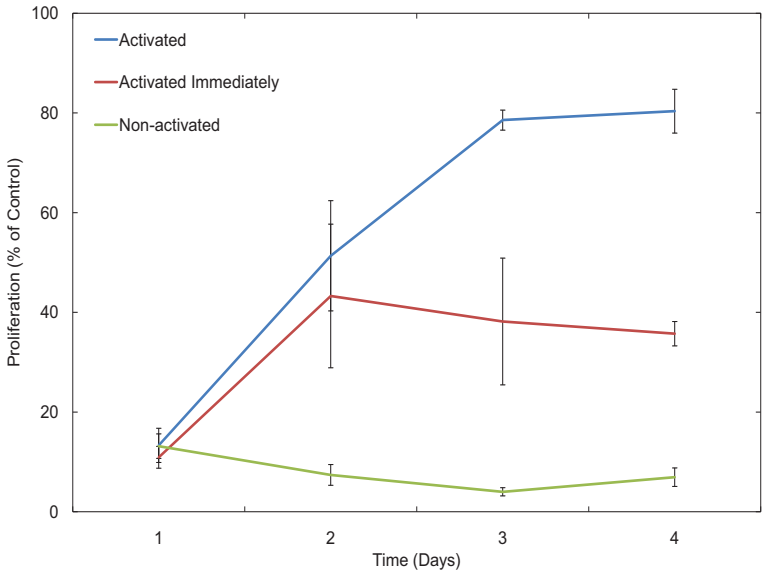

Figure 2.15. HASMC proliferation on 30:1 PDMS with and without different surface treatments.

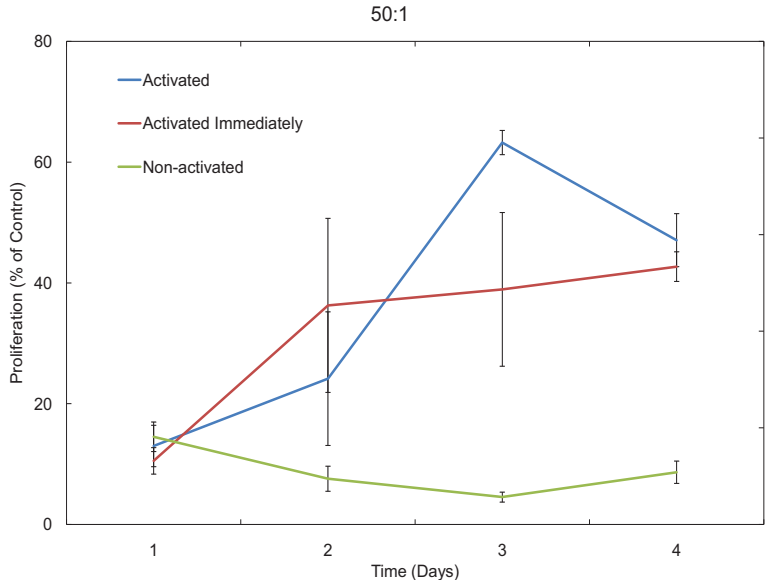

Figure 2.16. HASMC proliferation on 50:1 PDMS with and without different surface treatments.

1. PDMS activated 24 hours prior to cell seeding had highest number of cells
2. non-activated PDMS had the lowest number of cells
3. Changes in the composition of the PDMS did not affect PC-3 cells
4. HASMC's preferred PDMS that was activated 24 hours prior to cell seeding and having the mixing ratios 10:1 and 30:1

Thus, PDMS has the potential to be used as a cell culture substratum. In our proposed design, PDMS forms a superstructure confining the media and the cells on a cell culture substratum as will be discussed in Chapter 4. The cells attach and proliferate on the standard culture plate and conventional cell culture protocols were implemented for the experiments.

CHAPTER 3

DYNAMIC MICROFLUIDIC PLATFORM

We have proposed a PDMS microfluidic device that allows continuous monitoring of the gradients formed and the effects of these gradients on the prostate cancer cells (PC-3). The gradients generated can be controlled by the rate at which the chemokines are introduced into the channels. The fabrication and experimental results of the various experiments conducted to analyze the gradients formed by different flow rates are presented in the following sections.

3.1 Fabrication

A master pattern was first formed by photolithography on a silicon wafer. The pattern was hard baked to prepare it for the next step. The device pattern from the master was transferred onto the PDMS by soft lithography. The following sections describe the process in detail.

3.1.1 Photolithography

The dynamic microfluidic platform consists of a set of serpentine channels connected to three inlet channels and an outlet channel. The height of the channels was maintained 100 μm throughout. The negative-tone resist SU-8-100 (Microchem, MA) was used to create the master on the silicon wafer. The photoresist was spin coated and baked in preparation for photolithography. It was then exposed to UV light, baked and developed. This master on silicon was hard baked at 140°C for 1 hour. The complete process is summarized in Table 3.1.

Table 3.1. Process parameters for SU-8-100 to obtain 100 μm feature height

Process Step	Parameters
Singe the wafer	1 hour at 150°C
Spin coat	500rpm with a ramp of 100 rpm/s. Hold for 5s 3000rpm with a ramp of 300 rpm/s. Hold for 30s
Soft Bake	30m at 65° 45m at 95°C
Expose	32s
Post exposure bake (PEB)	30m at 65°C 45m at 95°C
Develop	10m in developer. Rinse with Isopropylalcohol (IPA)
Hard bake	45m at 150°C

Once the master pattern was created on the silicon wafer, the wafer was placed on a Pyrex® plate and PDMS was poured onto the mold and cured as shown in Fig. 2.1. As the PDMS cured, the patterns were transferred onto the PDMS from the master. The cured PDMS layer was cut and peeled from the silicon wafer. It was then diced and cleaned. Openings were made for the three inlets and the outlet using a luer connector having an inner diameter of 100 μm. The surface of the PDMS was then cleaned using scotch-tape (3M, MN)followed by 20 minutes soak in 75% Ethyl alcohol.

3.1.2 PDMS Bonding

The device was made by bonding the cleaned PDMS die to a clean glass substrate. PDMS was bonded permanently to glass by activating the surface of the PDMS with ionized oxygen in the chamber of a reactive ion etcher (RIE) for 20 seconds. The activated surface was brought in contact with glass forming a permanent chemical bond sealing the contacting surfaces. The permanent bond is required to prevent leaks in the device.

3.2 Design and Analysis

The design of a microfluidic device is based on the fluidic interactions in the micro-scale channels and structures. Fluids consist of molecules that are widely separated and molecular properties such as velocity and density vary. However, in microfluidics the continuum approximation [61] for almost all the properties is valid and holds true for dimensions approaching several molecular diameters. Continuum approach allows analysis of microfluidic flow using the principles governing macroscale fluidics.

In microfluidic devices, the fluid flow is laminar, that is, the Reynolds number (Eq. 3.1) for microchannels is less than 1 [61]. Thus, microfluidic devices with multiple fluidic inputs allow several parallel streamlines of fluid to flow within the microchannels without mixing. In order to create mixing of fluids or turbulent flow, structural designs have to be incorporated in the design to disrupt the parallel streamlines thereby mixing the fluid [62]. In the absence of turbulence or structures causing disruption in flow, the fluid returns once again into a laminar flow pattern in the microchannel. When multiple fluids of different concentrations are mixed, the laminar flow after mixing has a clear concentration gradient formed across the width of the microchannel. For fluids driven under pressure, maximum velocity is at the center of the microchannel and is called Poiseuille flow. The concentration gradient varies equally from center to the edges with the highest concentration located at the center for Poiseuille flow. By varying the velocity with which the various fluids are introduced into the microchannels, gradients of different shapes can be generated [63, 64]. By introducing cells into these microchannels the effect of gradients on cell growth and migration can then be analyzed.

The Reynolds number is directly proportional to the diameter, d. The channel dimensions in the microfluidic devices are in the order of micrometers rendering Re

very small compared to one. The laminar flows lead to simple Poiseuille flow with a parabolic velocity profile with the maximum velocity being at the center of the channel. Laminar flow is required in many microfluidic applications but is a drawback in applications where mixing is required.

$$\mathrm{Re} = \frac{\rho V d}{v} \tag{3.1}$$

where ρ is the density, V is the velocity, v is the kinematic viscosity and d is the channel diameter.

The design presented in this section includes a microfluidic mixer network that allows gradual mixing in stages of the fluids at the input to generate a fluid gradient at the output. The mask design of the device structure is as shown in Fig. 3.1. The device consists of three inlets and one outlet. The two inlets, inlet A and B in Fig.3.1, are connected via connectors and microtubes to a syringe pump allowing introduction of fluids at a controlled rate into the microfluidic device while the third inlet, labeled cell inlet allows introduction of cells. The two inlets lead into a mixing network guiding the fluids towards the cell inlet and finally into an outlet channel. By varying the velocity of the fluid at the two inputs different gradient profiles were generated by the mixing action created in the mixer network. The device is 2 cm (l) x 1.5 cm (w) and 0.7 mm (h). The height of the channels is 100 μm throughout. The mixing was carried out in two stages and the concentration of the fluids was varied from 2 levels at the input to 5 levels at the end of the mixing stage. By varying the velocity of the fluid at the two inputs, different gradient profiles were generated. By introducing cells into this gradient environment, the effect of the gradient on the migration of the cells was monitored and analyzed.

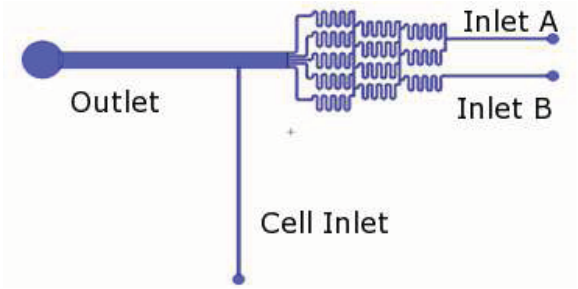

Figure 3.1. Mask layout of microfluidic device.

The analysis of the microfluidic device comprises of determining the mixing of fractions of the fluid entering the channel intersections. for a system having the same flow rate for each of the inputs, all other parameters being same or comparable, it can be assumed that the fluid divides into equal parts at each intersection. Thus, each successive stage in the fluidic network decreases the concentration of the fluid by a known factor and mixes it with the other streams entering the mixing stage. Therefore for a system having n channels in a branched network or order B=n, each channel arriving at a mixing stage is labeled from V=0 to V=B-1 as shown in Fig.3.2 [65,66].

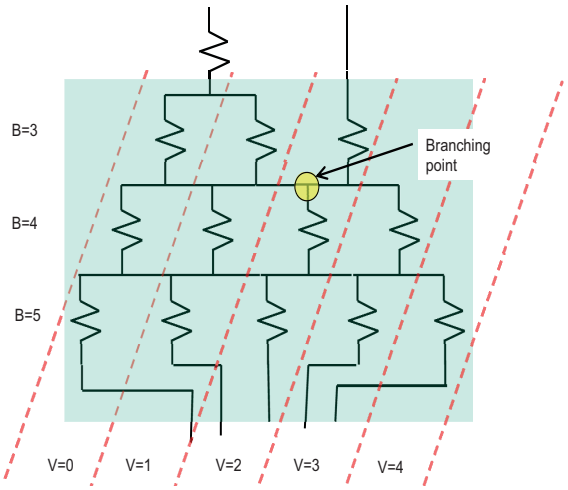

Figure 3.2. The ordering of the branches and channels for a branched network with order B having V=B-1 branches at every intersection or branching point.

The equations determining the quantity and therefore the concentration of the fluids entering a channel at any branching point is shown in Fig.3.3. In order to demonstrate the mixing action, we have used F.D.& C green and yellow colors mixed in cell culture media DMEM as the two input fluids.

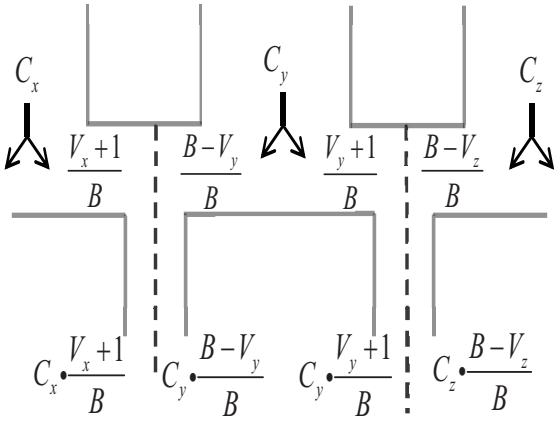

Figure 3.3. Representation of the branch equations determining the concentration of the fluids emerging at any intersection as separate parallel streams. For the streams C_x, C_y and C_z, the equations for the output streams are as shown above.

Using the branch equations, the concentration of the two fluid streams at the branching point shown in the Fig. 3.3 should be equal. This can be seen clearly in Fig.3.4. The two parallel streams mix as they flow further into the channel and the individual colors fade away as a new mixed color emerges towards to end of the "U" shaped mixing structures along the channel. The experiment procedure is explained in section 3.3.

The device was first primed with cell culture media DMEM to ensure the channels were not blocked and to ensure fluid flow was continuous without any air gaps. A 10-ml syringe filled with DMEM was used to prime the mixer device as shown in Fig. 3.5. The two inlets were individually connected via metal tubes and polyethylene

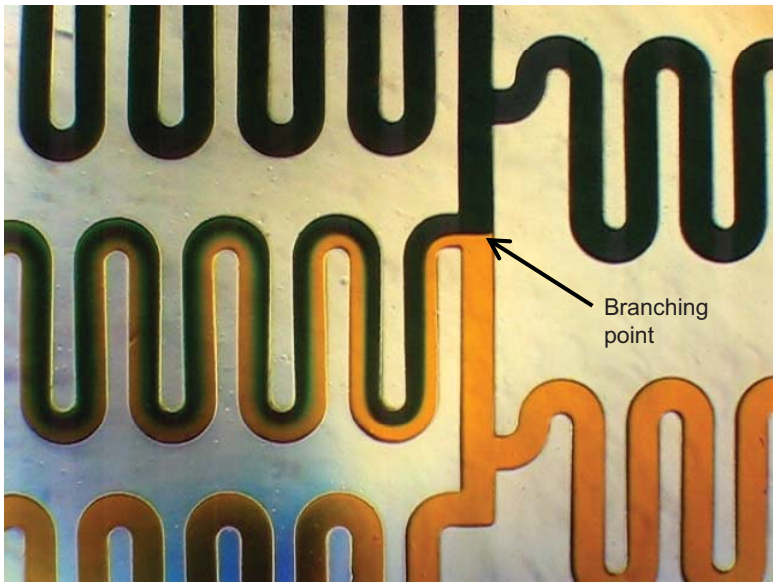

Figure 3.4. The color of the two streams at the branching point shown in Fig.3.2 can be seen to be equal to two streams of distinct colors that mix further along the mixing network to form a new color.

tubing having an inner diameter of 100 μm to a syringe pump (Harvard Apparatus, Holliston, MA) whose flow rate can be incremented in steps of 0.01 μl.

3.3 Experimental Verification of Gradient Formation

To demonstrate the gradient formation, we used equal quantities of F.D & C yellow and green colors mixed with culture media DMEM at the inlets. The two color streams flow into the mixer structure and combine in the outlet channel giving rise to a concentration gradient across the channel. By analyzing the color gradient, and assuming green represents hundred percent concentration and yellow represents zero percent, the gradient profile for the colors formed across the channel can be graphed as percentage of green.

For flow rates of 2, 3, 6, 8, 10 μl/min, images were taken every 5 minutes for 35 minutes and each of the images were analyzed. Pictures were captured using a

Nikon microscope attached to a Canon powershot digital camera. We used Matlab to analyze the color information in each pixel and graph the gradient profile along a line across the width of the channel. As can be seen from Fig. 3.6 the top most part of the outlet channel was green while the lower most was yellow with shades between green and yellow towards the center where the mixing was highest.

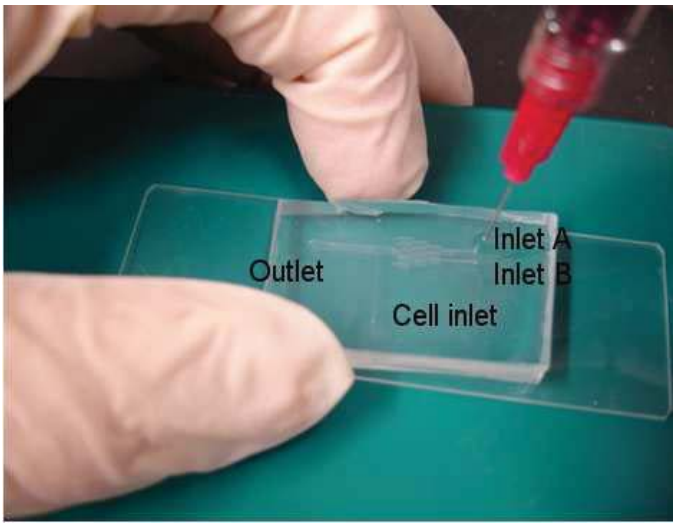

Figure 3.5. Bonded microfluidic device being primed by a 10-ml syringe.

As previously mentioned, in order to demonstrate the gradient formation in the microfluidic device, we used color (F. D & C green and yellow) infused cell culture media in the channels. By taking time -lapsed pictures under a microscope of the media in the channels and the diffusion, the gradient established over time for different flow rates was determined. Flow rates of 2, 3, 6, 8 and 10 μl/min were used and images were taken at 5-minute intervals for an hour. The fluidic gradients formed were found to be repeatable and easily controlled. The gradient profile for 2 μl/min monitored at 5-minute intervals up to 35 minutes is shown in Fig. 3.7.

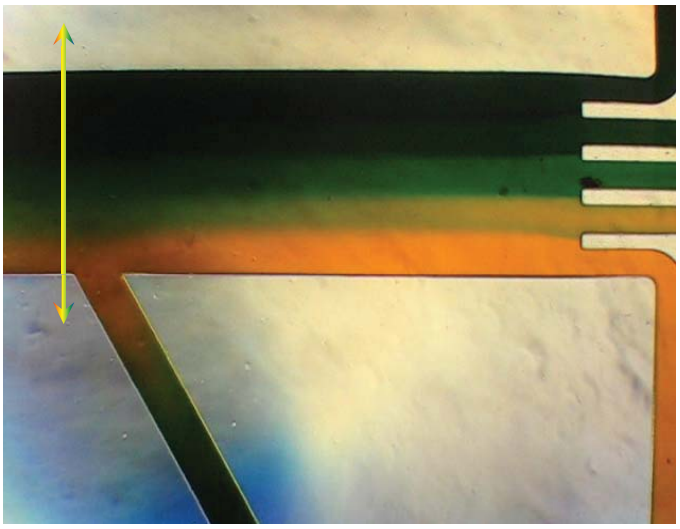

Figure 3.6. The gradient formed at the outlet channel.

Similarly, gradient profiles for 3, 6, 8 and 10 μl/min monitored at 5-minute intervals is shown in Figs. 3.8, 3.9, 3.10 and 3.11, respectively. From the gradient profiles, it appears that the gradient starts at a higher level and gradually falls off. This may be explained by understanding the experimental setup. In order to ensure that the image of the gradient being captured was a result of the fluid flow being used, after each experiment set, the syringe pump was switched off and the color gradient was allowed to diffuse. Thus, each dataset started similarly with a diffused pattern and when the syringe pump was turned on, at the onset of flow in the outlet, the gradient level appears higher before equilibrium is reached.

Flow rates of 3, 6, 8 and 10 μl/min have similar gradient profiles. The difference was in the time taken for diffusion to occur and the distance over which diffusion occurs. As the flow rate increased, the tendency towards diffusion decreased. The force of the fluid tended to keep the different gradients formed by mixing separated until the force gradually diminished along the length of the outlet channel and diffusion took precedence. The diffusion was observed further down the channel towards

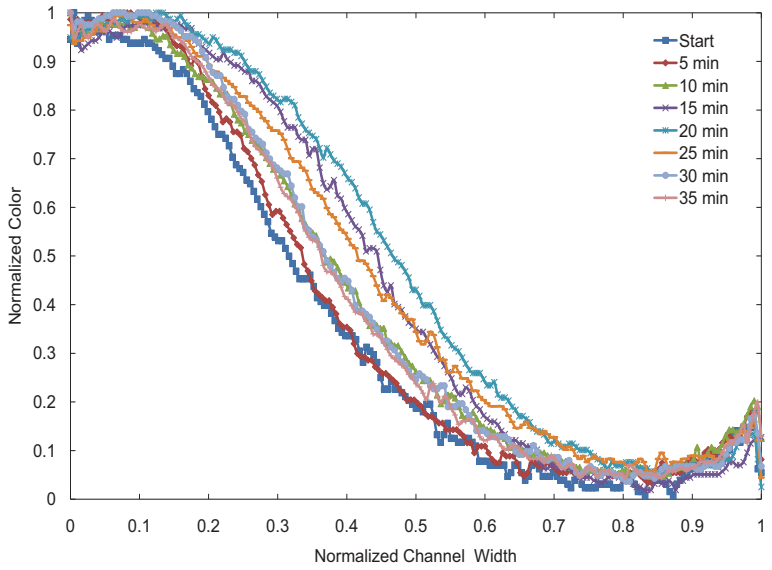

Figure 3.7. Gradient profiles for 2 μl/min over time.

the outlet as the flow rate increased. In the region before the diffusion pattern was observed, the five streams of fluid flowing into the outlet channel remained separated. In order to obtain the response of the cells in a gradually changing gradient environment, the cell inlet was placed far along down the outlet channel where diffusion took precedence. The gradient profiles were all taken in the area near the cell inlet and across the width of the channel.

The gradient profiles for different flow rates of 2, 3, 6, 8 and 10 μl/min characterized at 5 minute intervals are as shown in Figs. 3.12 - 3.19. It was seen that after 35 minutes, the shape of the gradient formed by the different flow rates were similar in profile but the distance over which pure green or pure yellow was retained was different i.e., the length over which the five streams remained separated varied. In order to analyze the color gradients, all the images were taken at the very beginning just after the flow was started but after enough time had been allowed for the pre-existing fluids to diffuse completely and have no more flow. This ensured that

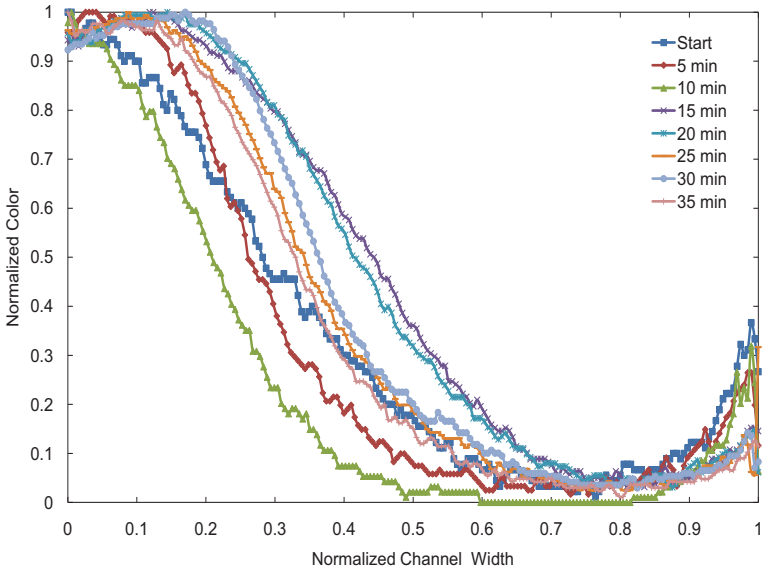

Figure 3.8. Gradient profiles for 3 μl/min over time.

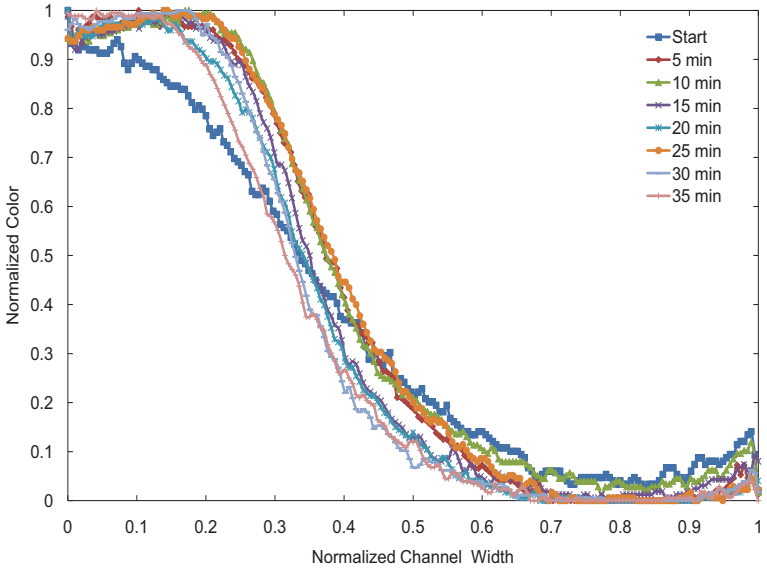

Figure 3.9. Gradient profiles for 6 μl/min over time.

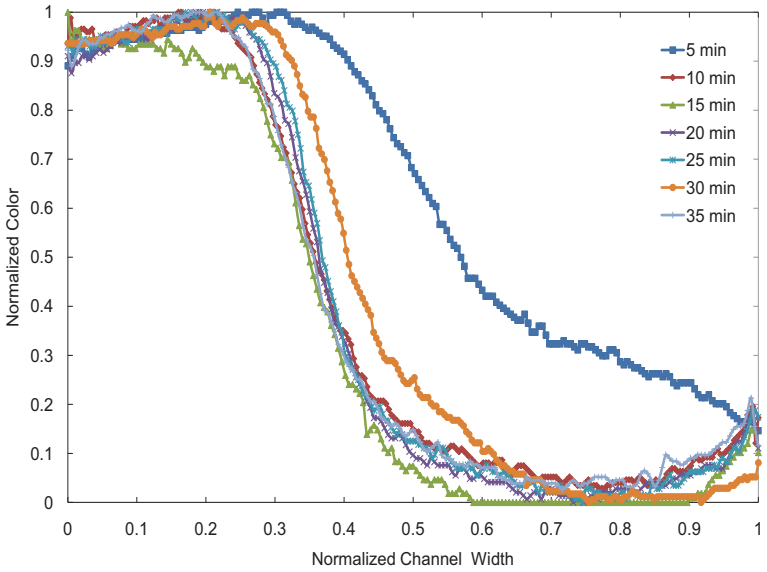

Figure 3.10. Gradient profiles for 8 μl/min over time.

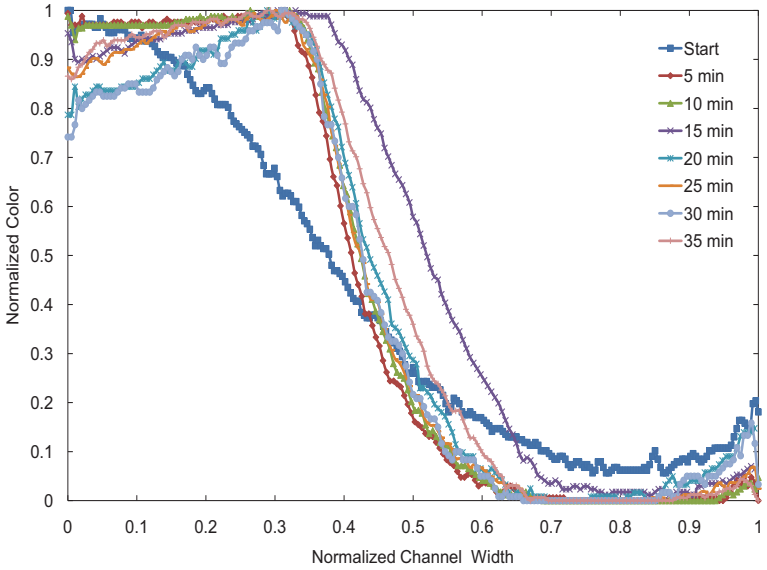

Figure 3.11. Gradient profiles for 10 μl/min over time.

all the starting point for the different flow rates tested were the same. The gradient measured at the beginning of every flow rate is shown in Fig. 3.12.16. It can be seen that the gradient profiles are very similar indicating that the diffusion that had occurred was same in each and every case. It was observed that at higher flow rates the distance over which the separate streams remain undisturbed with a step-like profile in cross-section was longer and had minimum diffusion. Similarly, at lower flow rates diffusion took a higher precedence and the fluid streams were blended into a gradual gradient change instead of a step-like profile [21, 25, 28]. It can also be inferred that in order to maintain a gradient condition within the channels, the fluid flow should be maintained constant. Any point along the channel will exhibit the same gradient profile only as long as the flow rate remains unaltered. When the flow was cut-off there was diffusion mixing between the flow streams.

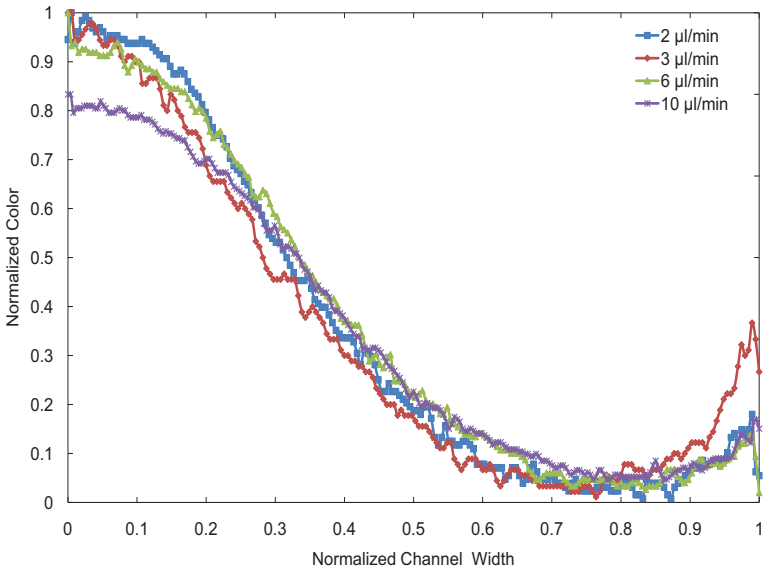

Figure 3.12. Gradient profiles at start of fluid flows of 2, 3, 6, 10 μl/min.

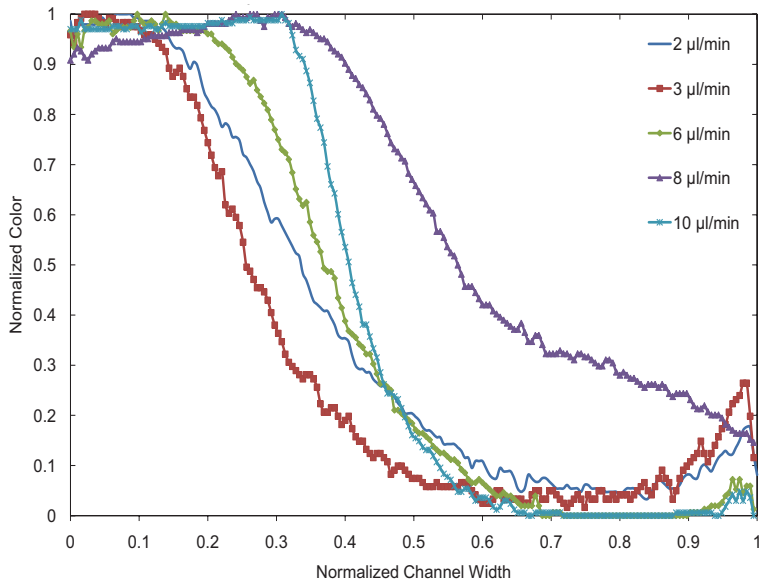

Figure 3.13. Gradient profiles after five minutes from start for fluid flows of 2, 3, 6, 8, 10 μl/min.

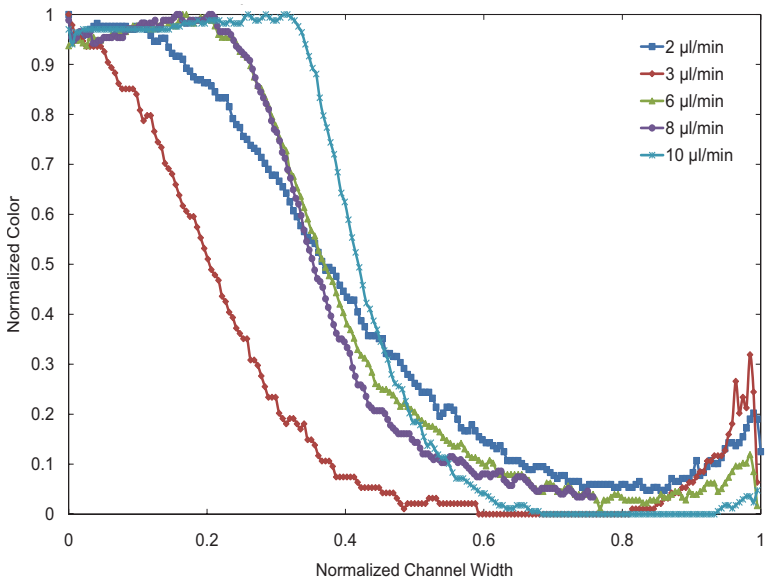

Figure 3.14. Gradient profiles after ten minutes from start for fluid flows of 2, 3, 6, 8, 10 μl/min.

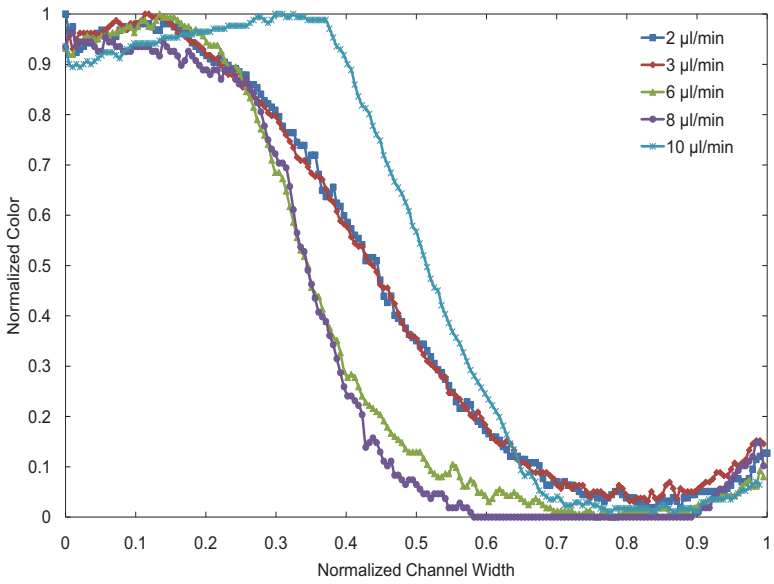

Figure 3.15. Gradient profiles after fifteen minutes from start for fluid flows of 2, 3, 6, 8, 10 μl/min.

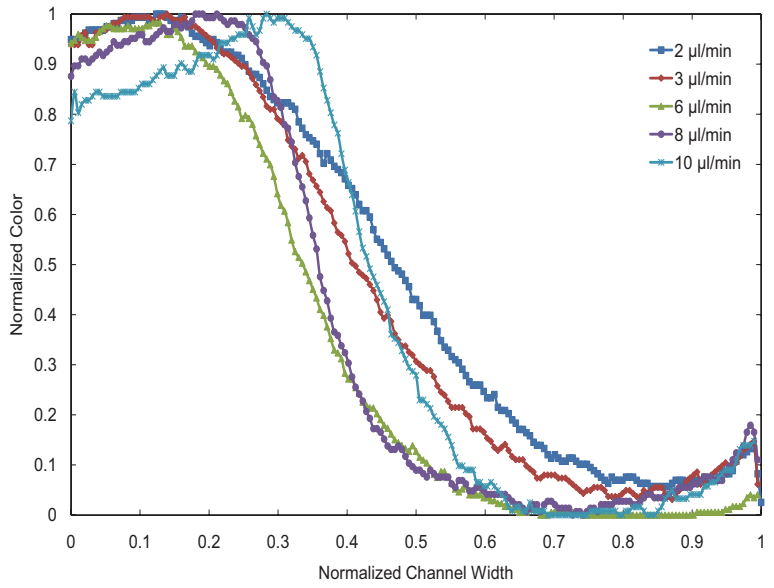

Figure 3.16. Gradient profiles after twenty minutes from start for fluid flows of 2, 3, 6, 8, 10 μl/min.

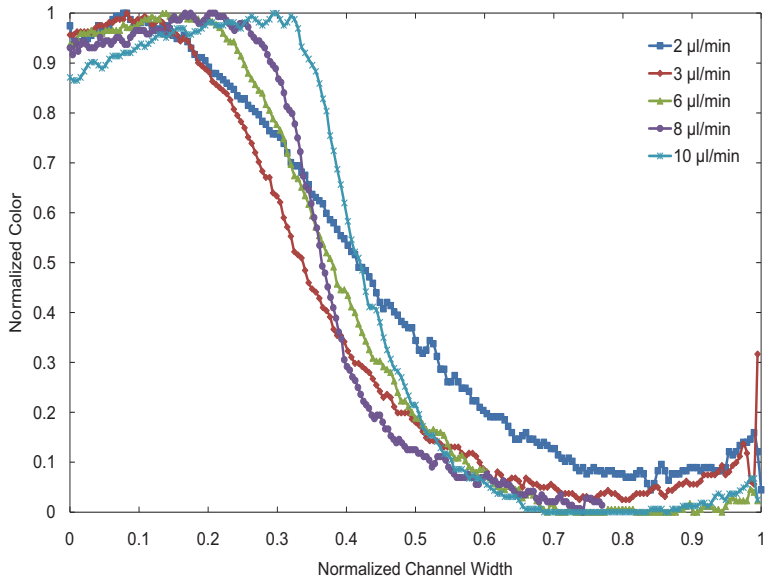

Figure 3.17. Gradient profiles after twenty-five minutes from start for fluid flows of 2, 3, 6, 8, 10 μl/min.

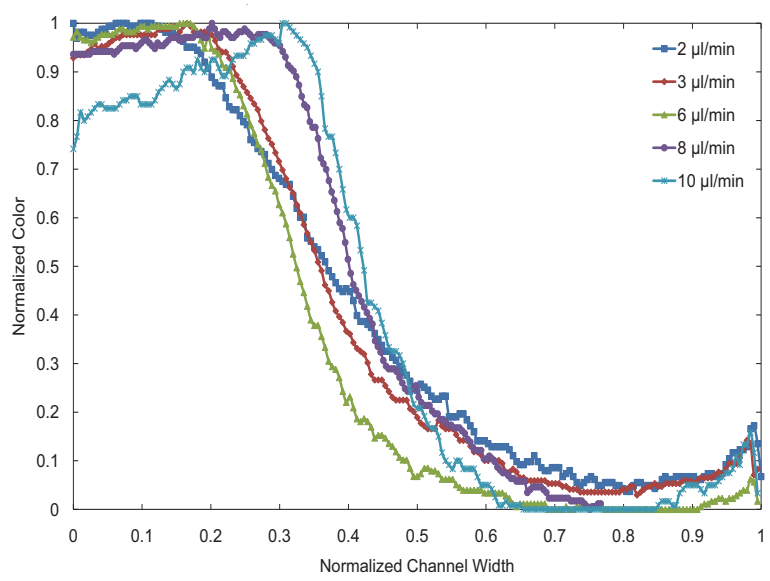

Figure 3.18. Gradient profiles after thirty minutes from start for fluid flows of 2, 3, 6, 8, 10 μl/min.

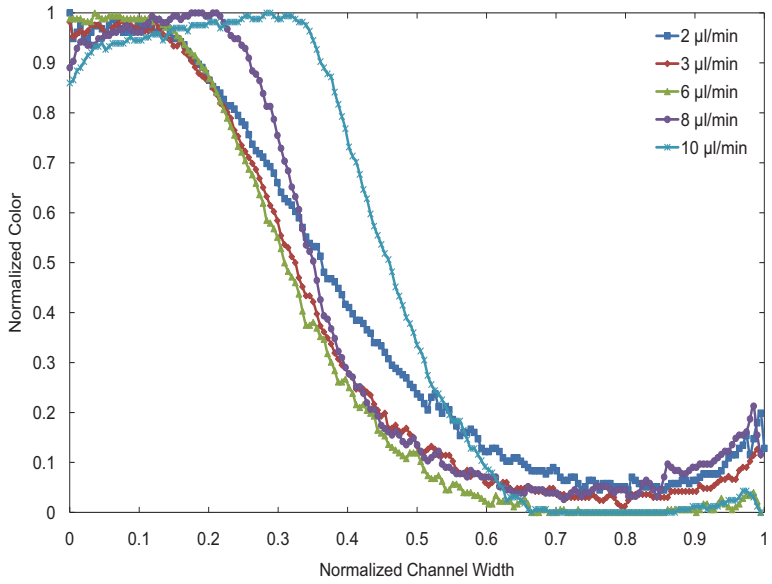

Figure 3.19. Gradient profiles after thirty-five minutes from start for fluid flows of 2, 3, 6, 8, 10 μl/min.

Furthermore, cells introduced in the cell inlet were monitored under the influence of different flow rates. The cells were seeded from the cell inlet and allowed to attach for 2 hours. The microfluidic device was then connected to the syringe pump with cell media and vascular endothelial growth factor, VEGF in inlets A and B respectively. The cells were monitored at the outlet as shown in Fig. 3.20. The flow rate of the fluids was varied from 2 μl/min to 20 μl/min. It was found that for flow rates above 2 μl/min, the cells were detached by the fluid force and tended to float away with the media. Thus, in order to use the microfluidic device, the flow rate would have to be maintained less that 2 μl/min.

3.4 Challenges

The PDMS microfluidic device configured to provide fluid mixing leading to a gradient across the outlet channel has been fabricated and demonstrated. By varying the flow rate of the media at the inlets, different gradient profiles were generated.

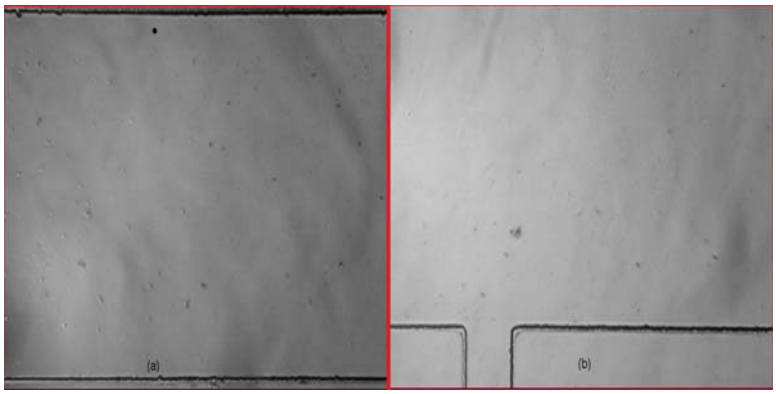

Figure 3.20. Prostate cancer cell in the cell outlet (a)After seeding and (b)After VEGF gradient formation at 3 μl/min flowrate.

A flow rate less than 2 μl/min was determined to be of interest for monitoring cell migration in the presence of chemokines since the cells in the channels are not affected by the flow rate. At flow rates above 8 μl/min, the gradient steps are well defined but turbulence was observed. Also, the cells tend to flow away with the media at a higher flow rate. There was also no significant difference in the gradient formed after 35 minutes that is, the gradient profiles observed remained unaltered after 35 minutes and had similar profiles for all the flow rates tested.

There were also a few difficulties in monitoring the cells in the channels:

1. The entire channel length could not be imaged in a single field of view without moving the device under the microscope
2. The duration of cell attachment prior to fluid flow needs to be determined
3. The quantity of the chemokine in the fluid and the resulting gradients in order to influence the cell migration needs to be well established
4. In order to study the effect of the gradient on the cells, the chemokine flow would have to remain constant over extended periods of time. This would increase chemokine consumption and costs related to testing

5. Once the fluid flow was stopped, the sharper gradient profiles were lost due to diffusion

In order to address these concerns, an alternative design has been proposed and its design, experiments and results are presented in the following chapter.

CHAPTER 4

STATIC FLOW DEVICE

4.1 Introduction

The mixing network with continuous flow generates gradients under sustained flow. However, over extended periods of time, it increases chemokine consumption. It has also been reported that there are shear stresses in the microfluidic channels with flow and could affect the cells present in these channels [67, 68].

In order to assess cell migration in the presence of gradients or chemoattractants, several devices have been proposed and used. These include Boyden chamber or transwell assay [69], under-agarose assay [70], Zigmond chamber [71], Dunn chamber [72], and micropipette assay [73]. The Boyden chamber provides means to measure chemotaxis in terms of the number of cells that migrate across a barrier usually a porous membrane between two chambers containing reagents in solution. The disadvantage of this method is that it provides only an end-point measure of number of cells without any information regarding cell migration. In the under-agarose assay, agarose gel with holes punched in it for the cells and chemoattractant on a glass coverslip is used to monitor cell migration. This method provides cell migration information but it cannot be quantified as the path of the cell is not defined and can be random. In the Zigmond and Dunn chambers, cells migrate across two wells separated by a bridge with a gradient between them on glass [32, 74]. There is a cover slip that encloses the chambers and provides a narrow gap in which the cells need to traverse. The effective volume of the chambers plays a very important role in maintaining a steady gradient across the bridge. Recently optical assays with

gradients across microgrooves or patterns in silicon for neutrophils chemotaxis has been reported [75]. Silicon however is not considered to be biocompatible.

A microfluidic device that uses static fluidic flow was proposed by Campenot [76, 77] in 1977. In this method, a culture dish was coated with collagen and parallel lines spaced 300 μm apart were scratched in the collagen. Silicone grease was used to seal a three chamber teflon atachment to the culture plate. Neurites grown in this set-up outwards from one compartment to the remaining two and were aligned parallel to the scratches. A modified Campenot chamber was developed by Ivins et al. that reduced the distance of the parallel grooves from 300 to 150 μm and used a glass coverslip attached to a hemisected Teflon tube. PDMS was used for the attachment and the apparatus with silicone vacuum grease was placed on a tissue culture dish. Provided that the distance between the glass coverslip and the culture plate was narrow enough, neurites extended across the vacuum grease barrier. Irimia et al. have proposed a microfluidic device that allowed observation of cellular chemotaxis and localized treatment of the polarized ends of a cell in a convection free, stationary gradient environments that were separated by an array of channels [78]. A three channel microfluidic chip with stationary linear gradient fabricated by laser etching of a nitrocellulose membrane placed between a polycarbonate manifold and a Borofloat glass was proposed by Diao et al. [79]. A similar device has been proposed by Shamloo et al. [80]. Anne Taylor et al. have proposed a multicompartment device for neuronal cultures [47] using PDMS and glass or tissue culture dish. The compartments are separated by micron-size grooves across which the growth of neurites was characterized. Our proposed device is based on the same principles as the aforementioned devices and provides means to monitor cell migration and quantify the results along with continuous monitoring abilites.

In order to overcome some of the drawbacks of our previously proposed fluidic mixer device, a new device incorporating the principles of conventional migration assays and other linear stationary gradient generation devices has been designed, fabricated and tested. The most important advantage of the newly proposed device is that a continuous fluid flow is not required to analyze cell migration.

4.2 Design

The device configuration consists of a series of parallel narrow microchannels (60 in number) that connect two growth chambers and was fabricated by soft lithography of PDMS. The growth chambers in turn have two inlets or reservoirs each that can be interfaced to external fluidic components. The dimensions of this prototype design were 2.4 cm (l) x 2.4 cm (w) x 100 μm (h). The microchannels connecting the chambers were 1000 μm (l) x 25 μm (w) x 10 μm (h). The PDMS microfluidic devices were fabricated according to the processes described in section 2.3. The thickness of the PDMS device was controlled and maintained at 6 mm. The cured devices were peeled from the silicon substrate and diced. Using a 5 mm tissue punch (Harris Unicore) holes were punched in the PDMS device to form four reservoirs, two each for the cell side and chemoattractant side. Having a pair of seeding wells ensures easier device priming, removal of air gaps and helps in equilibrating the sides. The dies were cleaned according to procedures described in section 2.3.2.1 and was soft bonded to standard 60 mm culture dishes (Corning^{TM} 60 mm TC-Treated Culture Dish). Such a PDMS microfluidic prototype device bonded to a culture dish is shown in Fig. 4.1. The inset shows the microchannels connecting the two growth chambers in detail.

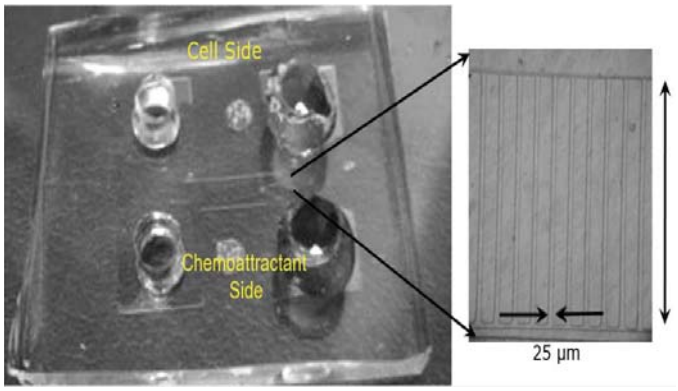

Figure 4.1. The prototype PDMS microfluidic platform soft bonded to a tissue culture dish. Inset: Microchannels connecting the cell side and chemoattractant side.

4.3 Fabrication

A master pattern was first formed by photolithography on a silicon wafer. The pattern was hard baked to prepare it for the next step. The device pattern from the master was transferred onto the PDMS by soft lithography. The following sections describe the process in detail.

4.3.1 Photolithography

The static microfluidic platform consists of a set of parallel channels 10 μm (w) x μm (h) x 1000 μm (l). The two reservoirs on each side of the channels are in turn connected by a chamber that is 4 mm (w) x 100 μm (h) x 16 mm (l). Thus, a two step lithography is required to create the master with two different heights. The negative-tone resists SU-8-100 and SU-8-10 (Microchem, MA) were used to create the master on the silicon wafer. In the first step, the 10 μm high patterns of the channels were created. In order to prevent alignment problems that may arise due to the thicker photoresist deposited on the patterned 10 μm layer, a two step process to create the 100 μm was adopted. The master pattern developed on silicon was hard baked at 140°C for 1 hour. The complete process is summarized in Table 4.1. Once the

Table 4.1. Process parameters for SU-8-100 and SU-8-10 to obtain 10 μm and 100 μm feature heights, respectively

Process Step	Parameters
Singe the wafer	1 hour at 150°C
Spin coat	500rpm with a ramp of 100 rpm/s. Hold for 5s 3000rpm with a ramp of 300 rpm/s. Hold for 30s
Soft Bake	2m at 65° 5m at 95°C
Expose	12s
Post exposure bake (PEB)	1m at 65°C 2m at 95°C
Develop	3m in developer. Rinse with Isopropylalcohol
Spin coat	500rpm with a ramp of 100 rpm/s. Hold for 5s 3000rpm with a ramp of 300 rpm/s. Hold for 30s
Soft Bake	30m at 65° 45m at 95°C
Expose	32s
Post exposure bake (PEB)	30m at 65°C 45m at 95°C
Develop	10m in developer. Rinse with Isopropylalcohol
Hard bake	45m at 150°C

master pattern was created on the silicon wafer, the wafer was placed on a Pyrex® plate and PDMS was poured onto the mold and cured as shown in Fig. 2.1. As the PDMS cured, the patterns were transferred onto the PDMS from the master. The cured PDMS layer was cut and peeled from the silicon wafer. It was then diced and cleaned. Openings were made for reservoirs using a 4 mm Harris Uni-core punch. The surface of the PDMS was then cleaned using scotch-tape (3M, MN) followed by a 20 minute soak in detergent, rinsing in distilled water and finally a 20 minutes soak in 75% Ethyl alcohol. The PDMS dies were then placed in a tissue culture hood under UV light for at least 20 minutes.

4.3.2 PDMS Bonding

The device was made by soft-bonding or temporary bonding of the PDMS to standard tissue culture plates (100 mm Corning TC-Treated Culture) inside a tissue culture hood to prevent contamination.

4.4 Analysis of the Static Flow Microfluidic Platform

The fluidic system in which there is no flow tends to have diffusion. Diffusion is a stochastic process in which the molecules move from region to region driven by random thermal motion of particles. Microfluidic devices have a combination of diffusive transport and convective flow of the bulk fluid. In order to compare the importance of each in a system, Sherwood number defined in Eq.4.1 is used. It is a dimensionless number that represents the ratio of the convective mass transfer to diffusive mass transfer. Sherwood number is defined as

$$Sh = \frac{kd}{D} \tag{4.1}$$

where k is the mass transfer coefficient, d is the characteristic length of the system such as channel diameter and D is the diffusion coefficient. In macro-scale systems, Sh is high resulting in convective transport. For microfluidic systems, Sh is low as it is directly proportional to d which is of the order of micrometers leading to diffusion taking precedence. The simplified mass transfer equation below can be used to estimate the diffusive transport without flow.

$$\frac{\partial C}{\partial t} = D\frac{\partial^2 C}{\partial x^2} \tag{4.2}$$

For a system with stationary fluid having a concentration C^* at all time t at a given location, provided that there is no other source of fluid interaction except diffusion, the concentration at time t will be $C^*/2$ at a distance $\sqrt{Dt}$ from the starting point. The concentration will be C^* at a distance $4\sqrt{Dt}$ making diffusion significant up to this point. The diffusion coefficient D for polymers and proteins is of the order of ˜$10^{-7} cm^2/s$. The time and distance over which diffusion remains significant is 10 seconds and 40 μm, respectively. At double that distance that is, at $8\sqrt{Dt}$, the concentration is further reduced to $10^{-8}C^*$ [61]. The profile for such a diffusion oriented system is shown in Fig.4.2.

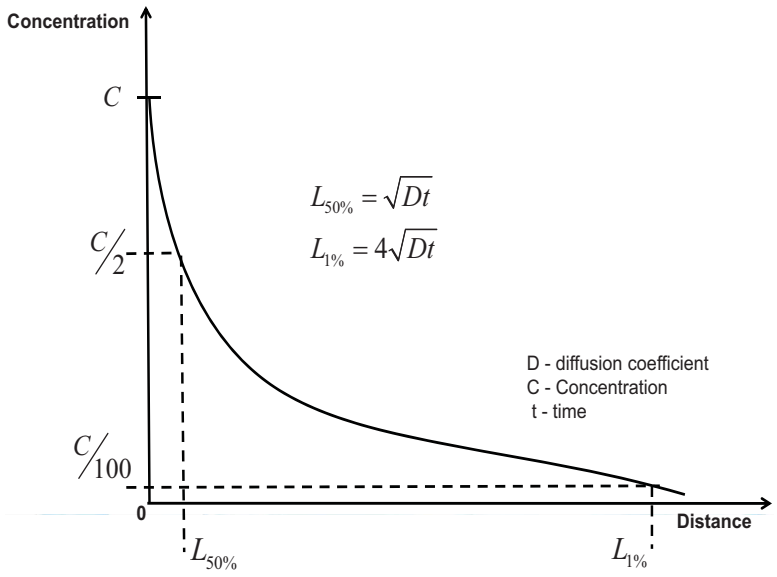

Figure 4.2. The diffusion profile for a system governed by diffusion alone and having a stationary liquid system.

In order to demonstrate that the concentration of the fluids in the static flow device was constant and remained dependant on diffusion alone, growth media mixed with F. D & C green was introduced on cell side and growth media with F.D & C yellow was introduced on the serum side of the device and allowed to diffuse.

The device was observed for over 24 hours. There was mixing of the two colors in the channels until the convection flow from the initial introduction of the fluids diminished after which the gradient was maintained and equilibrium was reached. As can be seen from Fig. 4.3, the two sides of the device are separated by the channels and provide a platform to monitor cell migration. The device effectively separates the cell and media containing the reagents as expected from theory. By monitoring the movement of the cells in the channels, the response of the cell to different chemoattractants was determined.

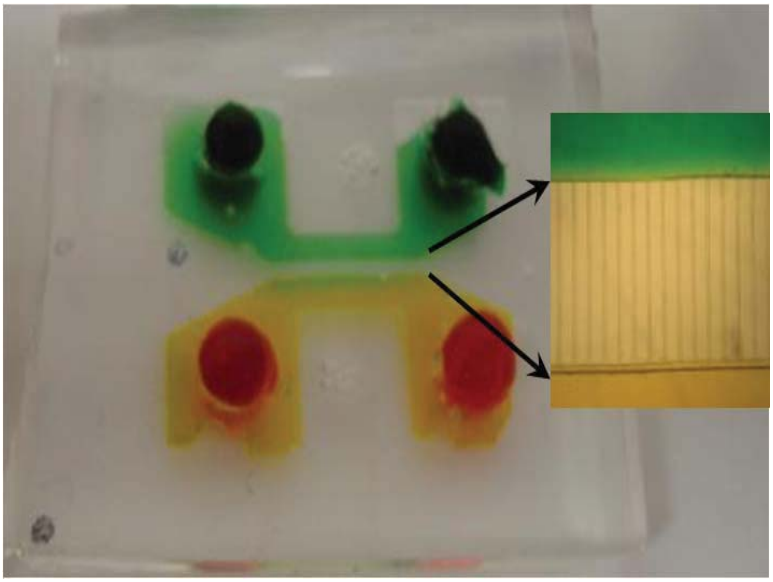

Figure 4.3. Prototype device with F.D & C green and yellow color infused culture media on cell side and chemoattractant sides of the device. Inset: Color mixing in the channel.

This prototype design has several advantages over the mixer network introduced earlier. The amount of the reagent used in the chemoattractant side was reduced considerably. The capacity of the growth area and the seeding wells combined together on one side of the device totals 200 μl. For the experiment, the device was first

primed using cell culture media (refer Appendix A). After ensuring that there was no air gap, the media from one side of the device was removed and replaced with 200 μl of cell suspension with a predetermined number of cells. After allowing for cell attachment, typically, 4-24 hrs, the media from the other side of the device was removed and replaced with media containing the reagent under test. The side on which the cells were introduced was marked as the cell side and the reagent was termed the chemoattractant side. By monitoring the cells and their migration through the channels at regular intervals, the migration rate, cell number and cell count was obtained. The images were taken using a Nikon Diaphot phase-contrast inverted microscope with a UV light source (HB-10101AF, Nikon) attached to a Nikon Coolpix 4500 digital camera.

4.5 Cell Migration Analysis

The protocol developed for using the prototype device allowed introduction of chemoattractants that developed a gradient environment across the microchannels connecting the two identical halves of the device. The cells were allowed to attach before the chemoattractants were introduced and the cell migration on the culture dish substratum was monitored over time. The device dimensions, mainly the microchannel length served as a guiding pathway for the cells enabling monitoring and measuring cell migration in real time. Allowing the cells to attach to the substratum before introduction of chemoattractants provided an environment analogous to physiological conditions. The following section explain the experiment methodology.

4.5.1 Cell Culture and Seeding Protocols

The microfluidic devices need to be prepared before the experiment. This was achieved by priming the devices with media and ensuring that there were no air

bubbles or blockages in the channels of the device. In order to prime the device, 100 μl of the appropriate media was pipetted into one of the reservoirs or wells. Using the broader side of a 20 μl pipette tip with the tip connected to a vacuum pump, the media from the reservoir was drawn into the channels and into the second reservoir on the same side of the device. After covering the third reservoir, media was drawn through the channels from the fourth reservoir. The devices were then checked under a microscope to make sure the channels were clear of any blockages or air bubbles. The devices were then placed in an incubator until the cells were prepared.

4.5.2 Cell Culture

The cell lines used in the experiments were red fluorescent protein (RFP) expressing human prostate cancer PC-3 line (PC-3R), green fluorescent protein (GFP) expressing lung-metastasized prostate cancer (PC-3-ML) cells and normal prostate epithelial cell line (PZ-HPV-7).

1. The cells were all cultured and maintained under 5% CO_2 atmosphere at 37°C. PC-3R cells were cultured in T-media (Invitrogen) supplemented with 5% fetal bovine serum (FBS), 100U/ml penicillin and 100 μg/ml streptomycin
2. PC-3-ML cells were cultured in RPMI 1640 (Cellgro) supplemented with 5% FBS, 100U/ml penicillin and 100 μg/ml streptomycin
3. PZ-HPV-7 cells were grown in PrEGM serum-free media (Clonetics) with 100U/ml penicillin and 100 μg/ml streptomycin

These cells were purchased from American Type Culture Collection (ATCC, Manassas, VA).

To prepare the cells for testing in the devices, cells in exponential growing condition were trypsinized. The cell suspension was placed in the incubator for 5 minutes and centrifuged to remove the trypsin containig media. The cells were re-

suspended in appropriate media and counted. Using the cell count obtained from the hemocytometer, cell suspension with the required number of cells was obtained by diluting in the appropriate media.

4.5.2.1 Cell Seeding

Cell suspension was prepared as explained earlier. The priming media present in the reservoirs on the cell side was removed carefully. Immediately, using a pipette, 100 μl of the cell suspension was introduced into the cell side reservoir(s). The seeded cells were allowed to attach to the substratum and grow for an additional 4-24 hours before the chemoattractant to be tested was introduced on the chemoattractant side of the devices. After 24 hrs, the media from all 4 wells was removed and 100μl of appropriate growth media was added to the wells on the cell side of the device, while 100μl growth media containing the chemoattractant to be tested was added to the wells on the chemoattractant side. In order to minimize the evaporation of the media in the devices, sterilized PBS was added around the PDMS device attached to the culture plate.

Precautions were taken to ensure that there was no contamination or cross-contamination. All the pipette tips used were sterilized and all the processes were carried out in a tissue culture hood.

4.5.3 Migration Analysis

The static flow platform was used to monitor the migration of normal human prostate cells (HPV-7). After the devices were primed, each of the cell side wells was filled with 2000 cells in 100 μl PrEGM. After 24 hrs, the chemoattractant side was replaced with PrEGM containing 5% FBS. Time-lapse images of HPV-7 cells in response to 5% FBS in PrEGM showed that the cells migrated into the channels and

began moving across the channels. The length of the channel was used to determine the distance the cells migrated over each 24 hr interval over which images were taken. The images were captured at 40X to show the overall cell distribution and at 200X for cell migration analyses. Once the images were obtained, the location of the cell within the channel and its distance from the cell side was determined by measuring the pixels using GIMP. First, the number of pixels x, representing the 1000 μm length of the channel was found. The number of pixels y, representing the distance from the starting point of the channel on the cell side to the leading edge of the cell was found. The actual distance, d of the cell was determined by using the following equation

$$d = \frac{y}{x} \times 1000 \tag{4.3}$$

The pixel lengths were determined using GIMP as shown in Fig. 4.4. The pixel distance y represents the actual length of the channel which from design is 1000 μm. The pixel distance x represents the cell location and the actual distance was determined using Eq.4.3. For example, the pixel distance representing the actual length of the microchannel was 781 pixels and the location of the cell was at 631 pixels. The actual location of the cell from the cell side of the device as calculated using Eq.4.3 was 807 μm. The location of the cells in the microchannels on different days as calculated using the equation 4.3 is shown in Fig. 4.5.

4.5.4 Significance of Cell Migration

Cell migration is considered to be a key step in cancer metastasis. The mechanism of cell migration has been studied and documented [81–83]. The techniques employed to quantify cell migration including the Boyden chamber, under-agarose assay, Zigmond chamber, Dunn chamber, and micropipette assay all have drawbacks

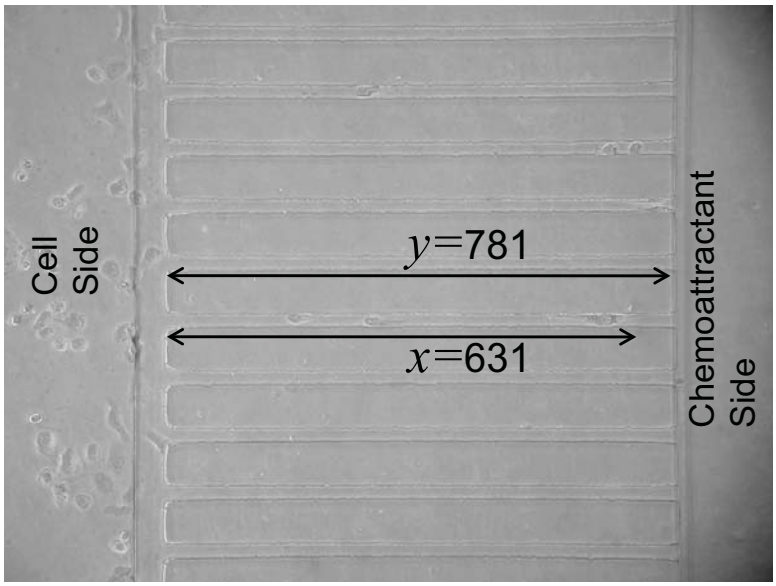

Figure 4.4. The migration distance is calculated by determining the location of the cell in the microchannel and the total length of the microchannel in pixels using Eq. 4.1.

as discussed earlier. The microfluidic platform provides a means to monitor cell migration in response to chemoattractants. The channels and growth chambers form a confined environment in which the cells migrate across from one side of the device to the other through the microchannels. By monitoring the microchannel, the distance the cells migrate and the number of cells that migrate can be easily determined. As shown in Fig. 4.5, the distance the HPV-7 cells have migrated can be determined. The images were captured using a Nikon Axiovert microscope connected to a Canon powershot. The images were then analyzed using GIMP, and the distance was measured using Carl Zeiss AxioVision. By comparing the distance measured on each day the migration rate was determined. Also, by comparing the migration rates and cell number for each of the chemoattractants tested, the chemoattractant with highest propensity for migration was identified.

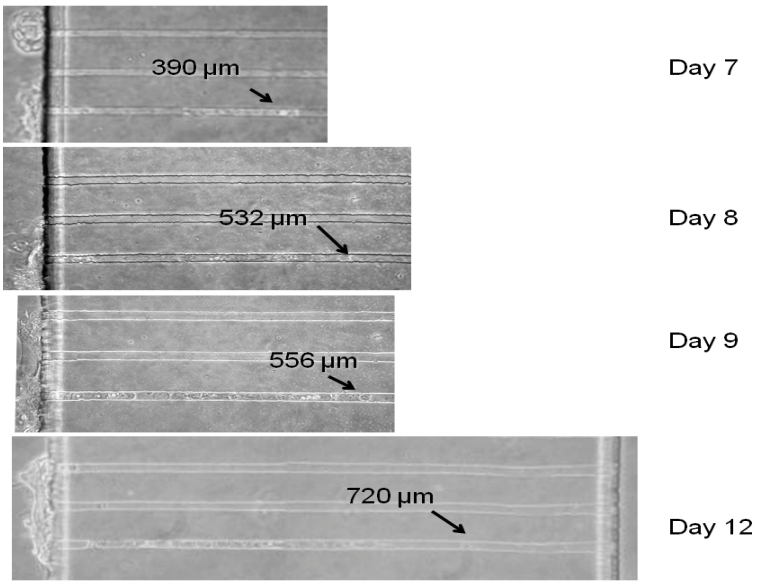

Figure 4.5. Migration distance measured for HPV-7 cells in response to 5% FBS is culture media PrEGM.

4.5.4.1 Comparison of Migration Distances

The response of cells to different chemoattractants was assessed by using different patient sera. The supernatant obtained by centrifuging the blood drawn from patients was collected. The protein content of each of the supernatants was determined by Bradford assay. Sera from three prostate cancer patient donors (with IRB-approved consent) was employed to assess their potential to promote cell migration. Fetal Bovine Serum (FBS) was used as a primary control and healthy donor's sera was used as a secondary control. The protein concentration of each serum was measured by protein assays and appropriate dilutions were made to maintain the protein concentration equivalent to that of FBS in the control (Appendix B).

To test the four sera designated as (Control, Serum-1, Serum-2, Serum-3) simultaneously, four devices were primed and red fluorescent expressing prostate cancer cells, PC-3R were seeded according to the methods described earlier. The quantity of patient serum added to the media was calculated to match the protein content in the

5% FBS containing media of the cell suspension. The protein concentration obtained for the patient sera using Bradford Assay is shown in Table 4.2. Cell density was 8 x 10^4 cells per 200 μl on the cell side, while 200 μl growth media without cells was introduced on the chemoattractant side. After allowing 24 hours for cell adhesion, the media in all 4 wells was removed. Immediately, 200 μl growth media was added to cell-side wells, while 200 μl of same media containing designated patient serum was added to the wells on on the chemoattractant side.

Table 4.2. The four patient sera tested were diluted in the cell culture media as 5% in 4 ml to match the quantity of FBS in the culture media used for the cell suspension. The protein concentration in each serum as obtained by Bradford assay was used to determine the 5% equivalent

Serum	Source	Bradford Protein Assay (μg/ml)	5% in 4 ml (μl)
Control	FBS	25	200
Serum-1	Y-pool	40	125
Serum-2	Patient 2546	34	147
Serum-3	Patient 2740	20	250

The devices were monitored individually at regular intervals of time and bright field and the corresponding fluorescent images were acquired. Figure 4.6 shows the images taken of the device showing cells in the channels on Days 4 and 5 in response to Serum-2. It is evident that there is a difference in the positions of the cells and by measuring this difference, the rate of migration was determined. The narrow channels serve to confine the cells and allow for identification and tracking of the cells over time. Also, in Fig. 4.6, another phenomenon evident is the deformation of the cell at the entrance to the channel. The cell appears to be stretched as it enters the

channel in response to the serum containing media. Our device thus offers a means of observing morphological changes of individual cells during migration in real time.

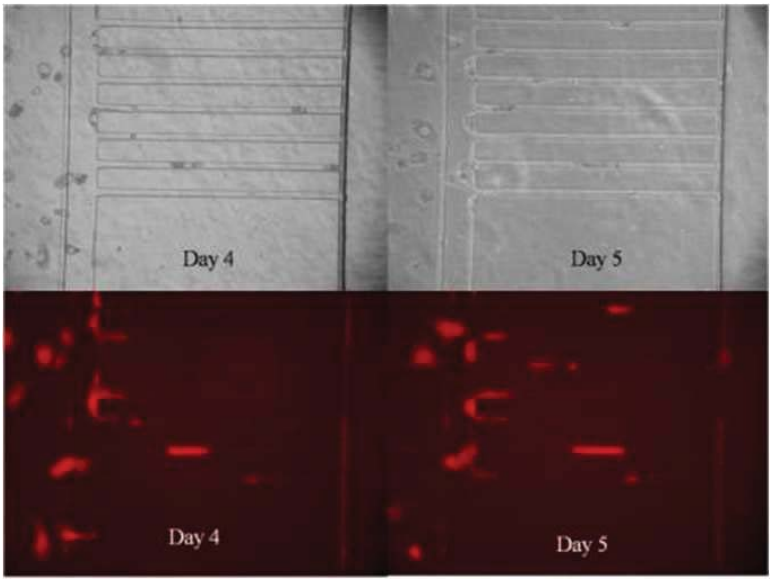

Figure 4.6. The response of the PC-3R cells to patient serum was monitored and captured. The brightfield and fluorescent images in response to Serum-1 on 4^{th} and 5^{th} day is shown in the left and right panels respectively.

The cell migration was observed and data collected for a period of 8 days. Images were acquired on each day and used to calculate the number of cells in the channels, distance moved and time taken for the relative speed at which the cells migrate towards the stimulant by comparison. In each image, the cells that moved into the channels were tracked and their migration distances were obtained by comparing with the images taken at 24 hour intervals. The numbers of tracked cells depend on the chemotaxis effect. For example, in five days, less than 20 cells were tracked in the device treated with healthy young donor serum and up to 113 cells were tracked in the device treated with Serum-2. The average migration rate of cell for each condition was obtained from the tracked cells. Results in Fig. 4.7 indicate that the

PC-3R cells migrating toward stimulating media treated with Serum-2 and Serum-3 exhibited much higher migration rates compared to those toward Serum-1 and Control. Repeated tests conducted under similar conditions provided similar results.

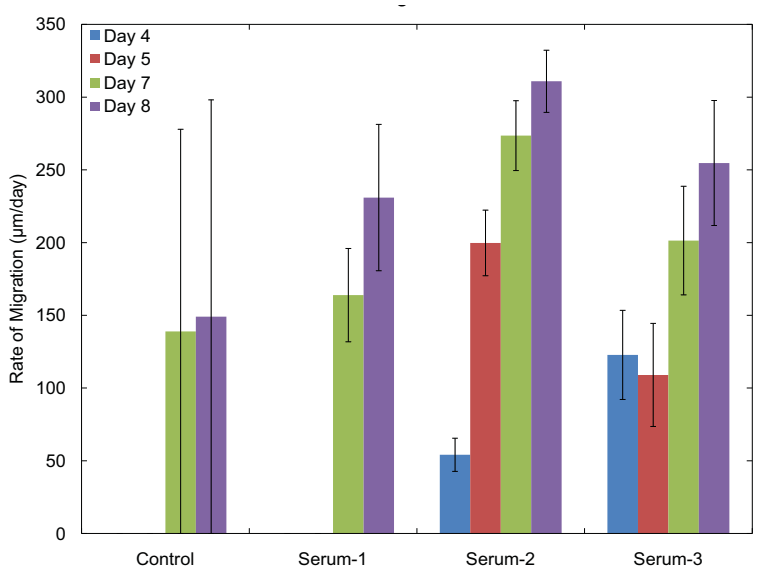

Figure 4.7. Different cell migration rates in different stimulating environments (Control, Serums 1, 2 and 3) for an observation period of 8 days demonstrating assessment of cell migration using our device.

In addition to measuring the rate of movement, the numbers of cells in the channels have also been recorded as a static indicative parameter for cell migration in response to chemoattractants. The number of cells in the channels was counted for each of the serum treatments at 24-hour intervals. As shown in Fig. 4.8, the numbers of cells moving in the channels toward Serum-2 and Serum-3 treated media was higher than those towards the Control on Days 4-7. Highest accumulation of cells was exhibited in the channels toward treatment with Serum-2. Relatively no significant increase in number of cells was observed after Day 4 for Serum-3. It

should be noted that Serum-1 and Control do not show any increase in cell number in the channels until Day 8, indicating a delayed response.

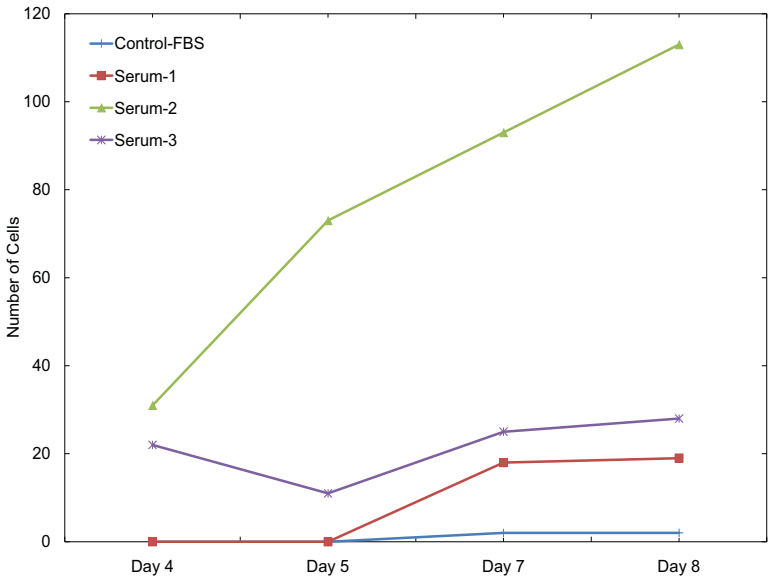

Figure 4.8. Number of cells observed in the channels for eight days under treatment of different stimulating environments (Control, Serums 1, 2 and 3).

From Fig. 4.7 and 4.8, it can be inferred that Serums 2 and 3 demonstrate a higher propensity for cell migration. It also indicates that that Serums 2 and 3 demonstrate higher average cell migration rates over a certain period of time when compared to Serum 1 and Control. There is a delay in the response for Serum-1 and Control and the rate of migration can be calculated only after cells were observed in the channel after 7 days.

The images taken at 100X cover ten channels and a small part of the cell and chemoattractant sides of the device. Thus, the brightfield and fluorescent images taken were aligned to show all the channels in the device. The fluorescent images were then compared. One such sample comparing the Control (T-media with 5% FBS) and Serum- 3 is shown in Fig.4.9. It can be seen that there is a very large

number of cells in response to Serum-3. Thus the static flow device can be used to compare migration response of cells for different stimulation conditions.

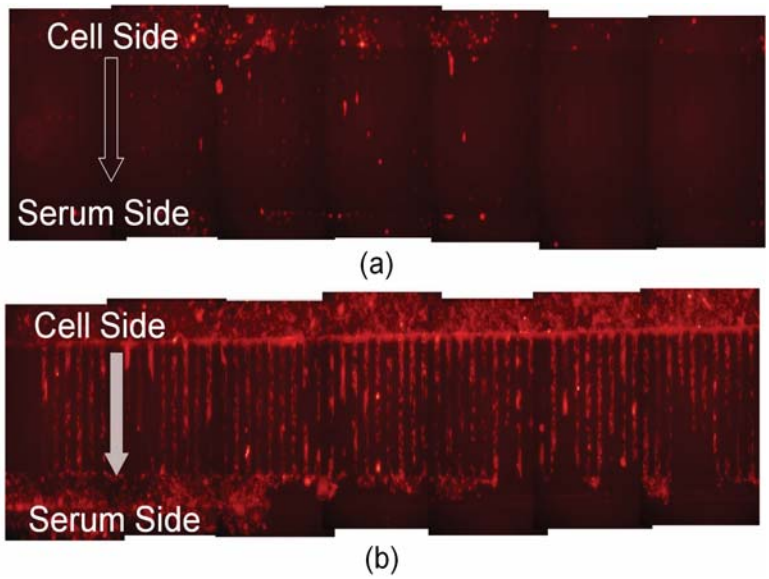

Figure 4.9. Images taken at 100X covers only ten channels and a small part of the cell and chemoattractant sides of the device. The fluorescent images taken were aligned to show all the channels in the device for PC-3R cells in response to Control (T-media with 5% FBS) and Serum- 3 showing higher response in terms of cell number and distance migrated in Serum-3.

One of the features of the static flow prototype device mentioned earlier was time-lapse. In order to demonstrate this capability, images were taken at 1 hour intervals for PC-3R cells migrating in response to Control and Serum-3. The images were then analyzed to determine the location of the cell. The images are shown in Figs.4.10 and 4.11.

From the images captured it was clearly evident that the cells did not migrate in response to the control. In the case of cells being analyzed for their response to Serum-3, it was seen that two cells migrated across half the length of the channel in 5 hours. Moreover, the changes in the cell morphology as they migrate across

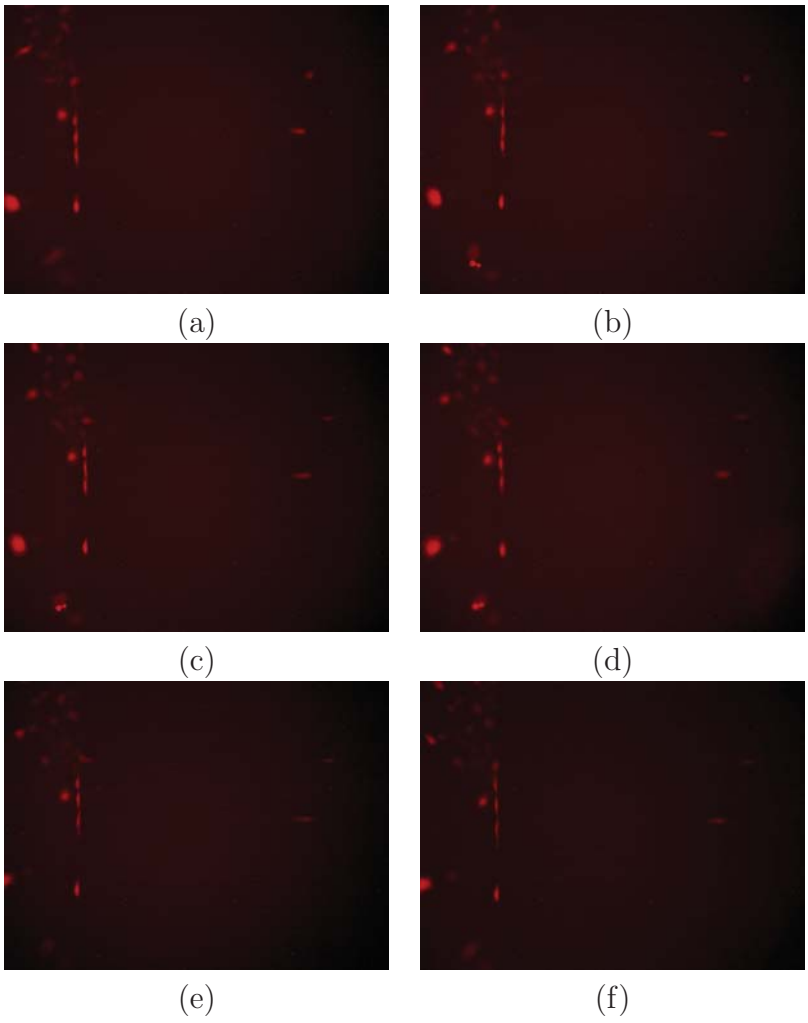

Figure 4.10. Location of PC-3 cells (a) at start of the experiment, (b) after 1 hour, (c) after 2 hours, (d) after 3 hours, (e) after 4 hours and (f) after 5 hours.

the channel was also observed in realtime in the brightfield images captured. Thus the microfluidic platform provides a means to monitor and analyze cell response to different chemoattractants in realtime.

The microfluidic device presented in this section provides a means to assess cell migration potential. The chemokine consumption is of the order of tens of microliters since each reservoir capacity is only 100 μl. One of the drawbacks of this device was that for each condition or chemoattractant under test a new device needs to be

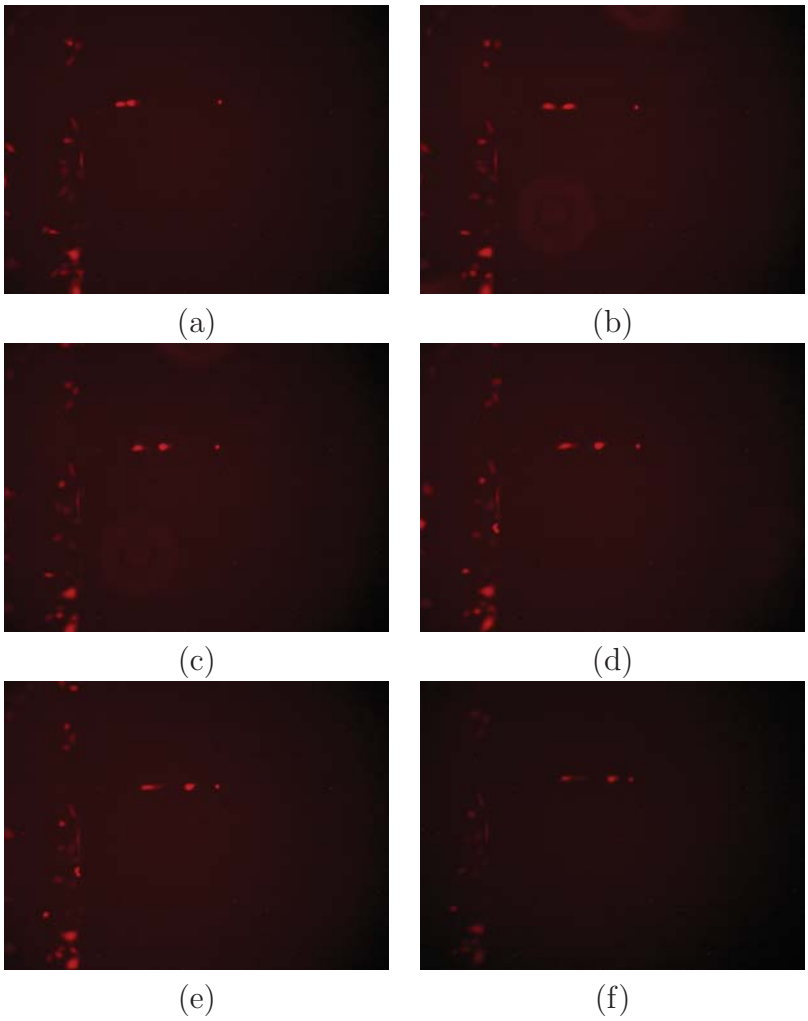

Figure 4.11. Location of PC-3 cells (a) at start of the experiment, (b) after 1 hour, (c) after 2 hours, (d) after 3 hours, (e) after 4 hours and (f) after 5 hours.

fabricated. Thus for the 4 patient sera experiment, 4 separate devices had to be used for sera alone and more devices were required as controls. This was time consuming and labor intensive. In order to address this issue, we have proposed a microfluidic platform for high throughput assays which is presented in Chapter 5.

CHAPTER 5

HIGH THROUGHPUT DEVICE

5.1 MiMiC^{TM}

In order to overcome the drawbacks of the static flow protoype device, namely a larger number of devices required for high throughput assays, a microfluidic platform called MiMiC^{TM} which stands for "'Microfluidics for Migration of Cells"' has been proposed. The platform has a layout similar to the conventional 96 well plate assay allowing for multiple tests to be conducted at one time. Figure 5.1 shows the design layout of the MiMiC^{TM} platform.

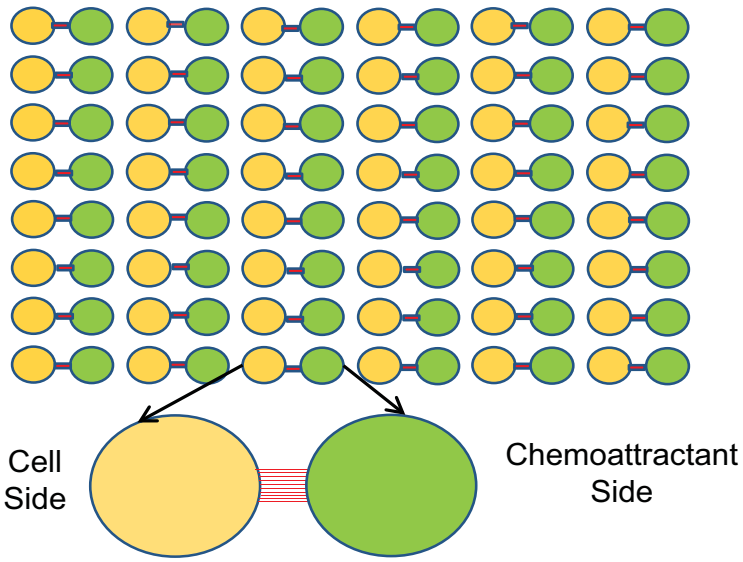

Figure 5.1. MiMiC^{TM}.

5.2 Fabrication

A master pattern was first formed by photolithography on a silicon wafer. The pattern was hard baked to prepare it for the next step. The device pattern from the master was transferred onto the PDMS by soft lithography. The following sections describe the process in detail.

5.2.1 Photolithography

The MiMiC^{TM} platform consists of a set of 10 parallel channels 10 μm (w) x 10 μm (h) x 1000 μm (l) connecting the two reservoirs. Photolithography was carried out using SU-8-10 (Microchem, MA) to obtain a 10 μm high pattern of the mask shown in Fig. 5.1. The complete process is summarized in Table 5.1.

Table 5.1. Process parameters for SU-8-10 to obtain 10 μm feature height

Process Step	Parameters
Singe the wafer	1 hour at 150°C
Spin coat	500rpm with a ramp of 100 rpm/s. Hold for 5s 3000rpm with a ramp of 300 rpm/s. Hold for 30s
Soft Bake	3m at 65° 5m at 95°C
Expose	12s
Post exposure bake (PEB)	1m at 65°C 45m at 2°C
Develop	3m in developer. Rinse with Isopropylalcohol (IPA)
Hard bake	45m at 150°C

Once the master pattern was created on the silicon wafer, the wafer was placed on a Pyrex® plate and PDMS was poured onto the mold and cured as shown in Fig. 2.1. As the PDMS cured, the patterns were transferred onto the PDMS from

the master. The cured PDMS layer was cut and peeled from the silicon wafer. It was then diced and cleaned. Openings were made for reservoirs using a 4 mm Harris Uni-core punch. The surface of the PDMS was then cleaned using scotch-tape (3M, MN)followed by a 20 minute soak in detergent, rinsing in distilled water and finally a 20 minutes soak in 75% Ethyl alcohol. The PDMS dies were then placed in a tissue culture hood under UV light for at least 20 minutes.

5.2.2 PDMS Bonding

The device was made by soft-bonding or temporary bonding of the PDMS to standard tissue culture plates (100 mm Corning TC-Treated Culture) inside a tissue culture hood to prevent contamination.

5.2.3 MiMiC^{TM}

The MiMiC^{TM} platform differs from the prototype design in many ways. The dimensions of the microchannels were retained the same. However, changes were made to the reservoirs and number of channels connecting the reservoirs. As opposed to the four reservoir configuration of the prototype, the MiMiC^{TM} platform has two reservoirs per device with ten microchannels connecting the reservoirs. There are 48 devices in each platform formed by devices placed along six columns and eight rows. The reservoir is 4 mm in diameter. The distance between each device is 1 mm. The total dimension of the device is 50 mm x 65 mm.

In order to validate the feasibility of using the MiMiC^{TM} platform for cell migration studies, several experiments were conducted using different cell lines and chemoattractants. The following sections describe the results of each of the experiments that were conducted.

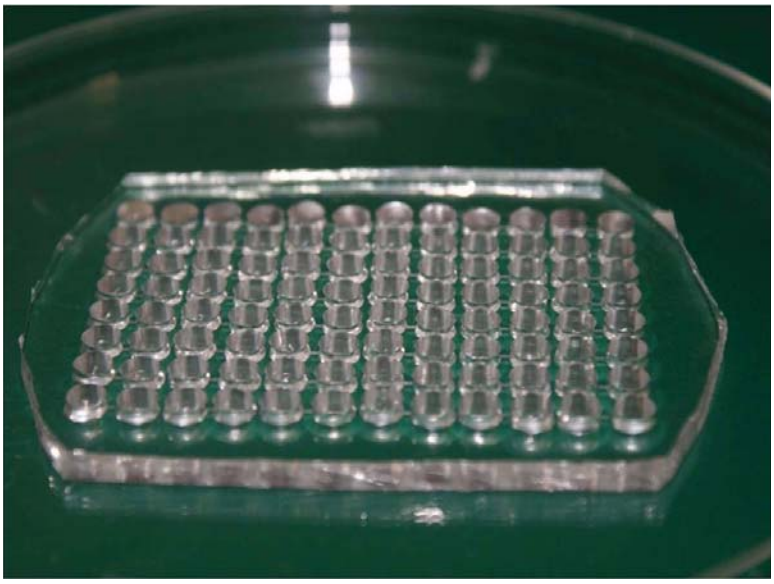

Figure 5.2. Mask layout for the MiMiC^{TM} platform.

5.2.4 Prostate Cancer Cells

Migration characteristics of prostate cancer cells was tested using the MiMiC^{TM} platform. Red fluorescent protein expressing prostate cancer (PC-3R) cells and green fluorescent protein expressing lung-metastasized prostate cancer (PC-3-ML) cells were assessed. We conducted a double blind study on the migration of PC-3R and PC-3-ML cells against patient blood serum extract. We were provided with 35 patient serum extracts by The Department of Urology, UTSW Medical Center, Dallas, TX. The samples were centrifuged, the supernatant was extracted and tested to determine their protein content as described in Appendix B. The following sections explain the experimental results.

5.2.4.1 PC-3-ML Cells

The MiMiC^{TM} overcomes the drawback of the prototype design in that it allows for multiple screenings to be carried out on a single culture plate. The 48 devices in a

single platform allow for 16 tests with n=3 to be carried out simultaneously. For our test with prostate cancer cells and 35 patient sera, three platforms were primed and prepared for the test. Each device was seeded with 1000 cells in 100 μl on the cell seeding side. There were 4 controls and 35 patient sera with n=3 with the controls being repeated in each platform. Thus there were 9 devices each for each type of control. A total of 141 devices out of the 144 devices were used. The controls were

1. Control 1: Culture media (RPMI 1640) with 1% FBS
2. Control 2: Culture media (RPMI 1640) with 3% FBS
3. Control 3: Culture media (RPMI 1640) with 1% FBS and 2% *y-pool*
4. Control 4: Culture media (RPMI 1640) with 5% FBS

The *y-pool* used in Control 3 was blood sera extract from healthy young adults in the age group 18-35 years of age with no known prior history of cancer. We were not privy to the patient medical history or the metastatic condition, if any, of the patients during the time of experimentation. The sera were randomly labeled from 1 through 35 and diluted by matching with the protein content in the culture media (refer Appendix B). Through our experiments, our goal was to demonstrate that different patient serum extracts led to different migration characteristics in the same cell type. Also, we intended to show that different cell types responded differently to the same stimulation conditions.

Cell seeding and serum addition was carried out according to protocols referred to previously. Brightfield and florescent images were captured at 24 hour intervals. The number of cells, the migration distance and migration rates were calculated for images captured up to 5 days. Also, the normalized average migration for the cells in the microchannels as percentage of highest value is shown in Fig. 5.3. By comparing

the results, it was observed that there appeared to be ranges in the number of cells marked by the location of the Controls in the plot.

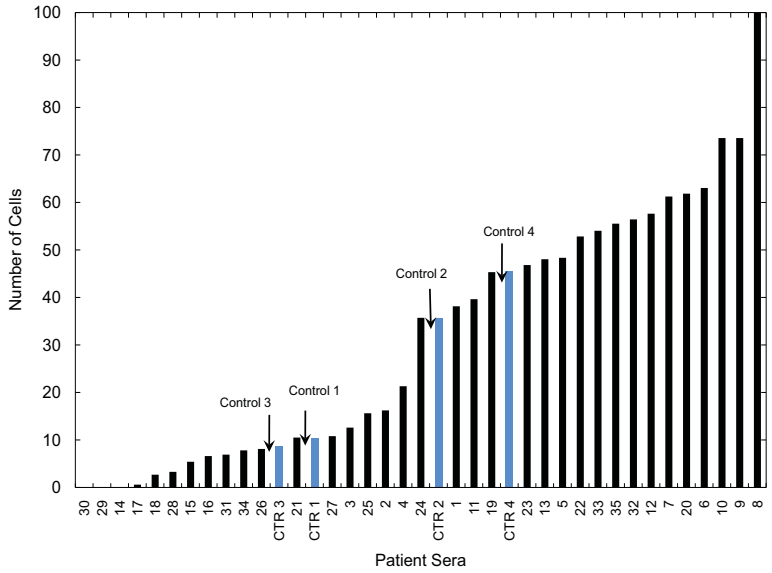

Figure 5.3. The normalized average migration of cells in the microchannels for 35 patient sera and four controls expressed as percentile.

The various images taken were arranged into panels to compare. The images showing cell response to the four controls and the patient extracts when arranged as panels appear as shown in Figs. 5.5 to 5.8. It can be seen from the images that the number of cells in response to patient serum 8 was highest while the lowest was in response to patient serum 30.

5.2.4.2 PC-3R Cells

Similar experiments were conducted with prostate cancer (PC-3R) cells. The normalized average number of cells in the microchannels represented as percentage of the highest value is shown in Fig. 5.8. The various images captured were aligned to show the difference and are as shown in Figs. 5.9 to 5.12. From these experiments,

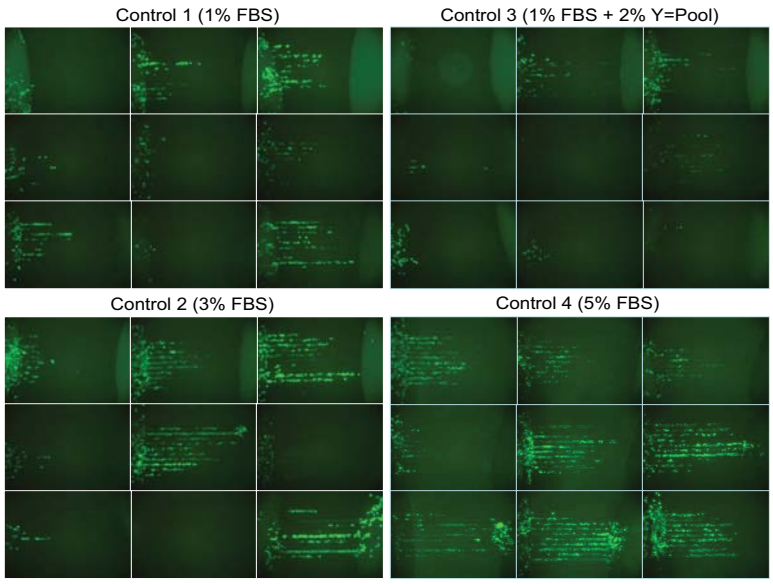

Figure 5.4. The images of PC-3-ML cells in the microchannels for the Controls used to assess migration in response to 35 patient blood serum extract after 6 days.

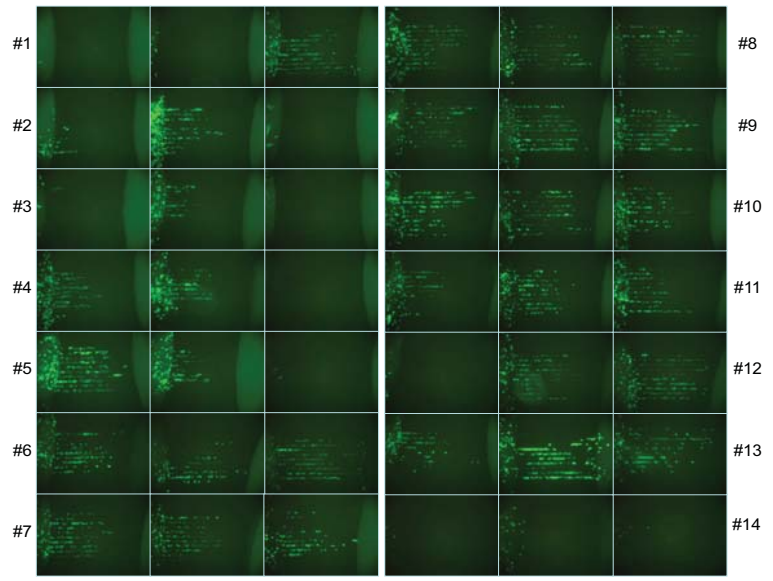

Figure 5.5. The images of PC-3-ML cells in the microchannels for patient sera 1 to 14 used to assess migration in response to 35 patient blood serum extract after 6 days.

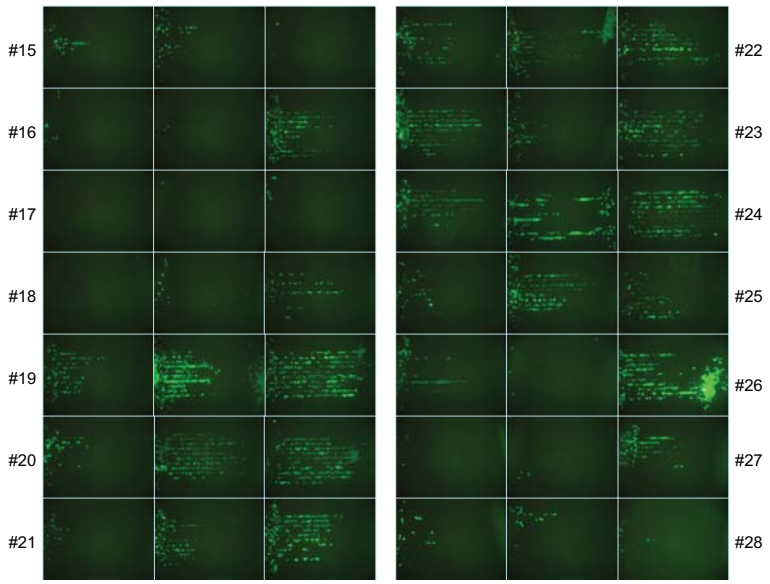

Figure 5.6. The images of PC-3-ML cells in the microchannels for patient sera 15 to 28 used to assess migration in response to 35 patient blood serum extract after 6 days.

it was evident that the response of different cell lines to the same conditions also varies. This is expected since PC-3-ML cells are derived from PC-3 cells after they have metastasized to the lungs in nude mice. Literature suggests that the response or migration characteristics of different cells for the same stimuli are different [82,84,85]. The experimental results suggest that there are certain factors in the patient serum extract that alters the response of the cells. The reasons for the varying migration rate or cell number for the same cell type are not yet clear. One of the factors that we were aware of regarding the patient sera supplied was that some of the patients were in an advanced stage of metastasized prostate cancer. At the time of the experimentation, we were not aware of the information required to make an informed decision regarding the relation between sera derived from cancer patients, normal patients and the corresponding cell migration results.

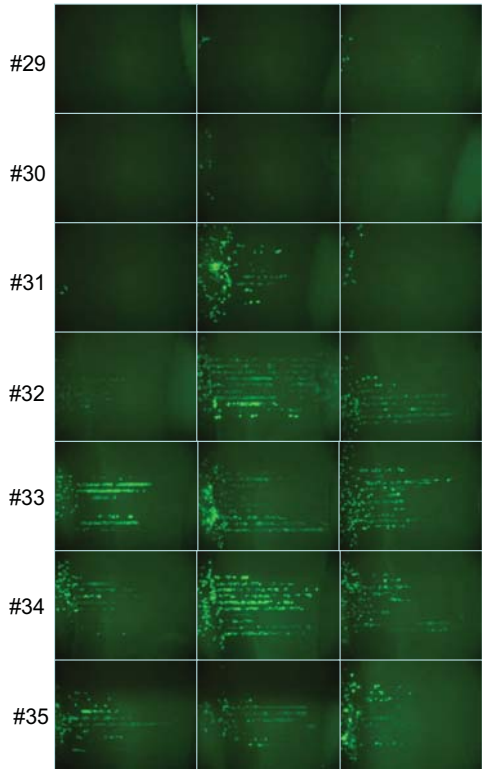

Figure 5.7. The images of PC-3-ML cells in the microchannels for patient sera 29 to 35 used to assess migration in response to 35 patient blood serum extract after 6 days.

In order to determine that the migration characteristics of cells in response to patient serum derived from patients with metastatic cancer and from patients without cancer are different, we conducted an experiment in which sera from 6 patients with metastatic prostate cancer was evaluated using the MiMiC^{TM}platform. Controls including serum from a pool of young men without prostate cancer and serum from women as negative control. The migration characteristics were clearly distinct for the patients with metastatic prostate cancer and the controls. An example of this distinct difference is shown in Fig.5.13. The data strongly indicates that migration of cells towards serum from men with metastatic prostate cancer were clearly distinct

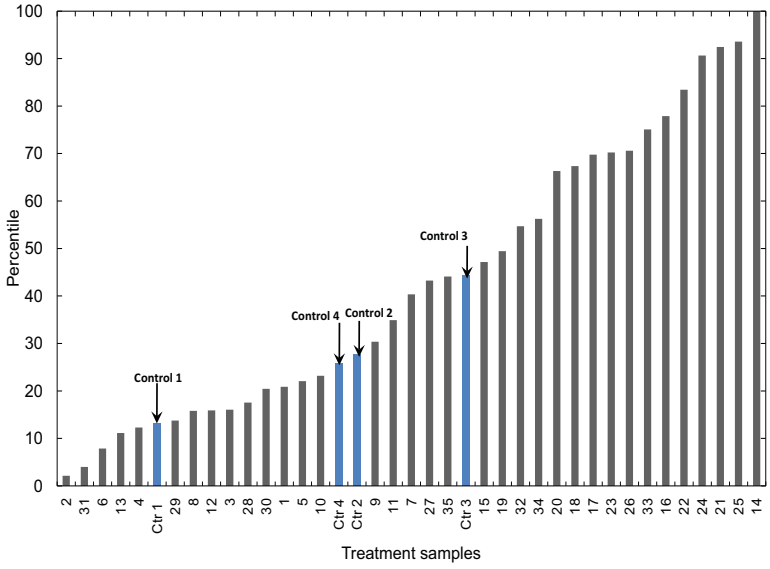

Figure 5.8. The normalized average migration of PC-3R cells in the microchannels for 35 patient sera and four controls expressed as percentile.

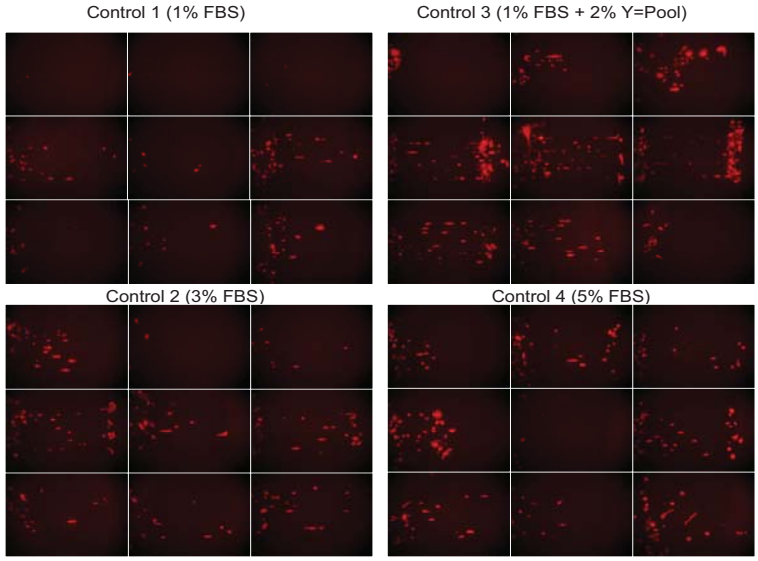

Figure 5.9. The images of PC-3R cells in the microchannels for the Controls used to assess migration in response to 35 patient blood serum extract after 6 days.

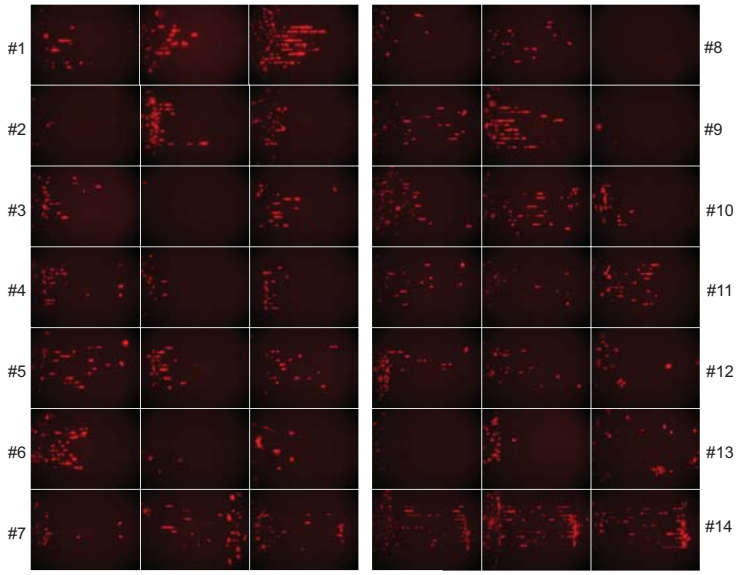

Figure 5.10. The images of PC-3R cells in the microchannels for patient sera 1 to 14 used to assess migration in response to 35 patient blood serum extract after 6 days.

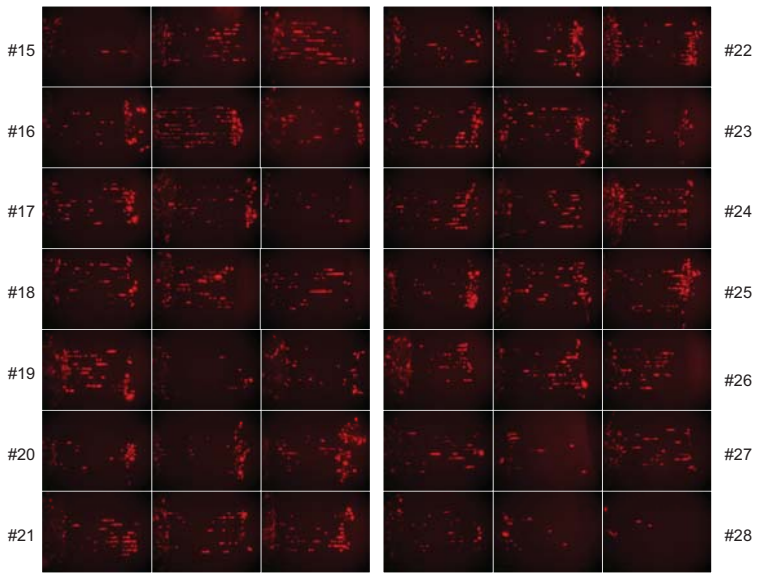

Figure 5.11. The images of PC-3R cells in the microchannels for patient sera 15 to 28 used to assess migration in response to 35 patient blood serum extract after 6 days.

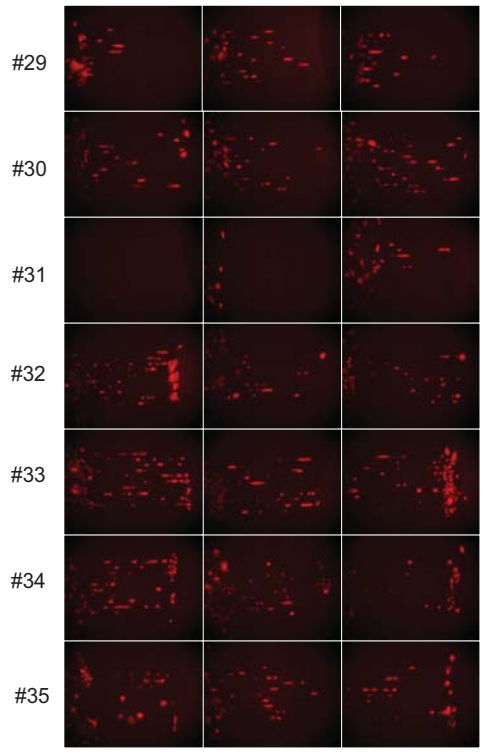

Figure 5.12. The images of PC-3R cells in the microchannels for patient sera 29 to 35 used to assess migration in response to 35 patient blood serum extract after 6 days.

from control patients. Thus the microfluidic assay works well in identifying patients with metastatic prostate cancer.

5.2.5 Human Aortic Vascular Smooth Muscle Cells

Vascular smooth muscle cells (VSMCs) are important in maintaining structure and function of blood vessels. They migrate in response to damage and promotes vascular diseases, such as atherosclerosis (hardening or narrowing of arteries) or restenosis. Thus the migration characteristics of VSMC's was tested. The response of the cells to different growth factors was monitored and analyzed. Previous studies have shown VSMC migration to be influenced by many chemical and cellular factors (stimulants) [86, 87]. In order to validate the results, migration of human aortic

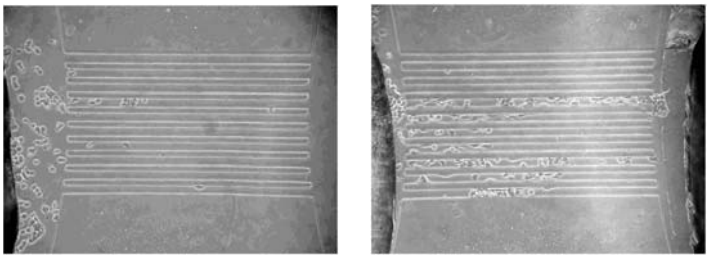

(a) (b)

Figure 5.13. Migration characteristics of prostate cancer PC-3-ML cells towards serum from (a)a patient without prostate cancer and (b) a patient with prostate cancer.

smooth muscle cells (HASMC) in response to growth factors EGF (50 ng/ml), FGF (10 ng/ml) and VEGF (10 ng/ml) was compared to a control (2% FBS in culture media DMEM). The average rate of migration and the number of cells in the microchannels for HASMC's in response to the different growth factors is shown in Fig. 5.14 and 5.15.

Simultaneously, conventional transwell plates were also prepared with the same growth factor concentrations and HASMC's. The response in the transwell plate is summarized in Table 5.2. In the transwell plates, it was seen that the highest percentage of cells was found in FGF and lowest percentage was in the Control.

To compare the performances of the MiMiC^{TM} platform and the transwell plates, the average number of cells and the average migration rate in the microchannels that migrated to the chemoattractant side was counted. The results are shown in Fig. 5.16. It can be seen that in the case of the MiMiC^{TM} platform also, the highest number of cells was in response to FGF and lowest was in the Control, while the migration rates were comparable for EGF, FGF and VEGF. However, it was clear that the overall response to FGF was high.

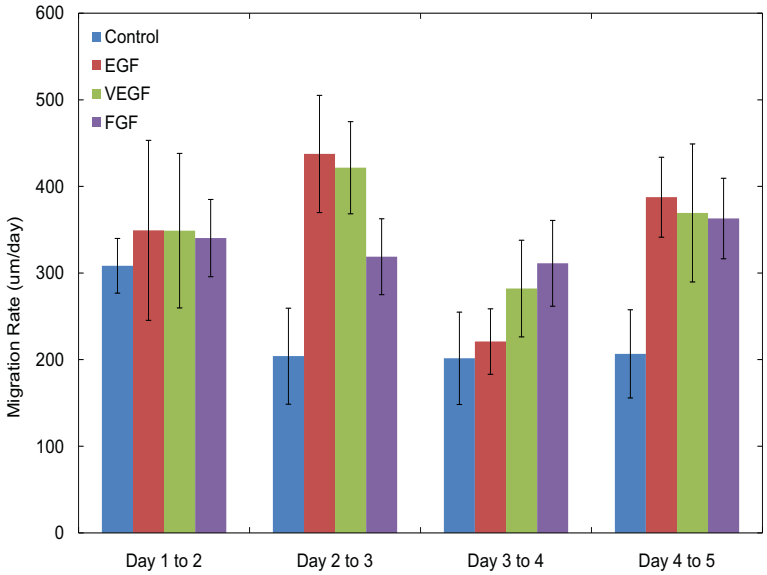

Figure 5.14. The average migration rate for Human Aortic Smooth Muscle HASMC) cells in response to growth factors EGF, FGF, VEGF compared to Control monitored for five days.

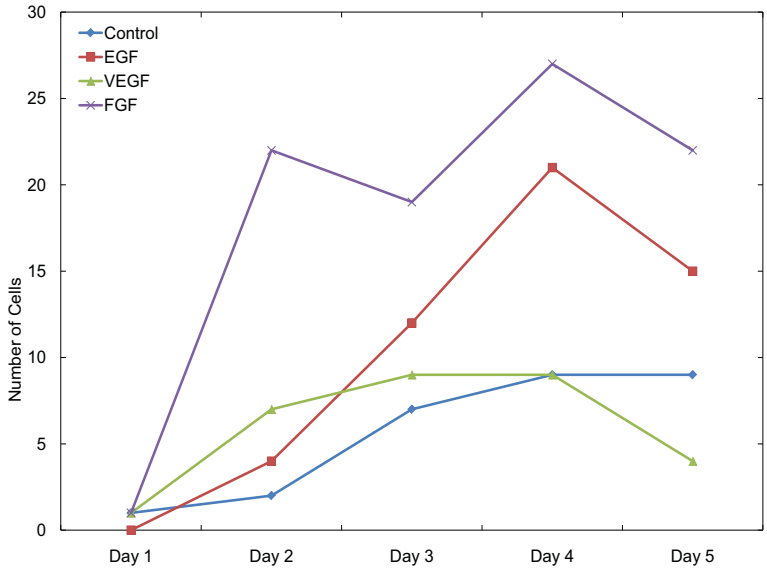

Figure 5.15. The number of HASMC's in the channels in response to growth factors EGF, FGF, VEGF compared to Control monitored for 5 days.

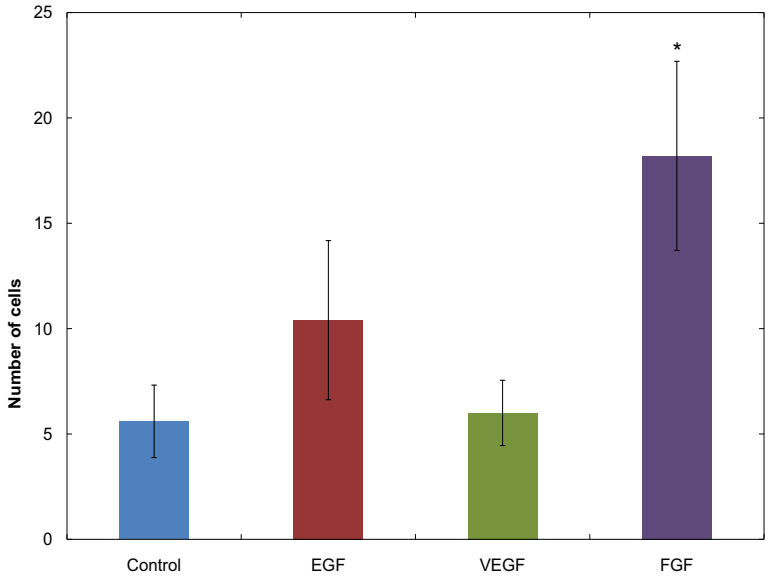

Figure 5.16. The average number of HASMC's in response to FGF, EGF, VEGF and Control over 5 days.

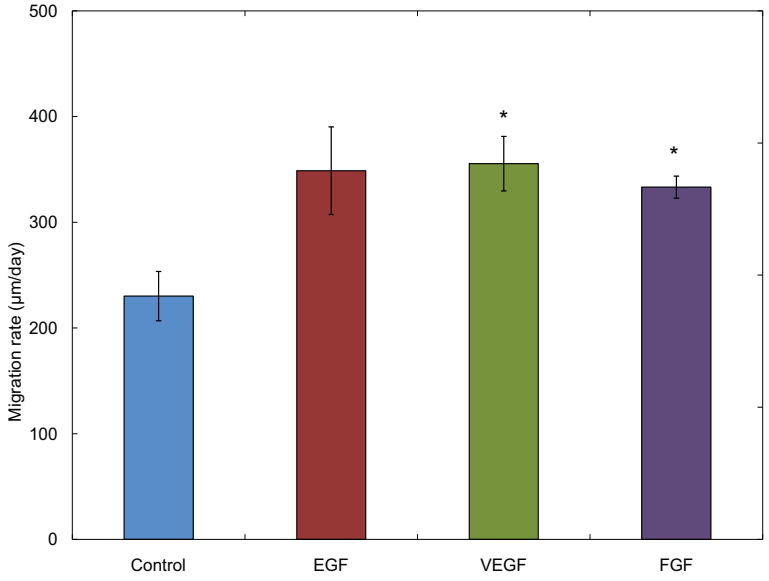

Figure 5.17. The average migration rate for HASMC's in response to FGF, EGF, VEGF and Control over five days.

Table 5.2. The migration of HASMC's in percentage in response to EGF (50 ng/ml), VEGF (10 ng/ml), FGF (10 ng/ml) and FBS (2%) in culture media DMEM on a Transwell®plate

Stimulant	Migration (percent)
Control	10%
EGF 50 ng/ml	23%
VEGF 10 ng/ml	37%
FGF 10 ng/ml	47%

5.2.6 Breast Cancer Cells

The MiMiC™ platform was used to assess the migration characteristics of breast cancer (MDA-MB-231) cells. This experiment was also used to compare the response of the cells when the number of cells that were seeded was varied. The experiment settings were as follows:

1. 10,000, 5,000 and 1,000 MDA-MB-231 cells in
    - 1% FBS in RPMI 1640
    - 5% FBS in RPMI 1640
    - 2% patient serum extract in RPMI 1640 with 1% FBS

Each experiment set was repeated five times thus giving n=5. Images were taken every 24 hours. The number of cells and average migration rate was calculated. The results shown in Figs. 5.18 suggests that there is an optimum number of cells that need to be used to obtain results for cell migration under all testing conditions. It was also evident that the response to the patient serum was higher than that for 1% FBS or 5% FBS containing media.

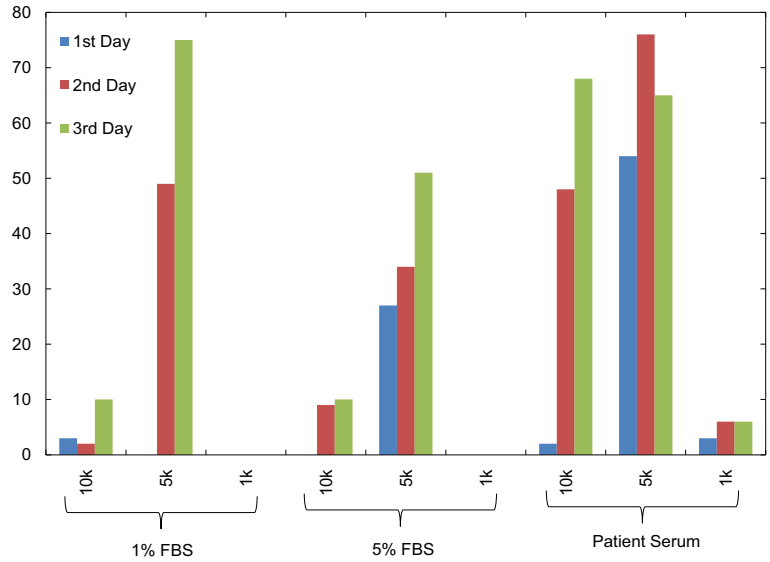

Figure 5.18. Total number of Breast cancer (MDA-MD-231) cells in the microchannels in response to 1% and 5% FBS in cell culture media, with 10,000, 5,000 and 1,000 cells with n=5.

5.2.7 Kidney Cancer Cells

The migration of Kidney Cancer (CaKi-2) cells and Human mesangial cells (HMC) was compared. The MiMiC^{TM} platform was primed and prepared to test different antibodies. The cells were seeded (1000 cells/well, in 50 μl media) and allowed to incubate for 24 hours after which 10 μl of the antibody was added to the wells. The antibodies added and the experiment configuration is shown in Fig.5.19. The cell migration characteristics were analyzed to obtain displacement towards gradients and cell numbers in the micro-channels. Migration speeds and the cell numbers in channels were the main parameters of interest.

The physiological processes involving RLIP76, HNE, GS-HNE can be simplified as follows. RLIP76 is a RAL-1 binding protein which is responsible for the removal of GS-HNE from the cells. HNE or 4-hydroxynonenal is the toxic aldehyde produced by the peroxidation of Omega-6 polyunsaturated fatty acids. The action of the enzyme

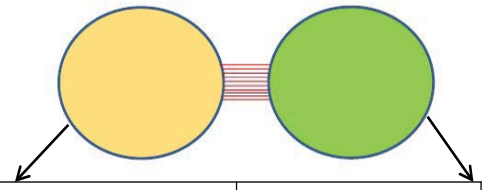

	Cell side	Attractant side
Control	2 % FBS	2% FBS
PIA_0	PIA	---
RLIP76_0	RLIP76	---
0_HNE	---	HNE
0_HNEGS	---	HNEGS
PIA_HNE	PIA	HNE
PIA_HNEGS	PIA	HNEGS
RLIP76_HNE	RLIP76	HNE
RLIP76_HNEGS	RLIP76	HNEGS
0_IONIC	---	IONIC

Figure 5.19. The treatment breakdown for the studies conducted with HMC and CaKi-2 cells with n=5.

glutathione S-transferase, converts the toxic HNE into a water soluble compound GS-HNE that is removed from the cytoplasm of the cell to the inter cellular spaces by RLIP76. the removal of GS-HNE is required to facilitate conversion of HNE to GS-HNE at normal rates. RLIP76 has been found to be present in elevated levels in metastatic cells. It has also been determined that controlling RLIP76 could affect cell migration and cancer metastasis. It can also improve the affect of the therapies used to alleviate cancer metastasis [88–96]

From the data obtained from the migration studies carried out for a period of 5 days it was observed that

1. Without HNE or GS-HNE, Caki-2 cells migrated faster than the mesangial cells
2. HMC showed very high attraction potential towards HNE
3. GS-HNE was an attractant to both HMC and CaKi-2 cells
4. The ionic liquid used showed no migration or attraction potential

5. The pre-immune antibody in the absence of HNE and HNE-GS increased cell motility in HMC and CaKi-2 cells
6. anti-RLIP76 inhibited cell motility
7. The presence of either pre-immune or anti-RLIP76 IgG changed the response of the cells to both HNE and GS-HNE. The response was reversed for CaKi-2 cells with HNE and for HMC with GS-HNE
8. Anti-RLIP76 inhibited the effect of GS-HNE and this was more pronounced in CaKi-2 cells
9. The results were matched with EMT analyses that showed repression of E-Cadherin. There was also activation of Fibronectin and Vimentin

The HMC and CaKi-2 cells present in the microchannels were analyzed for migration and cell numbers. The results obtained are shown in Figs.5.20 to 5.23

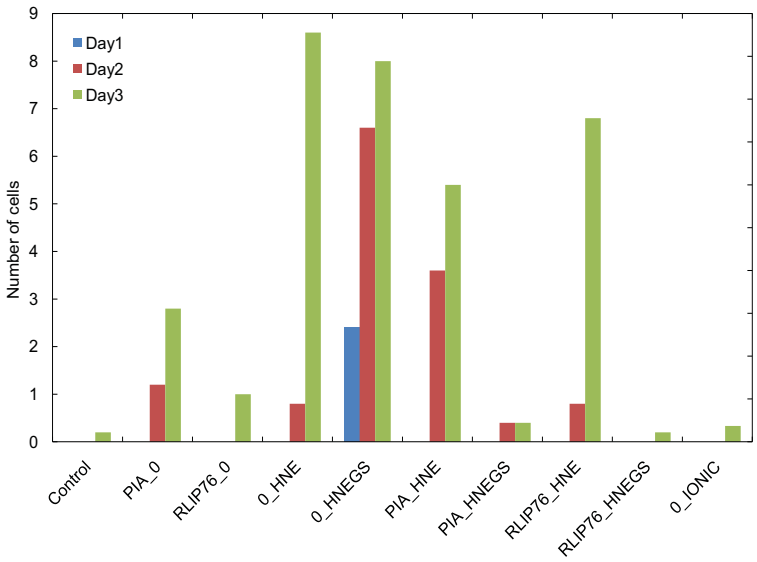

Figure 5.20. The number of HMC cells in the channels in response to the various chemoattractants.

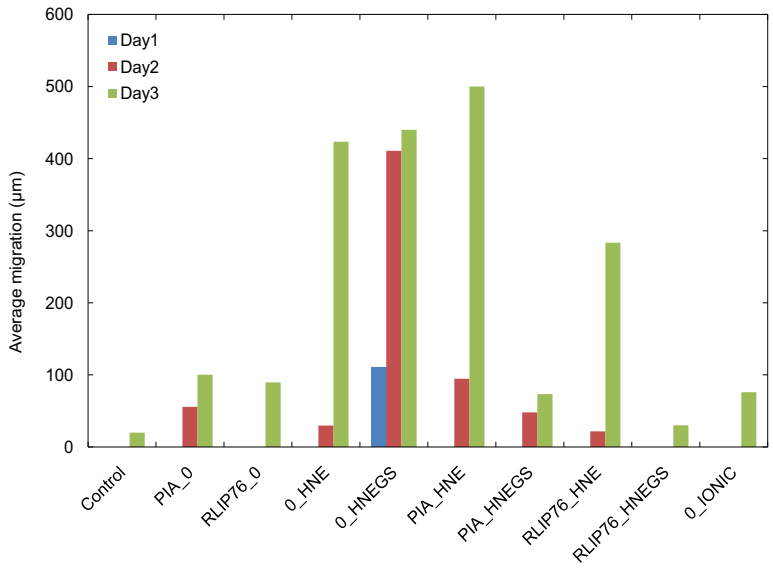

Figure 5.21. The location of the leading cell as average migration for HMC cells in response to various chemoattractants.

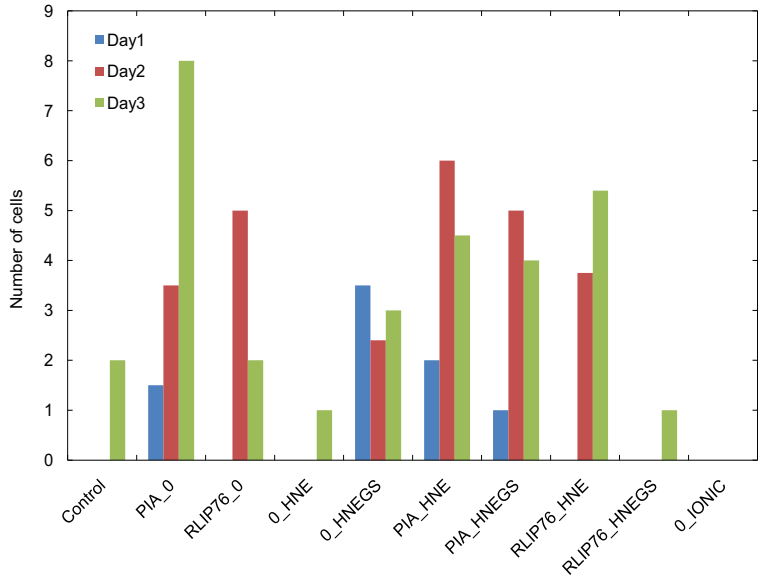

Figure 5.22. The number of HMC cells in the channels in response to the various chemoattractants.

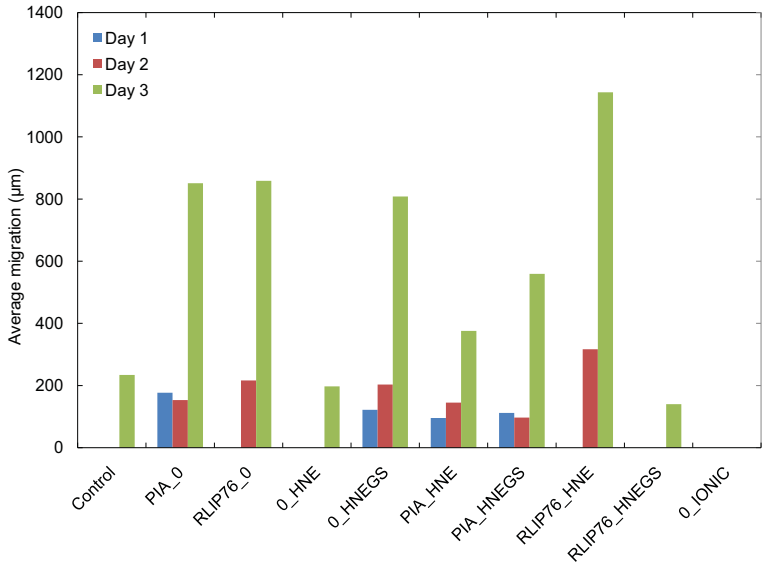

Figure 5.23. The location of the leading cell as average migration for CaKi-2 cells in response to various chemoattractants.

5.2.8 Immunocytochemistry using MiMiC^{TM}

The MiMiC^{TM} platform allows in-situ Immunocytochemistry (ICC) studies on the cells under test. As mentioned earlier, the PDMS devices were temporarily bonded by soft-bonding to 100 mm culture plates (Corning^{TM} 100 mm TC-Treated Culture Dish). HPV-7 cells were tested against 2 ng/ml of TGF-β in PrEGM media. The Control had no growth factors. The migration was monitored for 12 days after which the cells were fixed with 4% Paraformaldehyde (PFA). Seven different devices were chosen including one Control and treated with primary and FITC and TRITC containing secondary antibodies. The cells were finally treated with DAPI to stain the nuclei (Appendix C). The combination of primary and secondary antibodies chosen were to test for the following proteins:

1. Vimentin and n-cadherin
2. β-catenin and slug
3. Cytokeratin 14 (CK-14) and Cytokeratin-18 (CK-18)

4. E-cadherin and Desmin

The images captured were arranged to demonstrate the difference in the proteins present in the cells of the reservoirs on the cell side and chemoattractant side. The cells on the chemoattractant side were either due to migration or due to proliferation of the cells once they reached the chemoattractant side. A change in morphology and phenotype was evident on the chemoattractant side as seen by the widely spaced slightly elongated, flattened or larger cells. The fluorescent images captured of the cells after treatment with antibodies were compared (Fig. 5.24). It was seen that Vimentin which has long been considered as a marker for Mesenchymal cells [97] was expressed by the cells that migrated in response to TGF-β, Fig. 5.24(a) but not in the Control Fig. 5.24(b).

In the case of N-cadherin, it was seen that there was re-distribution of N-cadherin in the cells on the chemoattractant side. N-cadherin was uniformly expressed in the cytoplasm of the cells on the cell side but was confined to the region surrounding the nucleus on the chemoattractant side.

The results for E-cadherin, Desmin, β-catenin and slug were not conclusive. These results demonstrate the feasibility of using the MiMiC$^{\text{TM}}$ platform for immuno-cytochemistry studies. The microfluidic platform thus provides a means to study the cells in-situ after migration and test them for proteins for further analysis.

The high throughput device provides capabilities to monitor and analyze 48 test conditions on a single device. The 48 device platform can be fabricated in a single step process once the photoresist patterns on silicon were made. Various cell types were seeded in separate experiments and tested for their migration characteristics against different chemoattractants including chemokines and patient sera. Cancer cells were also tested against proteins and factors known to inhibit migration. These

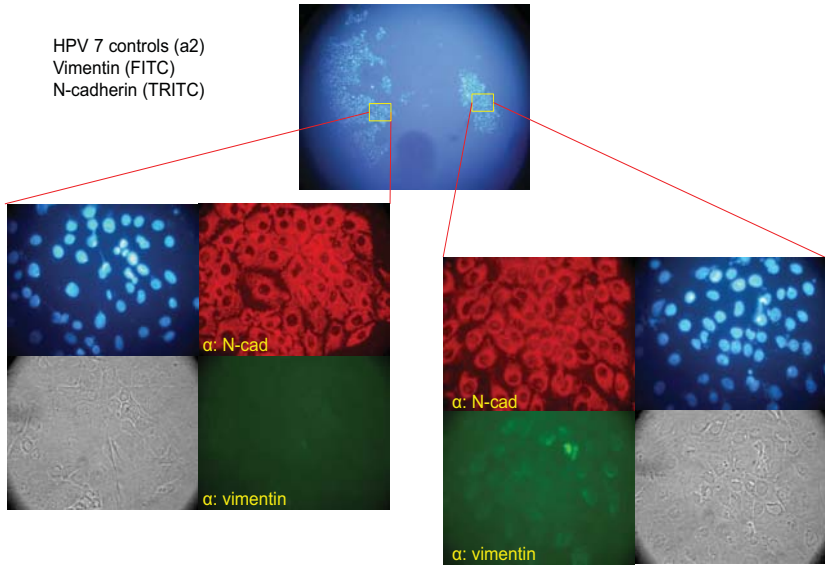

(a)

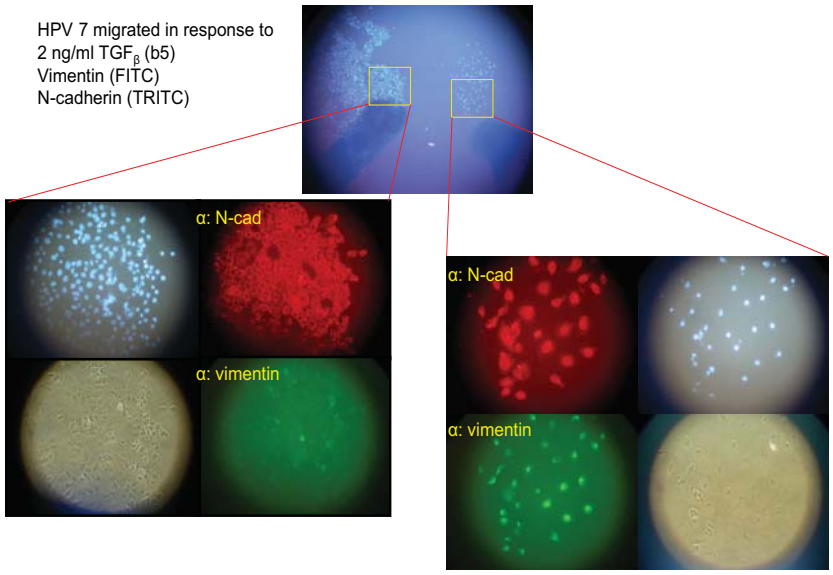

(b)

Figure 5.24. Immunocytochemistry results for HPV-7 cells in response to (a)control and (b) TGF–β. Vimentin was clearly observed in the cells on the chemoattractant side in response to TGF–β.

results were promising and further testing to establish a statistical significance are required to establish the MiMiC^{TM} platform as a high throughput assay system.

CHAPTER 6

FUTURE WORK

6.1 Discussion

The study of the migration of cells through microchannels in response to chemoattractants provides information regarding the mechanism involved in the phenomenon. Thus there are aspects of the studies that can be conducted using the MiMiC^{TM} platform that have implications in clinical applications and cell biology studies.

6.1.1 Clinical Applications

The MiMiC^{TM} platform was used to study the migration of prostate cancer cells, lung-mestastasized prostate cancer cells, breast cancer cells, vascular smooth muscle cells and kidney cancer cells. The platform provides means to monitor, analyze and assess the response of the cells to different chemoattractants. Determining the migration characteristics of the cell in response to patient serum extracts may provide important information regarding cancer metastasis. As seen from the experiments, there was a difference in the response of the cells to FBS and to patient serum extracts. The response was different in different patient serum extracts. This could be of tremendous importance and may help in cancer diagnosis.

Cell migration or inhibition characteristics can therefore be easily monitored using the MiMiC^{TM} platform. The device can also be used in drug trials and testing leading to personalized therapies. The high throughput capability allows for a large number of tests to be performed simultaneously and also obtain real time data for all the tests.

Thus the device has potential applications in cancer metastasis studies. By comparing the migration characteristics to prostate specific antigen (PSA) levels of the patient and the Gleason score, the results of the MiMiC^{TM} studies could be used to prognosticate cancer metastasis.

6.1.2 Biological Applications

As has been demonstrated, the MiMiC^{TM} platform was successfully used for Immunocytochemistry in-situ. Time-lapse studies allow for careful observation and understanding of cell migration characteristics. This could be of help to cell biologists as the device allows monitoring and manipulation. To further assess the device, we also conducted trial experiments to interrogate the cell in-situ using glass needles. This can be useful to selectively target cells in migration and determine changes to the cytoplasm, receptors, cell phenotype etc. Various chemical reagents may be delivered to the cells directly. By coating the needles with antibodies, we hope to extract genetic material from the cells. Probing different locations of the cell and analyzing the content of the materials extracted using microneedles will provide a better understanding of the biochemical changes that occur within a cell during migration.

6.2 Future Work

There were issues that became known during the course of the various experiments that were conducted. The thickness of the device had to be very strictly controlled and maintained in order to obtain devices with identical reservoir capacities. This was achieved by determining the volume of the PDMS mixture required to obtain the required height of the device. The mold that we fabricated and the PDMS soft-lithography processes involved formed a pattern area that consumed 20 ml of the PDMS mixture to obtain a uniform 6 mm height of the MiMiC^{TM} platform.

By maintaining a 6 mm thick device and using a 5 mm hole puncher for the reservoir, the capacity of the reservoirs can be controlled.

Another issue that arose was the time consuming and extremely difficult task of manually punching each of the 5 mm holes to form the reservoir wells. These reservoirs have a 1 mm separation between them and are in contact with the microchannels. Thus, the location of the punch is extremely critical during making the device. Dust particles very easily accumulate on the PDMS surface making it extremely difficult to clean. Particles in the channels not only impede viewing but also are a source of contamination. Once the devices were cleaned, they were never handled outside the tissue culture hoods. They had to be handled with sterilized tweezers and the side of the device that formed the temporary bond with the culture plate had to be protected from contact with any surface other than the culture plate.

The greatest challenge was in data processing. For example, for the 35 patient serum extract experiment, 141 devices were used. Images were taken in brightfield and fluorescence every 24 hours for six days. Thus, 282 pictures were generated daily and a total of 1692 images were collected and analyzed. This technique provided more information than conventional methods, but was time consuming and tedious. An alternative approach is to develop an integrated platform with photodetectors to automatically detect cell migration. A conceptual drawing of such a system is shown in Fig.6.1.

The application potential of the MiMiC^{TM} platform is vast and varied and many more are yet to be developed. In order to further the utilization of the device one of the challenges is to overcome the punching of holes to form the reservoirs and automating the imaging process. The punching of holes may be solved by using a hand press device with a pre-made cutting die having the hole punching mechanism attached to it. We have had some limited success with this method. The issue was in

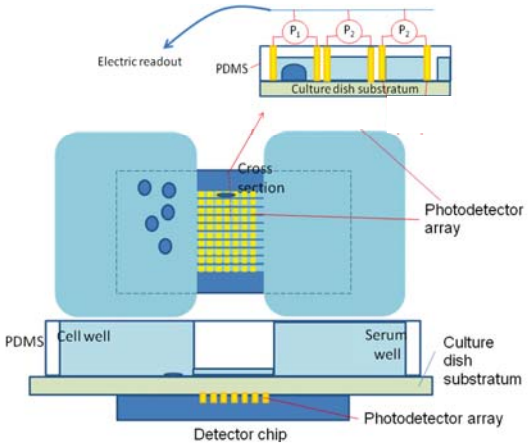

Figure 6.1. Conceptual design combining the MiMiC^{TM} platform with a photodetector array for automatic cell detection.

creating a cutting die that had to maintain strict tolerances. In our tested cutting die pattern, we used a 5 mm separation distance between the reservoirs. Although, the reservoirs could now be punched more accurately and simultaneously, the number of devices per platform was drastically reduced to 36 from 48. Also, making the process semi-automated or automated would reduce fabrication time and result in higher yields.

The various experiments conducted using the high throughput MiMiC^{TM} platform gave an insight into the various aspects of cell migration. It also provided a means to quantitatively assess the response of different cell types to the same chemoattractants. There seemed to be some discrepancy in the results. For example, for the same experiment set repeated within a experiment, there were different responses. This could be explained as being due to differing bilogical processes, device fabrication errors or oversight in cell seeding and/or addition of chemoattractants. In order to minimize these errors, a system needs to be developed to ensure that the position of the cells in each of the devices before the addition of the chemokine is the same.

In our experiments, we allowed cell attachment to occur over a period of 4 -24 hours depending on the cell type, checked the devices under a microscope to determine cell alignment, took pictures for reference and then added the chemokine. By improving the cell seeding technique the outcome of the experiments might be more consistent. Another issue was in data processing. The time-lapse images provide a large amount of information that is beneficial in analysis. However, it was labor intensive and time consuming to analyze. Obtaining a cell number from the time lapse images may be accomplished by using sofwares. The Cell Profiler^{TM} is a commonly used software for cell counting however, it does not provide information regarding cell position. In order to determine the migration rate of the cell, the position of the cell would have to be determined and compared.

The future direction of the work lies in automating the imaging and data analysis process. The images could be automatically captured using a programmed motorized stage with co-ordinates of each device location already fed-in. The number of cells can also be automatically determined using Matlab programs. However, analysis regarding cell migration that requires judgement will prove to be difficult to automate.

APPENDIX A

CELL CULTURE PROTOCOLS

A.1 Cell Culture

In this section, we present the methods of cell culture and seeding the cells in the microfluidic devices. The cell lines used in the experiments were red fluorescent protein (RFP) expressing human prostate cancer PC-3 line (PC-3R), green fluorescent protein (GFP) expressing lung-metastasized human prostate cancer (PC-3-ML) cells, normal prostate epithelial cell line (PZ-HPV-7), breast cancer (MDA-MB-231) cells, normal human mesangial cells (HMC), kidney cancer (CaKi-2) cells and human aortic smooth muscle cells (HASMC). These cells were used in the experiments to characterize the device. The conditions for the cell cultures and the culture media used with each type of cell is as listed below.

1. The cells were all cultured and maintained under 5% CO_2 atmosphere at 37°C. PC-3R cells were cultured in T-media (Invitrogen) supplemented with 5% fetal bovine serum (FBS), 100U/ml penicillin and 100 μg/ml streptomycin
2. PC-3-ML cells were cultured in RPMI 1640 (Cellgro) supplemented with 5% FBS, 100U/ml penicillin and 100 μg/ml streptomycin
3. PZ-HPV-7 cells were grown in PrEGM serum-free media (Clonetics) with 100U/ml penicillin and 100 μg/ml streptomycin
4. The CaKi-2 cells were grown in RPMI 1640 supplemented with 5% FBS, 100U/ml penicillin and 100 μg/ml streptomycin
5. The HMC were grown in DMEM supplemented with 20% FBS, 100U/ml penicillin and 100 μg/ml streptomycin
6. The HASMC were grown in DMEM with 10% NCS or 10% FBS, 100U/ml penicillin and 100 μg/ml streptomycin
7. Breast cancer cells (MDA-MB231) were cultured in RPMI 1640 with 5% FBS, 100U/ml penicillin and 100 μg/ml streptomycin

These cells were purchased from American Type Culture Collection (ATCC, Manassas, VA).

To prepare cells for testing in the devices, cells in exponential growing condition were trypsinized and counted. A cell suspension with the required number of cells was obtained by diluting in the appropriate media.

A.1.1 Device Priming

The microfluidic devices need to be prepared before the experiment. This was achieved by priming the devices with media and ensuring that there were no air bubbles or blockages in the channels of the device. In order to prime the device, 100 μl of the appropriate media was pipetted into one of the reservoirs or wells. Using the broader side of a 20 μl pipette tip with the tip connected to a vacuum pump, the media from the reservoir was drawn into the channels and into the second reservoir. In the case of the prototype device with four wells, the media was introduced into one of the reservoirs, and then drawn into the reservoir on the same side of the device. After covering the third reservoir, media was drawn through the channels from the fourth reservoir. The devices were then checked under a microscope to make sure the channels were clear of any blockages or air bubbles. The devices were then placed in an incubator until the cells were prepared.

A.1.1.1 Cell Seeding

Cell suspension was prepared as explained earlier. The priming media present in the reservoirs on the cell side was removed carefully. Immediately, using a pipette, 100 μl of the cell suspension was introduced into the cell side reservoir(s). The seeded cells were allowed to attach to the substratum and grow for an additional 4-24 hours before the chemokine or chemoattractant to be tested was introduced on the

chemoattractant side of the devices. After 24 hrs, the media from all 4 wells was removed and 100μl of appropriate growth media was added to the wells on the cell side of the device, while 100μl growth media containing the chemoattractant to be tested was added to the wells on the chemoattractant side. In order to minimize the evaporation of the media in the devices, sterilized PBS was added around the PDMS device attached to the culture plate.

Precautions were taken to ensure that there was no contamination or cross-contamination. All the pipette tips used were sterilized and all the processes were carried out in a tissue culture hood.

APPENDIX B

PATIENT PROTEIN ASSAY

B.1 Protein Assay

The Bradford protein is used to measure the concentration of protein in a solution. It is a spectroscopic analytical procedure dependent on the amino acid composition of the measured protein.

B.1.1 Principle

The Bradford assay is a colorimetric protein assay that is based on the absorbance shift Coomassie dye. The red colored Coomassie dye changes into coomassie blue by the binding of protein. The blue Coomassie dye is stabilized by the protein binding and the amount of the complex present in the solution providing an indication of the amount of protein in the solution.

The Bradford assay is linear over a short range, typically from 2 μg/ml to 120 μg/ml, often making dilutions of a sample necessary before analysis [98, 99]. Alternative protein assays are

1. UV spectroscopy
2. Biuret protein assay
3. Lowry protein assay
4. Bicinchoninic acid protein assay
5. Amido black protein assay
6. o-phthalaldehyde protein assay

B.1.2 Protein Content in the Patient Sera

The patient sera was centrifuged and the supernatant was drawn out. Centrifuge tubes of 2 ml capacity were filled with 99 μl of DI water each. The patient serum (1 μl) was added to each of the tubes and marked accordingly to identify the samples. Coomassie dye (500x) diluted to the appropriate concentration in DI water

was added to 1 ml cuvette tubes. A pipette was used to add 10 μl of the patient sera from the 2 ml tubes to the cuvettes. The cuvettes were then loaded onto the assay reader and readings were noted.

APPENDIX C

IMMUNOCYTOCHEMISTRY

C.1 Immunocytochemistry

In order to conduct Immunocytochemistry on the cells that were being tested using the microfluidic platform, the following steps were carried out.

1. The region of interest (channels and wells) were marked on the bottom side of the culture dish using a permanent marker
2. The media in the wells was pipetted out and the PDMS carefully peeled so that the cells remained attached to the culture plate
3. A wax pen (DAKO, Germany) was used to mark off the regions of the devices on the culture plate and the cells were fixed with 4% para-formaldehyde (PFA) for 30 mins at room temperature
4. The PFA was shaken-off and rinsed twice with PBS for 15 mins each on a rocker
5. Blocking buffer was used to shield the non-specific proteins in the device
6. After one hour, The blocking buffer was removed and primary antibodies suspended in incubation buffer was added to specific marked regions at room temperature for 2 hours
7. The primary antibody suspension was removed and the culture plate was once again washed with PBS twice for 15 mins each on a rocker
8. Secondary antibodies conjugated with fluorescent dyes (FITC or TRITC) suspended in incubation buffer was removed and rinsed with PBS as before
9. The culture plate was mounted with an anti-fade reagent DAPI, covered with glass coverslips and left overnight
10. Images were taken the next morning and compared

REFERENCES

[1] R. D. Loberg, C. J. Logothetis, E. T. Keller, and K. J. Pienta, "Pathogenesis and treatment of prostate cancer bone metastases: targeting the lethal phenotype,," *Journal of Clinical Oncology*, vol. 23, no. 32, pp. 8232–8241, Nov 2005. [Online]. Available: http://dx.doi.org/10.1200/JCO.2005.03.0841

[2] F. Saad, P. Perrotte, F. Bnard, M. McCormack, and P. I. Karakiewicz, "Bone health in men with prostate cancer: diagnostic and therapeutic considerations,," *Canadian Journal of Urology*, vol. 12 Suppl 2, pp. 9–15, Jun 2005.

[3] K. K. Yu and R. A. Hawkins, "The prostate: diagnostic evaluation of metastatic disease," *Radiologic Clinics of North America*, vol. 38, no. 1, pp. 139–57, ix, Jan 2000.

[4] I. Vela, L. Gregory, E. M. Gardiner, J. A. Clements, and D. L. Nicol, "Bone and prostate cancer cell interactions in metastatic prostate cancer,," *British Journal of Urology International*, vol. 99, no. 4, pp. 735–742, Apr 2007. [Online]. Available: http://dx.doi.org/10.1111/j.1464-410X.2006.06670.x

[5] F. W. Orr, H. H. Wang, R. M. Lafrenie, S. Scherbarth, and D. M. Nance, "Interactions between cancer cells and the endothelium in metastasis." *J Pathol*, vol. 190, no. 3, pp. 310–329, Feb 2000. [Online]. Available: http://dx.doi.org/3.0.CO;2-P

[6] E. W. Thompson and D. F. Newgreen, "Carcinoma invasion and metastasis: A role for epithelial-mesenchymal transition?" *Cancer Research*, vol. 65: (14), pp. 5991–5995, 2005.

[7] J. J. Christiansen and A. K. Rajasekaran, "Reassessing epithelial to mesenchymal transition as a prerequisite for carcinoma invasion and metastasis,," *Cancer Res*, vol. 66, no. 17, pp. 8319–8326, Sep 2006. [Online]. Available: http://dx.doi.org/10.1158/0008-5472.CAN-06-0410

[8] F. A. Ferrer, L. J. Miller, R. I. Andrawis, S. H. Kurtzman, P. C. Albertsen, V. P. Laudone, and D. L. Kreutzer, "Angiogenesis and prostate cancer: in vivo and in vitro expression of angiogenesis factors by prostate cancer cells,," *Urology*, vol. 51, no. 1, pp. 161–167, Jan 1998.

[9] B. Kaminska, A. Wesolowska, and M. Danilkiewicz, "Tgf beta signalling and its role in tumour pathogenesis,," *Acta Biochimica Polonica*, vol. 52, no. 2, pp. 329–337, 2005.

[10] S. Singh, U. P. Singh, W. E. Grizzle, and J. W. Lillard, "Cxcl12-cxcr4 interactions modulate prostate cancer cell migration, metalloproteinase expression and invasion,," *Lab Investigation*, vol. 84, no. 12, pp. 1666–1676, Dec 2004. [Online]. Available: http://dx.doi.org/10.1038/labinvest.3700181

[11] M. M. Marelli, R. M. Moretti, P. Procacci, M. Motta, and P. Limonta, "Insulin-like growth factor-i promotes migration in human androgen-independent prostate cancer cells via the alphavbeta3 integrin and pi3-k/akt signaling,," *International Journal of Oncology*, vol. 28, no. 3, pp. 723–730, Mar 2006.

[12] P. Wikstrm, P. Stattin, I. Franck-Lissbrant, J. E. Damber, and A. Bergh, "Transforming growth factor beta1 is associated with angiogenesis, metastasis, and poor clinical outcome in prostate cancer,," *Prostate*, vol. 37, no. 1, pp. 19–29, Sep 1998.

[13] S. Yang, C. Zhong, B. Frenkel, A. H. Reddi, and P. Roy-Burman, "Diverse biological effect and smad signaling of bone morphogenetic protein 7 in prostate tumor cells,," *Cancer Research*, vol. 65, no. 13, pp. 5769–5777, Jul 2005. [Online]. Available: http://dx.doi.org/10.1158/0008-5472.CAN-05-0289

[14] H.-L. Lee, K. J. Pienta, W.-J. Kim, and C. R. Cooper, "The effect of bone-associated growth factors and cytokines on the growth of prostate cancer cells derived from soft tissue versus bone metastases in vitro,," *International Journal of Oncology*, vol. 22, no. 4, pp. 921–926, Apr 2003.

[15] Y. Lu, Z. Cai, D. L. Galson, G. Xiao, Y. Liu, D. E. George, M. F. Melhem, Z. Yao, and J. Zhang, "Monocyte chemotactic protein-1 (mcp-1) acts as a paracrine and autocrine factor for prostate cancer growth and invasion,," *Prostate*, vol. 66, no. 12, pp. 1311–1318, Sep 2006. [Online]. Available: http://dx.doi.org/10.1002/pros.20464

[16] V. Michalaki, K. Syrigos, P. Charles, and J. Waxman, "Serum levels of il-6 and tnf-alpha correlate with clinicopathological features and patient survival in patients with prostate cancer,," *British Journal of Cancer*, vol. 90, no. 12, pp. 2312–2316, Jun 2004. [Online]. Available: http://dx.doi.org/10.1038/sj.bjc.6601814

[17] C. K. Ritchie, L. R. Andrews, K. G. Thomas, D. J. Tindall, and L. A. Fitzpatrick, "The effects of growth factors associated with osteoblasts on prostate carcinoma proliferation and chemotaxis: implications for the development of metastatic disease,," *Endocrinology*, vol. 138, no. 3, pp. 1145–1150, Mar 1997.

[18] R. D. Loberg, L. L. Day, J. Harwood, C. Ying, L. N. S. John, R. Giles, C. K. Neeley, and K. J. Pienta, "Ccl2 is a potent regulator of prostate cancer cell migration and proliferation,," *Neoplasia*, vol. 8, no. 7, pp. 578–586, Jul 2006. [Online]. Available: http://dx.doi.org/10.1593/neo.06280

[19] Y.-H. Li and C. Zhu, "A modified boyden chamber assay for tumor cell transendothelial migration in vitro," *Clinical & Experimental Metastasis*, vol. 17, p. 423429, 1999.

[20] M. M. Woo, C. M. Salamanca, A. Minor, and N. Auersperg, "An improved assay to quantitate the invasiveness of cells in modified boyden chambers,," *In Vitro Cellular & Developmental Biology - Animal*, vol. 43, pp. 7–9, 2007.

[21] F. Lin, C. M.-C. Nguyen, S.-J. Wang, W. Saadi, S. P. Gross, and N. L. Jeon, "Neutrophil migration in opposing chemoattractant gradients using microfluidic chemotaxis devices," *Annals of Biomedical Engineering*, vol. 33, pp. 475–482, 2005.

[22] N. L. Jeon, H. Baskaran, S. K. W. Dertinger, G. M. Whitesides, L. V. de Water, and M. Toner, "Neutrophil chemotaxis in linear and complex gradients of interleukin-8 formed in a microfabricated device,," *Nature Biotechnology*, vol. 20, no. 8, pp. 826–830, Aug 2002. [Online]. Available: http://dx.doi.org/10.1038/nbt712

[23] F. Lin, C. M.-C. Nguyen, S.-J. Wang, W. Saadi, S. P. Gross, and N. L. Jeon, "Effective neutrophil chemotaxis is strongly influenced by mean il-8 concentration,," *Biochemical and Biophysical Research Communications*, vol. 319, no. 2, pp. 576–581, Jun 2004. [Online]. Available: http://dx.doi.org/10.1016/j.bbrc.2004.05.029

[24] A. M. Taylor, S. W. Rhee, and N. L. Jeon, "Microfluidic chambers for cell migration and neuroscience research,," *Methods in Molecular Biology*, vol. 321, pp. 167–177, 2006.

[25] F. Lin and E. Butcher, "T cell chemotaxis in a simple microfluidic device,," *Lab on a chip*, vol. 6, no. 11, pp. 1462–1469, Nov 2006.

[26] R. S. Martin, P. D. Root, and D. M. Spence, "Microfluidic technologies as platforms for performing quantitative cellular analyses in an in vitro environment,," *Analyst*, vol. 131, no. 11, pp. 1197–1206, Nov 2006. [Online]. Available: http://dx.doi.org/10.1039/b611041j

[27] S. R. Quake and A. Scherer, "From micro- to nanofabrication with soft materials,," *Science*, vol. 290, no. 5496, pp. 1536–1540, Nov 2000.

[28] G. M. Walker, J. Sai, A. Richmond, M. Stremler, C. Y. Chung, and J. P. Wikswo, "Effects of flow and diffusion on chemotaxis studies in a microfabricated gradient generator,," *Lab Chip*, vol. 5, no. 6, pp. 611–618, Jun 2005. [Online]. Available: http://dx.doi.org/10.1039/b417245k

[29] M. Ghitun, E. Bonneil, M.-H. Fortier, H. Yin, K. Killeen, and P. Thibault, "Integrated microfluidic devices with enhanced separation performance: application to phosphoproteome analyses of differentiated cell model systems," *Journal of Seperation Science*, vol. 29, no. 11, pp. 1539–1549, Jul 2006.

[30] J. Li, T. LeRiche, T.-L. Tremblay, C. Wang, E. Bonneil, D. J. Harrison, and P. Thibault, "Application of microfluidic devices to proteomics research: identification of trace-level protein digests and affinity capture of target peptides,," *Molecular & Cellular Proteomics*, vol. 1, no. 2, pp. 157–168, Feb 2002.

[31] W. Saadi, S.-J. Wang, F. Lin, and N. L. Jeon, "A parallel-gradient microfluidic chamber for quantitative analysis of breast cancer cell chemotaxis,," *Biomedical Microdevices*, vol. 8, no. 2, pp. 109–118, Jun 2006. [Online]. Available: http://dx.doi.org/10.1007/s10544-006-7706-6

[32] J. W. Pollard and J. M. Walker, Eds., *Basic cell culture protocols,*. Humana Press Inc., Totowa, NJ, 1997.

[33] W. B. Jakoby and I. H. Pastan, *Methods In Enzymology: Cell Culture,*, S. Colowick and N. Kaplan, Eds. Academic Press, 1979, vol. 58.

[34] A. A. S. Bhagat, P. Jothimuthu, A. Pais, and I. Papautsky, "Re-usable quick-release interconnect for characterization of microfluidic systems," *Journal of Micromechanics and Microengineering*, vol. 17, no. 1, pp. 42–49, 2007. [Online]. Available: http://stacks.iop.org/0960-1317/17/42

[35] V. Saarela, S. Franssila, S. Tuomikoski, S. Marttila, P. stman, T. Sikanen, T. Kotiaho, and R. Kostiainen, "Re-usable multi-inlet pdms fluidic connector,," *Sensors and Actuators B: Chemical*, vol. 114, no. 1, pp. 552–557, March 2006.

[36] R. Lo and E. Meng, "Integrated and reusable in-plane microfluidic interconnects,," *Sensors and Actuators B: Chemical*, vol. 132, no. 2, pp. 531–539, June 2008.

[37] Z. Yang and R. Maeda, "Socket with built-in valves for the interconnection of microfluidic chips to macro constituents,," *Journal of Chromatography A*, vol. 1013, no. 1-2, pp. 29–33, September 2003.

[38] D. Sabourin, D. Snakenborg, and M. Dufva, "Interconnection blocks: a method for providing reusable, rapid, multiple, aligned and planar microfluidic interconnections," *Journal of Micromechanics and Microengineering*, vol. 19, no. 3, p. 035021 (9pp), 2009. [Online]. Available: http://stacks.iop.org/0960-1317/19/035021

[39] L. T. Canham, "Bioactive silicon structure fabrication through nanoetching techniques,," *Advanced Materials*, vol. 7, no. 12, pp. 1033–1037, 1995. [Online]. Available: http://dx.doi.org/10.1002/adma.19950071215

[40] P. R. Hernandez, C. Taboada, L. Leija, V. Tsutsumi, B. Vazquez, F. Valdes-Perezgasga, and J. L. Reyes, "Evaluation of biocompatibility of ph-isfet materials during long-term subcutaneous implantation,," *Sensors and Actuators B: Chemical*, vol. 46, no. 2, pp. 133 – 138, 1998. [Online]. Available: http://www.sciencedirect.com/science/article/B6THH-3SY3W9C-9/2/40130fd8b309be4ccf2f95a18df8a409

[41] U. Certa, R. Hochstrasser, H. Langen, M. Buess, and C. Moroni, "Biosensors in biomedical research: Development and applications of gene chips," *CHIMIA International Journal for Chemistry*, vol. 53, pp. 57–61(5), March 1999.

[Online]. Available: http://www.ingentaconnect.com/content/scs/chimia/1999/00000053/00000003/art00002

[42] G. Voskerician, M. S. Shive, R. S. Shawgo, H. von Recum, J. M. Anderson, M. J. Cima, and R. Langer, "Biocompatibility and biofouling of mems drug delivery devices,," *Biomaterials*, vol. 24, no. 11, pp. 1959 – 1967, 2003. [Online]. Available: http://www.sciencedirect.com/science/article/B6TWB-47VS5BP-7/2/03785737a42db8291177b62e195975e3

[43] J. D. Snyder and T. A. Desai, "Microscale three-dimensional polymeric platforms for in vitro cell culture systems,," *Journal of Biomaterials Science, Polymer Edition*, vol. 12, no. 8, pp. 921–932, 2001.

[44] B.-H. Jo, L. M. V. Lerberghe, K. M. Motsegood, and D. J. Beebe, "Three-dimensional micro-channel fabrication in polydimethylsiloxane (pdms) elastomer,," *Journal of Microelectromechanical Systems*, vol. 9, no. 1, pp. 76–81, 2000.

[45] U. Y. Schaff, M. M. Q. Xing, K. K. Lin, N. Pan, N. L. Jeon, and S. I. Simon, "Vascular mimetics based on microfluidics for imaging the leukocyte–endothelial inflammatory response." *Lab Chip*, vol. 7, no. 4, pp. 448–456, Apr 2007. [Online]. Available: http://dx.doi.org/10.1039/b617915k

[46] S.-J. Wang, W. Saadi, F. Lin, C. M.-C. Nguyen, and N. L. Jeon, "Differential effects of egf gradient profiles on mda-mb-231 breast cancer cell chemotaxis,," *Experimental Cell Research*, vol. 300, no. 1, pp. 180 – 189, 2004. [Online]. Available: http://www.sciencedirect.com/science/article/B6WFC-4D2FJD2-1/2/97eff61cc4259620f80371bd1a04bace

[47] A. M. Taylor, S. W. Rhee, C. H. Tu, D. H. Cribbs, C. W. Cotman, and N. L. Jeon, "Microfluidic multicompartment device for neuroscience research,," *Langmuir*, vol. 9, no. 5, pp. 1551–1556, 2003.

[48] S. A. Klasner, E. C. Metto, G. T. Roman, and C. T. Culbertson, "Synthesis and characterization of a poly(dimethylsiloxane)-poly(ethylene oxide) block copolymer for fabrication of amphiphilic surfaces on microfluidic devices,," *Langmuir*, vol. 25, no. 17, pp. 10 390–10 396, Sep 2009. [Online]. Available: http://dx.doi.org/10.1021/la900920q

[49] D. Fuard, T. Tzvetkova-Chevolleau, S. Decossas, P. Tracqui, and P. Schiavone, "Optimization of poly-di-methyl-siloxane (pdms) substrates for studying cellular adhesion and motility,," *Microelectronic Engineering*, vol. 85, pp. 1289–1293, 2008.

[50] E. Leclerc, Y. Sakai, and T. Fujii, "A multi-layer pdms microfluidic device for tissue engineering applications," in *IEEE The Sixteenth Annual International Conference on Micro Electro Mechanical Systems*. IEEE, January 2003, pp. 415–418.

[51] J. Kuncova-Kallio and P. J. Kallio, "Pdms and its suitability for analytical microfluidic devices," in *Proc. 28th Annual International Conference of the IEEE Engineering in Medicine and Biology Society EMBS '06*, Aug. 2006, pp. 2486–2489.

[52] W. Noll, *Chemistry and Technology of Silicones,*. Academic Press, New York,, 1968.

[53] T. Kendrick, B. Parbhoo, and J. White, *Siloxane Polymers and Copolymers in The Chemistry of Organic Silicon Compounds Pt 2*, S. Patai and Z. Rappoport, Eds. John Wiley, Chichester, 1989, vol. 21.

[54] J. White and R. Treadgold, *Organofunctional Siloxanes in Siloxane Polymers*, S. Clarson and J. Semlyen, Eds. Prentice Hall, New Jersey, 1993, vol. 4, no. 193-215.

[55] S. Clarson and J. Semlyen, Eds., *Siloxane Polymers*. Prentice Hall, New Jersey, 1993.

[56] W. Gardiner and J. White, *Specialty Silicones as Building Blocks for Organic Polymer Modification in High Value Polymers*, A. Fawcett, Ed. Royal Society of Chemistry, Cambridge, 1990.

[57] W. Wang and S. A. Soper, Eds., *Bio-MEMS technologies and applications,*. CRC Press, Boca Raton, FL, 2006.

[58] K. Efimenko, W. E. Wallace, and J. Genzer, "Surface modification of sylgard-184 poly(dimethyl siloxane) networks by ultraviolet and ultraviolet/ozone treatment,," *Journal of Colloid and Interface Science*, vol. 254, pp. 306–315, 2002.

[59] M. A. Eddings, M. A. Johnson, and B. K. Gale, "Determining the optimal pdms-pdms bonding technique for microfluidic devices," *Journal of Micromechanics and Microengineering*, vol. 18, no. 6, p. 067001 (4pp), 2008. [Online]. Available: http://stacks.iop.org/0960-1317/18/067001

[60] J. B. Christen and A. G. Andreou, "Hybrid silicon/silicone (polydimethylsiloxane) microsystem for cell culture,," in *Proceedings of the 28th IEEE EMBS Annual International Conference*, 2006, pp. 2490–2493.

[61] E. F. Wei-Cheng Tian, Ed., *Microfluidics for biological applications,*. Springer Science + Business Media, New York, 2008.

[62] J. Cha, J. Kim, S.-K. Ryu, J. Park, Y. Jeong, S. Park, S. Park, H. C. Kim, and K. Chun, "A highly efficient 3d micromixer using soft pdms bonding," *Journal of Micromechanics Microengineering*, vol. 16, pp. 1778–1782, 2006.

[63] *2-D Modeling and Simulation of Fluidic Microsystems for Biological Fluids Analysis*, 2003.

[64] D. Irimia, D. A. Geba, and M. Toner, "Universal microfluidic gradient generator,," *Anal Chem*, vol. 78, no. 10, pp. 3472–3477, May 2006. [Online]. Available: http://dx.doi.org/10.1021/ac0518710

[65] S. K. W. Dertinger, D. T. Chiu, N. L. Jeon, and G. M. Whitesides, "Generation of gradients having complex shapes using microfluidic networks,," *Analytical Chemistry*, vol. 73, pp. 1240–1246, 2001.

[66] N. L. Jeon, S. K. W. Dertinger, D. T. Chiu, I. S. Choi, A. D. Stroock, and G. M. Whitesides, "Generation of solution and surface gradients using microfluidic systems,," *Langmuir*, vol. 16, no. 22, p. 83118316, 2000.

[67] D. P. Gaver and S. M. Kute, "A theoretical model study of the influence of fluid stresses on a cell adhering to a microchannel wall." *Biophys J*, vol. 75, no. 2, pp. 721–733, Aug 1998. [Online]. Available: http://dx.doi.org/10.1016/S0006-3495(98)77562-9

[68] H. Dailey, H. Yalcin, and S. Ghadiali, "Fluid-structure modeling of flow-induced alveolar epithelial cell deformation," *Computers & Structures*, vol. 85, no. 11-14, pp. 1066 – 1071, 2007, fourth MIT Conference on Computational Fluid and Solid Mechanics. [Online]. Available: http://www.sciencedirect.com/science/article/B6V28-4MSY8B9-2/2/fcbec75cd40c6225b3e18d30901711c2

[69] S. Boyden, "The chemotactic effect of mixtures of antibody and antigen on polymorphonuclear leucocytes,," *The Journal of Experimental Medicine*, vol. 115, pp. 453–466, 1962.

[70] R. D. Nelson, P. Quie, and R. L. Simmons, "A new and simple method for measuring chemotaxis and spontaneous migration of human polymorphonuclear leukocytes and monocytes,," *Journal of Immunology*, vol. 115, pp. 1650–1656, 1975.

[71] S. H. Zigmond, "Ability of polymorphonuclear leukocytes to orient in gradients of chemotactic factors." *J Cell Biol*, vol. 75, no. 2 Pt 1, pp. 606–616, Nov 1977.

[72] D. Zicha, G. Dunn, and A. F. Brown, "A new direct-viewing chemotaxis chamber," *Journal of Cell Science*, vol. 99, Pt 4, pp. 769–775, 1991.

[73] G. Gerisch and H. U. Keller, "Chemotactic reorientation of granulocytes stimulated with micropipettes containing fmet-leu-phe." *Journal of Cell Science*, vol. 52, pp. 1–10, Dec 1981.

[74] O. Debeir, I. Camby, R. Kiss, P. V. Ham, and C. Decaestecker, "A model-based approach for automated in vitro cell tracking and chemotaxis analyses," *Cytometry A*, vol. 60, no. 1, pp. 29–40, Jul 2004. [Online]. Available: http://dx.doi.org/10.1002/cyto.a.20040

[75] N. Nitta, T. Tsuchiya, A. Yamauchi, T. Tamatani, and S. Kanegasaki, "Quantitative analysis of eosinophil chemotaxis tracked using a novel optical device – taxiscan," *Journal of Immunological Methods*, vol. 320, no. 1-2, pp. 155 – 163, 2007. [Online]. Available: http://www.sciencedirect.com/science/article/B6T2Y-4MW8WKX-2/2/f61d357271b1731ac96335704df29d80

[76] R. B. Campenot, "Local control of neurite development by nerve growth factor," *Proc. of National Academy of Sciences*, vol. 74, pp. 4516–4519, 1977.

[77] ——, "Development of sympathetic neurons in compartmentalized cultures. il local control of neurite growth by nerve growth factor." *Dev Biol*, vol. 93, no. 1, pp. 1–12, Sep 1982.

[78] D. Irimia, G. Charras, N. Agrawal, T. Mitchison, and M. Toner, "Polar stimulation andcconstrained cell migration in microfluidic channels," *Lab Chip*, vol. 7, pp. 1783 – 1790, 2007.

[79] J. Diao, L. Young, S. Kim, E. A. Fogarty, S. M. Heilman, P. Zhou, M. L. Shuler, M. Wu, and M. P. DeLisa, "A three-channel microfluidic device for

generating static linear gradients and its application to the quantitative analysis of bacterial chemotaxis." *Lab Chip*, vol. 6, no. 3, pp. 381–388, Mar 2006. [Online]. Available: http://dx.doi.org/10.1039/b511958h

[80] A. Shamloo, N. Ma, M.-M. Poo, L. L. Sohn, and S. C. Heilshorn, "Endothelial cell polarization and chemotaxis in a microfluidic device." *Lab Chip*, vol. 8, no. 8, pp. 1292–1299, Aug 2008. [Online]. Available: http://dx.doi.org/10.1039/b719788h

[81] G. G. Martins and J. Kolega, "Endothelial cell protrusion and migration in three-dimensional collagen matrices." *Cell Motil Cytoskeleton*, vol. 63, no. 2, pp. 101–115, Feb 2006. [Online]. Available: http://dx.doi.org/10.1002/cm.20104

[82] M. Vicente-Manzanares, D. J. Webb, and A. R. Horwitz, "Cell migration at a glance," *J Cell Sci*, vol. 118, no. Pt 21, pp. 4917–4919, Nov 2005. [Online]. Available: http://dx.doi.org/10.1242/jcs.02662

[83] A. J. Ridley., M. A. Schwartz, K. Burridge, R. A. Firtel, M. H. Ginsberg, G. Borisy, T. J. Parsons, and A. R. Horwitz, "Cell migration: Integrating signals from front to back," *Science*, vol. 302, no. 5651, pp. 1704–1709, 2003. [Online]. Available: http://www.sciencemag.org/cgi/content/abstract/302/5651/1704

[84] R. Horwitz and D. Webb, "Cell migration," *Current Biology*, vol. 13, no. 19, pp. R756–R759, September 2003.

[85] L. L. Soon, "A discourse on cancer cell chemotaxis: Where to from here?" *IUBMB*, vol. 59, pp. 60–67, 2007.

[86] T. Kanzaki, R. Shiina, Y. Saito, H. Oohashi, and N. Morisaki, "Role of latent tgf-beta1 binding protein in vascular remodeling," *Biochemical and Biophysical Research Communications*, vol. 246, pp. 26–30, 1998.

[87] C. Pross, M. M. Farooq, J. S. Lane, N. Angle, C. K. Tomono, A. E. Xavier, J. A. Freischlag, A. E. Collins, R. E. Law, and H. A. Gelabert, "Rat and human aortic

smooth muscle cells display differing migration and matrix metalloproteinase activities in response to dexamethasone," *J Vasc Surg*, vol. 35, no. 6, pp. 1253–1259, Jun 2002.

[88] S. Awasthi, J. Cheng, S. S. Singhal, M. K. Saini, U. Pandya, S. Pikula, J. Bandorowicz-Pikula, S. V. Singh, P. Zimniak, and Y. C. Awasthi, "Novel function of human rlip76: Atp-dependent transport of glutathione conjugates and doxorubicin," *Biochemistry*, vol. 39, pp. 9327–9334, 2000.

[89] S. S. Singhal, J. Singhal, J. Cheng, S. Piku?a, R. Sharma, P. Zimniak, Y. C. Awasthi, and S. Awasthi, "Purification and functional reconstitution of intact ral-binding gtpase activating protein, rlip76, in artificial liposomes." *Acta Biochim Pol*, vol. 48, pp. 551–562, 2001.

[90] S. Awasthi, R. Sharma, S. S. Singhal, P. Zimniak, and Y. C. Awasthi, "Rlip76, a novel transporter catalyzing atp-dependent efflux of xenobiotics," *Drug Metab Dispos*, vol. 30, pp. 1300–1310, 2002.

[91] S. S. Singhal, J. Singhal, R. Sharma, S. V. Singh, P. Zimniak, Y. C. Awasthi, and S. Awasthi, "Role of rlip76 in lung cancer doxorubicin resistance: I. the atpase activity of rlip76 correlates with doxorubicin and 4-hydroxynonenal resistance in lung cancer cells," *Int J Oncol*, vol. 22, pp. 365–375, 2003.

[92] S. Awasthi, S. S. Singhal, J. Singhal, Y. Yang, P. Zimniak, and Y. C. Awasthi, "Role of rlip76 in lung cancer doxorubicin resistance: Iii. anti-rlip76 antibodies trigger apoptosis in lung cancer cells and synergistically increase doxorubicin cytotoxicity," *Int J Oncol*, vol. 22, pp. 721–732, 2003.

[93] J. Singhal, S. S. Singhal, S. Yadav, S. Suzuki, M. M. Warnke, A. Yacoub, P. Dent, S. Bae, R. Sharma, Y. C. Awasthi, D. W. Armstrong, and S. Awasthi, "Rlip76 in defense of radiation poisoning," *Int J Radiat Oncol Biol Phys*, vol. 72, pp. 553–561, 2008.

[94] S. Awasthi, S. S. Singhal, J. Singhal, J. Cheng, P. Zimniak, and Y. C. Awasthi, "Role of rlip76 in lung cancer doxorubicin resistance: Ii. doxorubicin transport in lung cancer by rlip76," *Int J Oncol*, vol. 22, pp. 713–720, 2003.

[95] R. Sharma, S. S. Singhal, J. Cheng, Y. Yang, A. Sharma, P. Zimniak, S. Awasthi, and Y. C. Awasthi, "Rlip76 is the major atp-dependent transporter of glutathione-conjugates and doxorubicin in human erythrocytes," *Arch Biochem Biophys*, vol. 391, pp. 171–179, 2001.

[96] Y. C. Awasthi, G. A. S. Ansari, and S. Awasthi, "Regulation of 4-hydroxynonenal mediated signaling by glutathione s-transferases," *Methods Enzymol*, vol. 401, pp. 379–407, 2005.

[97] E. Korsching, J. Packeisen, C. Liedtke, D. Hungermann, P. Wulfing, P. J. van Diest, B. Brandt, W. Boecker, and H. Buerger, "The origin of vimentin expression in invasive breast cancer: epithelialmesenchymal transition, myoepithelial histogenesis or histogenesis from progenitor cells with bilinear differentiation potential?" *Journal of Pathology*, vol. 206, pp. 451–457, 2005.

[98] M. M. Bradford, "A rapid and sensitive method for the quantitation of microgram quantities of protein utilizing the principle of protein-dye binding," *Analytical Biochemistry*, vol. 72, pp. 248–254, 1976.

[99] T. Zor and Z. Selinger, "Linearization of the bradford protein assay increases its sensitivity: Theoretical and experimental studies," *Analytical Biochemistry*, vol. 236, no. 2, pp. 302 – 308, 1996. [Online]. Available: http://www.sciencedirect.com/science/article/B6W9V-45N4PDS-CG/2/6f0bdd3c1f5d07a2d9f0eb178fca72e7

BIOGRAPHICAL STATEMENT

Smitha Malalur Nagaraja Rao was born in Mysore, India, in 1979. She received her Bachelor of Engineering in Telecommunication degree from Bangalore University, India, in 2000, her M.S. and Ph.D.in Eectrical Engineering from The University of Texas at Arlington in 2004 and 2009, respectively. Her current research interest is in the area of cell migration, cancer cell migration and metastasis, biomedical sensing systems and imaging applications. She is a member of IEEE, BMES and SPIE societies.